STUDYING SOURCE CONTRIBUTIONS TO AMBIENT FINE PARTICULATE MATTER AND ESTIMATING ITS HISTORICAL CONCENTRATIONS

by

Jun Meng

Submitted in partial fulfilment of the requirements
for the degree of Doctor of Philosophy

at

Dalhousie University
Halifax, Nova Scotia
September 2020

致

我的父母

TABLE OF CONTENTS

LIST OF TABLES

LIST OF FIGURES

ABSTRACT

Long-term exposure to ambient fine particulate matter ($PM_{2.5}$) is a major health concern. This thesis presents three projects that take advantage of chemical transport modeling, ground-based monitoring and satellite remote sensing to advance the understanding of historical concentrations, source contributions, and chemical composition of $PM_{2.5}$.

Historical $PM_{2.5}$ concentrations across North America from 1981 to 2016 were estimated by fusing satellite derived $PM_{2.5}$ data and ground-based measurements with GEOS-Chem chemical transport model simulations. Comparison with ground-based $PM_{2.5}$ measurements indicates consistency of the estimated $PM_{2.5}$ concentrations with observations, especially in the later years with extensive $PM_{2.5}$ monitoring. The estimated population-weighted annual average $PM_{2.5}$ over North America decreased from 22 ± 6.4 μg m^{-3} in 1981 to 7.9 ± 2.1 μg m^{-3} in 2016, with an overall trend of -0.33 μg m^{-3} yr^{-1} (95% CI: -0.35 -0.30), reflecting the significant reduction of anthropogenic emissions over the past decades.

Sensitivity simulations were conducted using the GEOS-Chem chemical transport model to investigate the sectoral contribution to $PM_{2.5}$ for Canada. We found that annually about 70% of population-weighted $PM_{2.5}$ originates from Canadian sources and about 30% from the contiguous United States, with wildfires, transportation and residential combustion as the leading sectors in 2013. The relative contribution to population-weighted $PM_{2.5}$ of different sectors varied regionally and seasonally. Sectoral trend analysis showed that the contribution from anthropogenic sources to population-weighted $PM_{2.5}$ decreased from 7.1 μg/m^3 in 1990 to 3.4 μg/m^3 in 2013.

Offline grid independent dust emissions driven by native high resolution meteorological fields were generated to harmonize dust emissions across simulations of different resolutions. The updated offline dust emissions can better resolve weak dust source regions, such as southern South America, southern Africa and the southwestern United States. We find that the performance of simulated aerosol optical depth (AOD) versus measurements from the Aerosol Robotic Network (AERONET) network and satellite remote sensing improves significantly when using the updated offline dust emissions with the total global annual dust emission strength of 2,000 Tg yr^{-1}. The offline high resolution dust emissions are easily implemented in chemical transport models, with potential to promote model development and evaluation.

LIST OF ABBREVIATIONS AND SYMBOLS USED

Symbol	Unit	Description
AERONET		Aerosol Robotic Network
AOD		Aerosol Optical Depth
APEI		Air Pollutant Emission Inventory
BAM		Beta Attenuation Monitoring
BC		Black Carbon
BLUP		Best Linear Unbiased Prediction
CAC		Criteria Air Contaminants
CanCHEC		Canadian Census Health and Environment Cohorts
CASTNET		Clean Air Status and Trends Network
CCME		Canadian Council of Ministers of the Environment
CEDS		Community Emissions Data System
CSN		Chemical Speciation Network
CTM		Chemical Transport Models
DB		Deep Blue
DJF		December, January and February
DMS		Dimethyl Sulfide
DOD		Dust Optical Depth
EPA		Environmental Protection Agency
ERF	$W\ m^{-2}$	Effective Radiative Forcing
FRM		Federal Reference Method
GBD		Global Burden of Disease
GEOS		Goddard Earth Observation System
GMAO		Global Modeling and Assimilation Office
GWR		Geographically Weighted Regression
HEI		Health Effects Institute
HO_2		Hydroperoxyl Radical
IMPROVE		Interagency Monitoring of Protected Visual Environments
IPN		Inhalable Particle Network
JJA		June, July and August
MAIAC		Multi-Angle Implementation of Atmospheric Correction
MAM		March, April and May
MB		Mean Bias
MODIS		Moderate-Resolution Imaging Spectroradiometer
N_2O_5		Dinitrogen Pentoxide
NAPS		National Air Pollutant Surveillance

NEI2011		2011 National Emissions Inventory
NH_3		Ammonia
NO_x		Nitrogen Oxides
OC		Organic Carbon
PM		Particulate Matter
PM_{10}	$\mu g\ m^{-3}$	Aerosol particles with an aerodynamic diameter below 10 μm
$PM_{2.5}$	$\mu g\ m^{-3}$	Aerosol particles with an aerodynamic diameter below 2.5 μm
PM_{sat}	$\mu g\ m^{-3}$	Satellite-based $PM_{2.5}$ concentration estimates
POC		Primary Organic Carbon
r		Correlation
R^2		Coefficient of determination
RMSD		Root Mean Square Difference
RMSE		Root Mean Square Error
SEDAC		Space Administration Socioeconomic Data and Application Center
SIA		Secondary Inorganic Aerosol
SNA		Sulfate-Nitrate-Ammonium
SO_2		Sulfur Dioxide
SOA		Secondary Organic Aerosol
SOC		Secondary Organic Carbon
SON		September, October and November
TSP		Total Suspended Particles
VOC		Volatile Organic Compound
WHO		World Health Organization
Θ	degree	Satellite viewing angle
τ_a		Aerosol optical depth
ϖ		Aerosol single-scattering albedo

ACKNOWLEDGEMENTS

Firstly, I would like to thank my supervisor Dr. Randall Martin for his encouragement, guidance and financial support. This work will be impossible without his insightful comments and advices. I would also like to thank my committee members, Dr. Glen Lesins and Dr. Rachel Chang, for their helpful and constructive comments for my research throughout the PhD program.

I would also like to express my thanks to all my co-authors for their contributions in the two published articles presented in Chapter 2 and Chapter 3. This includes Chi Li, Aaron van Donkelaar, Perry Hystad, Xu Yue, Jun-Wei Xu, Crystal Weagle, Zitely Tzompa-Sosa, Richard Burnett and Michael Brauer. Thanks also to the seven anonymous reviewers who helped to review and improve the manuscripts that are presented in those chapters. I would also like to acknowledge the contributions to the Chapter 4 from Paul Ginoux, David Ridley, Melanie Hammer and Aaron van Donkelaar.

Additionally, to all my office mates, no matter in Dalhousie University or Washington University, thanks for all the great conversations and technical supports. To my friends in the North End Runners group and Mexpats, thanks for the moral support while running all those beautiful streets and trails in Halifax with me.

Finally, I would like to thank my parents and younger sister for their continuous and altruistic support. Especially, I would like to thank my parents for not complaining about being visited for only once and my absence from all the Chinese New Year reunions in the past four years.

CHAPTER 1 INTRODUCTION

1.1 ATMOSPHERIC AEROSOLS

Atmospheric aerosols are a complex and dynamic mixture of solid and liquid particles with a wide range in size from a few nanometers (nm) to tens of micrometers (μm) in diameter. Atmospheric aerosol consists of many chemical components, commonly including sulfates, ammonium compounds, elemental carbon (soot), organic compounds, dust particles, and sea salt particles, rising from natural and anthropogenic sources. Atmospheric aerosol can either be primary particles that emitted directly into the atmosphere or secondary particles that formed by chemical reactions of precursor gases in the atmosphere, such as sulfur dioxide (SO_2), nitrogen oxides (NO_X), ammonia (NH_3), and volatile organic compounds (VOC) (Seinfeld & Pandis, 2016).

The dynamic processes of atmospheric aerosols change the particle size distribution and ultimately determine the fate of the aerosols. Newly emitted or formed aerosols are predominantly in the ultrafine size range with an aerodynamic diameter less than 0.1 μm (nucleation mode). Then particles can rapidly grow to accumulation mode (aerodynamic diameter in 0.1 – 2.5 μm) through condensation of vapor species, coagulation with other particles, and activating in the presence of water supersaturation to cloud droplets. The further growth from accumulation mode particles to coarse mode particles (aerodynamic diameter larger than 2.5 μm) is slow due to the low condensation and coagulation rates in large particles (Seinfeld & Pandis, 2016). Atmospheric aerosols are eventually removed from the atmosphere by two mechanisms: dry deposition and wet deposition. Dry deposition is the settling of aerosol particles without precipitation through Brownian diffusion for nucleation mode particles and gravitational settling for coarse mode particles. Wet deposition is the process that aerosol

particles are removed through precipitation, including washout by incorporating into cloud droplets and below-cloud rainout. Thus, residence times of aerosol particles in the troposphere vary from a few days to a few weeks (Seinfeld & Pandis, 2016).

Atmospheric aerosol has a profound impact on earth system since the composition and mass concentration of aerosol have been changed significantly during the past century due to anthropogenic emissions. Aerosol plays a significant role in atmospheric radiation and climate change by scattering and absorbing solar radiation and serving as condensation nuclei for cloud droplet formation and ice nucleation (Lohmann & Feichter, 2005; Ramanathan et al., 2001; Seinfeld & Pandis, 2016). The estimated aerosol effective radiative forcing (ERF) excluding black carbon on snow and ice is -0.9 (5 to 95% confidence interval, -1.9 to -0.1) W m^{-2} (IPCC, 2013). The negative ERF indicates an overall cooling effect to the climate system. However, the large uncertainties in aerosol ERF contributes dominantly to the uncertainties in overall net anthropogenic forcing (IPCC, 2013). Besides, aerosol could affect the environment, such as causing the soil and surface water acidification by acid rain (Eney & Petzold, 1987; Glass et al., 1980), nourishing the rainforest by dust deposition (H. Yu et al., 2015) and impairing human health by degrading air quality (Fairlie et al., 2007). A more advanced understanding of the sources, chemical composition, and dynamic processes of aerosol will benefit the quantifying of the effect of aerosol on earth system with a small uncertainty.

Fine aerosol with an aerodynamic diameter smaller than 2.5 μm ($PM_{2.5}$), especially, has adverse effects on human health due to the fact that it is small enough to penetrate into human lungs and consequently cause cardiovascular and respiratory diseases (Beelen et al., 2014; Boldo et al., 2006; Caiazzo et al., 2013; Pope et al., 2009). This thesis will focus primarily on $PM_{2.5}$ and aim to shed more light on $PM_{2.5}$ historical concentrations and sources contributions.

1.1.1 Sources and Chemical Compositions of $PM_{2.5}$

$PM_{2.5}$ consists of several chemical compositions from both natural and anthropogenic sources. Secondary inorganic aerosol (SIA) species, including sulfuric acid, ammonium sulfate and ammonium nitrate, are the dominant components of $PM_{2.5}$ over industrial regions (R.-J. Huang et al., 2014; D. Wang et al., 2014). SIA forms from their precursor gases, including SO_2, NO_x and NH_3, through chemical oxidation (Aksoyoglu et al., 2017; Squizzato et al., 2013). SO_2 and NO_x are mostly from human activities, such as combustion engines, solid-fuel (coal, heavy oil and biomass) combustion for energy generation in households and industry, and other industrial activities (i.e. mining, building, and manufacture) (Qu et al., 2016). They also have natural origins, such as volcanic eruption (Carn et al., 2016; Wallace, 2001) and marine dimethyl sulfide (DMS) conversion (Amouroux et al., 2002) for SO_2 and lightning emitted NO_x (Hudman et al., 2018; Murray et al., 2012). NH_3 is mostly from the agriculture sector (Behera et al., 2013).

Carbonaceous aerosols, including organic carbon (OC) and black carbon (BC), are another important component of $PM_{2.5}$. OC includes both primary and secondary OC. The primary organic carbon (POC) and BC are emitted directly from incomplete combustion of fossil fuels (e.g., coal, heavy oil, and gasoline) and biomass (e.g., wood, grass, and crop residues) (Briggs & Long, 2016; Y. Huang et al., 2015). The sectoral contributions vary over regions, for example the OC and BC emission from residential combustion for home heating and cooking is profound in developing countries or rural regions; while the emission from vehicle engine combustion is significant in developed urban regions (Bond et al., 2004). The secondary OC (SOC), also called secondary organic aerosol (SOA), formed in the atmosphere through chemical oxidation of VOC from both fossil sources and non-fossil sources (e.g. household biomass burning and wildfires) (Carlton et al., 2009; Jacobson et al., 2000; Kroll & Seinfeld, 2008). The

understanding of SOA is still limited due to the complexities of the formation pathways and large numbers of precursor chemical species.

Sea salt and mineral dust aerosol are primary particles emitted from natural sources. Fine mode sea salt aerosol emitted from sea spray is the dominant component of $PM_{2.5}$ over coastal and remote ocean region (Jaeglé et al., 2011) . Soil and fine mode dust particle re-suspension is also a contributing component of $PM_{2.5}$, particularly in desert regions, arid areas or during episodes of long-range transport of dust (Claiborn et al., 2000). Besides the natural emission source of mineral dust, dust aerosol can also be emitted from anthropogenic source, such as the anthropogenic fugitive, combustion and industrial dust in urban area (Philip et al., 2017). Both sea salt and mineral dust emissions are related to meteorological parameters, such as wind speed (Gillette & Passi, 1988; Grythe et al., 2014). The uncertainties of emission estimation for sea salt and dust are quite large due to poor understanding of their emission mechanism.

1.1.2 $PM_{2.5}$ and Human Health

$PM_{2.5}$ has been recognized as the leading environmental risk factor for the global burden of disease (GBD) with an estimated over 4 million attributable deaths globally in 2016 (Gakidou et al., 2017). Numerous epidemiological studies have linked $PM_{2.5}$ to heart disease (Amsalu et al., 2019; Du et al., 2016), lung cancer (Tomczak et al., 2016), and even neurological disorders (Fu et al., 2019). Although air quality has been improved significantly in developed countries in the last decades due to the large anthropogenic emission reduction. Adverse effects were still reported from long-term exposure to $PM_{2.5}$ levels even below the World Health Organization (WHO) guideline of annual average 10 $\mu g\ m^{-3}$ (Crouse et al., 2012; Hales et al., 2012; Schwartz

et al., 2017). The historical $PM_{2.5}$ concentrations study could benefit the investigations of the long-term health effects at low level $PM_{2.5}$ environments (Brauer et al., 2019).

1.2 Monitoring of Atmospheric Aerosols

Observations of aerosol concentrations and optical properties are significantly important to better understand aerosol sources, chemical processes, and spatial and vertical distributions. Besides, these in situ measurements are the best resources to use as truth to evaluate and improve numerical models (see Section 1.3), even though they can have their own biases. This section will present two most common atmospheric aerosol monitoring systems, ground-based (in situ) monitoring and satellite remote sensing.

1.2.1 Ground-based Measurements

Ground-based observations provide comprehensive samplings of aerosol mass, chemical composition and optical properties. The measurements of aerosol mass concentrations are generally performed through an inlet that transports the aerosol particles to a collector or detector (filter). The measured aerosol size can be determined by controlling the inlet airflow. Besides mass concentrations, the aerosol optical properties, such as aerosol optical depth (AOD), are retrieved from ground-based sunphotometers network, such as the global Aerosol Robotic Network (AERONET) (Giles et al., 2019; Holben et al., 1998), which can provide valuable information for model validation and satellite retrieving constraints.

1.2.1.1 Total Aerosol Mass Concentration Measurements

The aerosol total mass concentrations can be determined by weighing the filter that has collected aerosol particles below specific size before and after sampling under controlled temperature and humidity conditions. This method is known as Federal Reference Method (FRM). Another common approach is by measuring the attenuation of β-radiation through a particle-laden filter. Because the attenuation, caused by electron scattering in the filter media, is proportional to the total number of atomic electrons, this can provide information about the total mass density of the sample. This technique is also called beta attenuation monitoring (BAM).

There have been several aerosol monitoring networks across North America since 1980s, mostly measuring the concentrations of PM_{10} and total suspended particles (TSP). Those PM_{10} and TSP measurements in the earlier years could be very useful to help to estimate the historical $PM_{2.5}$ concentrations. The $PM_{2.5}$ monitoring network across U.S. was established in the late 1990s (Solomon et al., 2014). These aerosol monitoring networks are very helpful to investigate the health impact of long-term exposure to air pollution.

1.2.1.2 Aerosol Chemical Composition Mass Concentration Measurements

The mass contributions of aerosol chemical composition can be measured by collecting particles on filters and then analyzing the filter substrate. This analysis can be done by aqueous or organic extraction, in which the chemical species are dissolved. The composition of the liquid sample is then determined by various techniques. For the non-volatile species, such as non-volatile elemental carbon, a thermal method, in which the filter is heated to evaporate volatile organic carbon out of total carbon, is used to determine the mass concentration. The chemical composition data sets are great resources to infer the aerosol source and chemical processes.

1.2.1.3 Aerosol Optical Depth Measurements

Ground-based aerosol remote sensing is based on the extinction of solar radiation by aerosol reflecting and absorbing, which can be described by Beer-Lambert extinction law as,

$$I_\lambda = I_{0\lambda} \exp(-\tau_\lambda/\cos\theta) \qquad \textit{(Equation 1–1)}$$

where I_λ is the solar intensity observed by a ground-based instrument at wavelength λ, $I_{0\lambda}$ is the solar intensity at the top of the atmosphere, τ_λ is the total atmospheric optical depth at wavelength λ, and θ is the solar zenith angle. Aerosol optical depth is then determined by excluding the optical depth contributing from ozone, NO_2 and Rayleigh scattering from the total atmospheric optical depth (Chance & Martin, 2017).

1.2.2 Satellite Remote Sensing

Satellite remote sensing is a monitoring technique that can retrieve aerosol abundance based on the collection of spectroscopic data along a selected atmospheric path by remote sensing instruments on board satellites. The high spatial and temporal resolution of satellite remote sensing data are unprecedented valuable for estimating long-term high resolution surface air pollutants concentration (van Donkelaar et al., 2010), and constraining emission inventories (Goldberg et al., 2017).

AOD is one of the most common aerosol optical properties that can be retrieved from satellite remote sensing, which measure the reflectance of the solar backscatter radiation at different wavelengths. The total measured reflectance R at a specific wavelength are approximately the sum of the reflectance due to molecular scattering R_m, the reflectance due to aerosol scattering R_a and the surface reflectance R_s. This can be described as

$$R(\Theta) = R_m(\Theta) + R_a(\Theta) + R_s(\Theta) \quad \text{(Equation 1–2)}$$

where Θ is the satellite viewing angle. The reflectance due to aerosol scattering R_a is a function of aerosol optical depth τ_a , the aerosol single-scattering albedo ϖ that quantifies the scatter fraction of incident radiation, and the aerosol scattering phase function P describing the angular distribution of radiation scattered by aerosol. Then AOD is approximately proportional to the aerosol reflectance,

$$\tau_a \approx \frac{Ra(\Theta)}{P(\Theta)\varpi} \quad \text{(Equation 1–3)}$$

The above relationship is more accurate when the surface reflectance R_s estimation has higher accuracy (Chance & Martin, 2017). Therefore, evaluations and error quantifications are needed before using specific satellite remote sensing product, such as evaluating models using satellite AOD products over bright surface regions.

1.3 Modeling of Atmospheric Aerosols

Ground-based observations are usually too sparse for a large research domain and also have errors themselves. The satellite retrievals exhibit systematic uncertainties due to their retrieval algorithms. Modeling can cover large research domains at fine resolution and offer additional information with the independent knowledge of mathematical representations of the physical atmosphere. Besides, models could be used to interpret the measurements to understand aerosol sources or processes (Weagle et al., 2018) that observations alone could not be possible.

Models, such as the GEOS-Chem chemical transport models (CTM) used in this thesis, solve differential equations that describe the evolution of atmospheric chemistry on space and time scale. CTMs, in particular, solve continuity equations that express mass conservation within an elemental volume of air. The local mass concentration for a specific chemical component will

be affected by many processes in the atmosphere, such as emission, meteorological transport, chemistry production and loss, and deposition. The sources and processes of atmospheric aerosol can be inferred by conducting sensitivity simulations under specific assumed scenarios, such as the study presented in Chapter 3 of this thesis.

1.4 GOALS OF THIS WORK

Chemical transport modeling, satellite remote sensing and ground-based monitoring can help us to understand many aspects of $PM_{2.5}$, such as its historical concentration, source contribution and its chemical composition distribution. This thesis brings together research that interprets the satellite and ground-based measurements using a chemical transport model to better understand the source and distribution of $PM_{2.5}$ in relatively low level $PM_{2.5}$ environments and its human health impact.

The shape of the concentration-response function at low $PM_{2.5}$ concentrations remains uncertain. Accurate data concerning historical $PM_{2.5}$ concentrations are needed to assess long-term changes in exposure and associated health risks. In Chapter 2, we estimate the historical surface $PM_{2.5}$ concentrations across North America from 1981 to 2016 by combining information from chemical transport modeling, satellite remote sensing and ground-based monitoring. These estimates can be used to investigate the long-term health impacts associated with low levels of $PM_{2.5}$. This work was published in Environmental Science and Technology in 2019.

A better understanding of the sources contributing to $PM_{2.5}$ concentrations could inform future air quality management and help to investigate the association of health outcomes with different emission sectors. In Chapter 3, we study the contributions of different emission sectors to $PM_{2.5}$ across Canada from both Canadian and U.S sources using a chemical transport model

GEOS-Chem. We also investigate the trend of the sectoral contributions of different sectors to $PM_{2.5}$ concentrations across Canada. This work was also published in Environmental Science and Technology in 2019.

Mineral dust, as the most abundant aerosol in the atmosphere in terms of mass, has significant impacts on climate, weather, and air quality (Querol et al., 2019; Kerstin Schepanski, 2018). However, dust emissions are highly uncertain because of the lack of direct dust emission observation and poor understanding of the emission processes. Models are usually used to estimate the dust emissions in a large scale. In the last part of this thesis, an offline dust emission dataset is calculated by running a dust module driven by the native resolution meteorological fields and then use these offline dust emissions in GEOS-Chem simulations. The goal of this work is to assess the availability and strengths of using offline high resolution dust emissions in a chemical transport model.

CHAPTER 2 ESTIMATED LONG-TERM (1981-2016) CONCENTRATIONS OF AMBIENT FINE PARTICULATE MATTER ACROSS NORTH AMERICA FROM CHEMICAL TRANSPORT MODELING, SATELLITE REMOTE SENSING AND GROUND-BASED MEASUREMENTS

Authors: Jun Meng[1], Chi Li[1], Randall V. Martin[1,2], Aaron van Donkelaar[1], Perry Hystad[3], Michael Brauer[4]

[1]Department of Physics and Atmospheric Science, Dalhousie University, Halifax, Nova Scotia, B3H 4R2, Canada

[2]Smithsonian Astrophysical Observatory, Harvard-Smithsonian Center for Astrophysics, Cambridge, MA 02138, USA

[3]College of Public Health and Human Sciences, Oregon State University, Corvallis, OR 97331, USA

[4]School of Population and Public Health, The University of British Columbia, 2206 East Mall, Vancouver, British Columbia, V6T 1Z3, Canada

Adapted with permission from "Meng, J., Li, C., Martin, R.V., van Donkelaar, A., Hystad, P., Brauer, M., Estimated Long-term (1981- 2016) Concentrations of Ambient Fine Particulate Matter across North America from Chemical Transport Modeling, Satellite Remote Sensing and Ground-based Measurements. Environmental Science & Technology, 2019, 53, 9, 5071-5079, doi:10.1021/acs.est.8b06875". Copyright (2019) by American Chemical Society. https://pubs.acs.org/doi/10.1021/acs.est.8b06875.

2.1 Abstract

Accurate data concerning historical $PM_{2.5}$ concentrations are needed to assess long-term changes in exposure and associated health risks. We estimated historical $PM_{2.5}$ concentrations over North America from 1981-2016 for the first time by combining chemical transport modeling, satellite remote sensing and ground-based measurements. We constrained and evaluated our estimates with direct ground-based $PM_{2.5}$ measurements when available and otherwise with historical estimates of $PM_{2.5}$ from PM_{10} measurements or TSP measurements. The estimated $PM_{2.5}$ concentrations were generally consistent with direct ground-based $PM_{2.5}$ measurements over their duration from 1988 onward (R^2 = 0.6-0.85) and to a lesser extent with $PM_{2.5}$ inferred from PM_{10} measurements from 1985 to 1998 (R^2 =0.5-0.6). The collocated comparison of the trends of population-weighted annual average $PM_{2.5}$ from our estimates and ground-based measurements were highly consistent (RMSD = 0.66 μg m^{-3}). The population-weighted annual average $PM_{2.5}$ over North America decreased from 22 ± 6.4 μg m^{-3} in 1981, to 12 ± 3.2 μg m^{-3} in 1998, and to 7.9 ± 2.1 μg m^{-3} in 2016, with an overall trend of -0.33 μg m^{-3} yr^{-1} (95% CI: -0.35 -0.30).

2.2 Introduction

$PM_{2.5}$ is recognized as the leading environmental risk factor for the global burden of disease with an estimated 4.1 million [3.6 million to 4.6 million] attributable deaths in 2016 (Gakidou et al., 2017). Long-term exposure to high $PM_{2.5}$ adversely affects human health (Beelen et al., 2014; Boldo et al., 2006; Caiazzo et al., 2013; Pope et al., 2009; Schwartz, 2000; Weichenthal et al., 2014; Y. Zhang et al., 2018). Several epidemiological studies reported adverse effects from long-term exposure at levels of $PM_{2.5}$ concentrations (Crouse et al., 2012; Hales et al., 2012; Schwartz

et al., 2017; Shi et al., 2016) below the WHO guideline (10 μg m^{-3} annual average), the U.S. standard (12 μg m^{-3} annual average) and the Canadian standard (10 μg m^{-3} annual average, to be reduced to 8.8 μg m^{-3} in 2020). However, the shape of the concentration-response function at these low $PM_{2.5}$ concentrations remains uncertain. Information about historical $PM_{2.5}$ concentrations across Canada and the United States is needed to understand long-term changes in exposure and their implications for health effects research.

Understanding historical long-term exposure is complicated by the paucity of $PM_{2.5}$ monitoring sites across North America before the late 1990s and by the spatial variation of monitoring sites over time. Ground-based monitoring provides historical time series at specific points for $PM_{2.5}$, PM_{10}, and TSP. Several cohort studies have attempted to infer historical PM estimates using monitoring data for urban areas in later years (Beelen et al., 2008; Caiazzo et al., 2013; Lepeule et al., 2012). A recent study by Kim et al. (2017) demonstrated that historical measurements of PM_{10} and TSP offer valuable information for prediction of historical $PM_{2.5}$ concentrations across the continental United States.

Additional sources of data are available to inform estimates of historical $PM_{2.5}$ spatial and temporal variations to improve the overall representativeness. Chemical transport modeling offers additional valuable information about historical $PM_{2.5}$ concentrations through the representation of atmospheric processes with historical emission inventories (Hoesly et al., 2018; C. Li et al., 2017; U.S. EPA, 2018). Satellite remote sensing offers a powerful additional constraint on $PM_{2.5}$ spatial distributions (van Donkelaar et al., 2015; Z. Ma et al., 2016) especially after 2002 when both the Terra and Aqua satellites were in orbit. Some studies (Lall et al., 2004; Parkhurst et al., 1999) have developed prediction models to estimate historical $PM_{2.5}$ by back-casting using the ratio between $PM_{2.5}$ and PM_{10} or TSP observations. Other studies

(Beckerman et al., 2013; Eeftens et al., 2012; L. Li et al., 2017; Z. Ma et al., 2016) use land-use regression, which included predictor variables derived from geographic information systems, or combine information from other particulate matter (PM) measurements or satellite data. However, those studies either focused on smaller regions (L. Li et al., 2017; Parkhurst et al., 1999) or shorter durations (Z. Ma et al., 2016).

In this paper, we present historical estimates of $PM_{2.5}$ across North America by combining information from chemical transport modeling, satellite-derived $PM_{2.5}$ estimates and ground-based monitoring from 1981-2016. These estimates can be used to assess long-term health impacts associated with low levels of $PM_{2.5}$ throughout North America.

2.3 Materials and Methods

Figure 2-1 provides an overview of our method to develop estimates of historical $PM_{2.5}$ concentrations across North America by incorporating information from ground-based monitoring, chemical transport modeling, and satellite-derived $PM_{2.5}$. We started with a fine resolution chemical transport model (GEOS-Chem) simulation with reliable anthropogenic emission inventories across North America for 1989–2016. We downscaled the simulation to 0.01° x 0.01° using a satellite-derived $PM_{2.5}$ dataset (van Donkelaar et al., 2015). We applied geographically weighted regression (GWR) to the downscaled simulation to incorporate information from ground-based measurements into the estimates. For the years 1981-1988, we relied on information on interannual variation from ground-based measurements to backcast the gridded $PM_{2.5}$ concentrations. Each step is described further below.

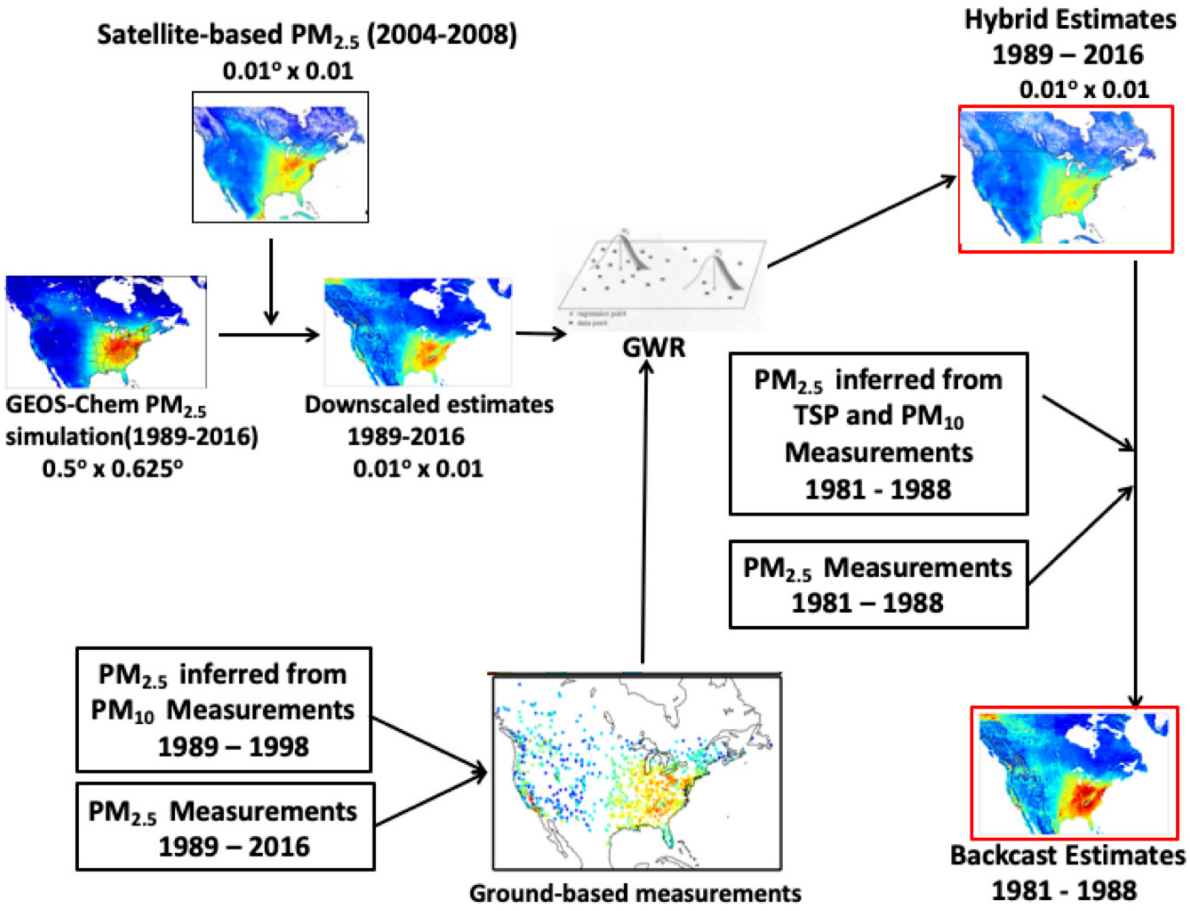

Figure 2-1. Overview of estimation method.

2.3.1 Historical Particulate Matter Monitoring Data

We collected ground-based measurements for 1981-2016 across Canada and the United States. Canadian particulate matter data were obtained from the National Air Pollutant Surveillance (NAPS) (http://maps-cartes.ec.gc.ca/rnspa-naps/data.aspx?lang=en). This database includes continuous PM measurement data, dichotomous sampler (dichot, PM_{10} and $PM_{2.5}$) data and TSP data. Instrument-specific calibrations were applied as recommended by the Canadian Council of Ministers of the Environment (CCME) (Canadian Council of Ministers of the Environment (CCME), 2011). Daily PM data for the United States were obtained from the US

Air Quality System Data Mart for PM_{10} and $PM_{2.5}$ (https://aqsdr1.epa.gov/aqsweb/aqstmp/airdata/download_files.html). In addition, data from the inhalable particle network (IPN) which consisted of $PM_{2.5}$ measurements in the early 1980's were included. Table 2-S1 summarizes available monitoring data by measurement type in selected years (1981-2016). In Canada, dichot $PM_{2.5}$ and PM_{10} sampling began in the mid 1980s, followed by continuous $PM_{2.5}$ monitoring in the late 1990s. In the United States, most PM_{10} sampling began in the late 1980s, followed by widespread $PM_{2.5}$ monitoring in 1999. Limited $PM_{2.5}$ measurements were available prior to 1999. Separate predictive models based on uniform method were created for Canada and US monitoring data since the larger number of monitoring stations in the US would overwhelm the Canadian dataset. Detailed information about the predictive models of inferring monthly $PM_{2.5}$ concentrations from the historical PM_{10} and TSP measurements is provided in section 2.7.

2.3.2 Estimated Historical Gridded $PM_{2.5}$ Data

2.3.2.1 GEOS-Chem Chemical Transport Model

We use the GEOS-Chem chemical transport model (version 11-01, http://www.geos-chem.org), with updated historical emissions inventories and meteorological data to consistently simulate $PM_{2.5}$ concentrations across North America for 1989-2016. GEOS-Chem includes detailed aerosol-oxidant chemistry (Bey et al., 2001; Park et al., 2004). The simulation of concentrations of $PM_{2.5}$ components includes the sulfate-nitrate-ammonium (SNA) aerosol system (Fountoukis & Nenes, 2007; Park et al., 2004), mineral dust (Fairlie et al., 2007), sea salt (Jaeglé et al., 2011), and carbonaceous aerosol (Park et al., 2003) with updates to black carbon (Q. Wang et al., 2014), and SOA (Marais et al., 2016; Pye et al., 2010) including an aqueous-

phase mechanism for SOA from isoprene (Marais et al., 2016). Our simulation used a relative humidity dependent and composition dependent fixed size distribution following Martin et al. (2003) with updates to organics (Drury et al., 2010) and mineral dust (Ridley et al., 2012). We drove the simulation using MERRA-2 meteorological data from NASA's Global Modeling and Assimilation Office (GMAO) with a nested resolution at 0.5˚ × 0.625˚ over North America for 1989-2016 for which updated historical emissions were available. Anthropogenic emissions over North America were from the 2011 National Emissions Inventory (NEI2011, http://ww.epa.gov/air-emissions-inventories) for the US and the Criteria Air Contaminants (CAC, http://www.ec.gc.ca/inrp-npri/) for Canada with historical scale factors applied to each simulating year. OC and BC emissions were calculated by applying sector-specific OC and BC to $PM_{2.5}$ emission ratios (C. Li et al., 2017; Reff et al., 2009; Ridley et al., 2018). Open fire emissions were from GFED4 (Giglio et al., 2013) for years 1997-2016 and from the RETRO fire emission inventory (Schultz et al., 2008) for earlier years.

2.3.2.2 Creation of Historical Gridded $PM_{2.5}$ Dataset

Given our objective of a consistent dataset over the entire 1989-2016 period, and the lack of satellite AOD for the entire period, we used the 5-year average from near the middle of the period (2004-2008) of geophysical satellite-based $PM_{2.5}$ estimates (referred to as PM_{sat}) (van Donkelaar et al., 2015), derived from both the Terra and Aqua satellites, to downscale GEOS-Chem model simulation (1989-2016) to a resolution relevant for exposure at 0.01˚ × 0.01˚ following C. Li et al. (2017). We calculated the ratio between PM_{sat} and the 5-yr average (2004-2008) of GEOS-Chem simulations. Then, we used this ratio to downscale simulations in all the years from 1989 to 2016. The downscaling process does not change the simulated relative

temporal variation of $PM_{2.5,}$ since the same scale factor was applied to all years. This downscaled estimate (referred to as PM_{scl}) contained fine-scale spatial information from satellite-derived $PM_{2.5}$ estimates (PM_{sat}) and long-term temporal information from the GEOS-Chem simulation. We evaluate the approach by excluding the satellite-based estimates.

Ground-based monitoring offers reliable information on $PM_{2.5}$ when and where available. We used this information to constrain our estimates. We included monitor information across both the US and Canada to produce a continuous surface for North America. Following van Donkelaar et al. (2015), we applied GWR to PM_{scl} over 1989-2016 using available $PM_{2.5}$ observations, and $PM_{2.5}$ concentrations inferred from PM_{10} observations. GWR (Brunsdon et al., 1996) is a multiple regression, an extension of least-squares regression, to allow predictor coefficients to vary by choosing different spatial weighting function at several geographic locations according to their inverse-squared distance from individual observation sites. We used GWR to regress the spatial relationship between multiple predictors and the bias between $PM_{2.5}$ estimates and $PM_{2.5}$ measurements. Our predictors in GWR include urban land cover, sub-grid elevation difference, and aerosol chemical composition from GEOS-Chem simulation. We fit the GWR model at the same resolution (0.01^{o} x 0.01^{o}) as the downscaled $PM_{2.5}$ estimates, which was scaled by satellite-driven $PM_{2.5}$, following the Equation 2–1 below:

$$(Measured\ PM_{2.5} - Estimated\ PM_{2.5}) = \alpha_1 ULC + \alpha_2 SED + \alpha_3 SUL + \alpha_4 NIT + \alpha_5 PrC + \alpha_6 SOA + \alpha_7 DST + \varepsilon \qquad Equation\ 2\text{–}1$$

where α_1 to α_7 represented the spatial weighted predictor coefficients for each predictor, and ε is the error. ULC was the percent of urban land cover from the 500-m spatial resolution MODIS land cover type product (Friedl et al., 2010). SED was the sub-grid elevation difference, which is the difference between the site elevation, which is from the ETOPO1 Global Relief Model of the

National Geophysical Data Center (Information (NCEI)), and the annual mean elevation of the GEOS-Chem grid cell. SUL, NIT, PrC, SOA and DST are sulfate, nitrate, primary carbon, secondary carbon and dust respectively as simulated with GEOS-Chem. We conducted sensitivity tests by changing the weight of PM_{10} observations in the GWR regression and found that a reduction by 75% of the weight of PM_{10} best represented its uncertainty compared to direct $PM_{2.5}$ measurements from ground-based measurements, GEOS-Chem transport model simulations and satellite remote sensing.

For years 1981-1988, reliable emission inventories were not available for GEOS-Chem simulation. Instead we used the information on inter-annual variation from ground-based measurements to back-cast the gridded $PM_{2.5}$ concentrations following previous studies (Lall et al., 2004; Parkhurst et al., 1999). Ground-based measurements include TSP measurements, PM_{10} measurements and $PM_{2.5}$ measurements. Ground-based $PM_{2.5}$ concentrations inferred from TSP measurements were included for this time period since fewer than 200 PM_{10} sites existed before 1986 and even fewer $PM_{2.5}$ monitoring sites existed. For each year (e.g. 1988), we calculated the ratio between the annual mean $PM_{2.5}$ of this year and the following 3-year mean $PM_{2.5}$ (e.g. 1989-1991) for each ground-based monitoring site. We used the ratios from TSP sites as the basis, which were overwritten by the ratios from PM_{10} sites, and then by the ratios from $PM_{2.5}$ sites. This ratio field from ground-based measurements was then interpolated to other grids using distance weighted interpolation. Finally, we applied this gridded ratio field to the following 3-year mean $PM_{2.5}$ estimates to get the estimated $PM_{2.5}$ for each year. The process is described by Equation 2–2 below:

$$Y(t) = \gamma\,[Y(t+1) + Y(t+2) + Y(t+3)]/3 \qquad \textit{Equation 2–2}$$

where Y(t) represents the $PM_{2.5}$ estimates in year t, and γ is the gridded ratio field.

We evaluated the backcasting method by repeating the procedure for the years 2001-2008 using measurements for the years 2001-2011, for comparison with our estimates for 2001-2008 (Table 2-S5).

We calculated the overall root mean square difference (RMSD) between the estimates and measurements for each year over 1981-2016 as a measure of uncertainty.

2.4 Results and Discussion

We first evaluated the approach in the years when only PM2.5 stations were used for GWR adjustment to statistically incorporate information from ground-based observations into the downscaled model results. Figure 2-2 shows scatter plots of 2004-2008 mean PM2.5 from the downscaled simulation (PMscl) before and after GWR adjustment, versus in situ PM2.5. As found by van Donkelaar et al. (2015), the GWR model significantly reduces the mean bias (MB) and RMSD over both Canada and the US. Out-of-sample cross validation using 50% of randomly selected sites to train the GWR model exhibits significantly improved performance (R2 = 0.69; RMSD = 2.3 μg m-3) (bottom left panel) compared with the base case (R2 = 0.52; RMSD = 3.1 μg m-3). In such a holdback analysis, GWR parameter coefficients are trained using only 50% of available ground-based monitors. The withheld sites provide an independent dataset with which to evaluate the quality of fused PM2.5 estimates in areas without ground-based observation. The improvement at these independent sites suggests improvement in the GWR adjusted surface even at locations away from ground-based observation. The bottom right panel of Figure 2-2 shows the 2004-2008 mean performance of GWR-adjusted values made using only the PM2.5 sites that were also available before 1998 (< 70 sites in total), consisting mostly of remote and rural U.S.-based sites. Limiting the GWR-based adjustment to only these

earlier-available PM2.5 sites provided no improvement in agreement compared to the initial estimates without GWR. The negative MB in PM_{scl} (-1.00 μg m^{-3}) (top left panel) is not corrected in the adjusted estimates (-0.83 μg m^{-3}) (bottom right panel), due to a lack of representative urban and eastern sites which generally have higher $PM_{2.5}$ levels. Complementary information from PM_{10} sites that are representative of urban environments is necessary for early years.

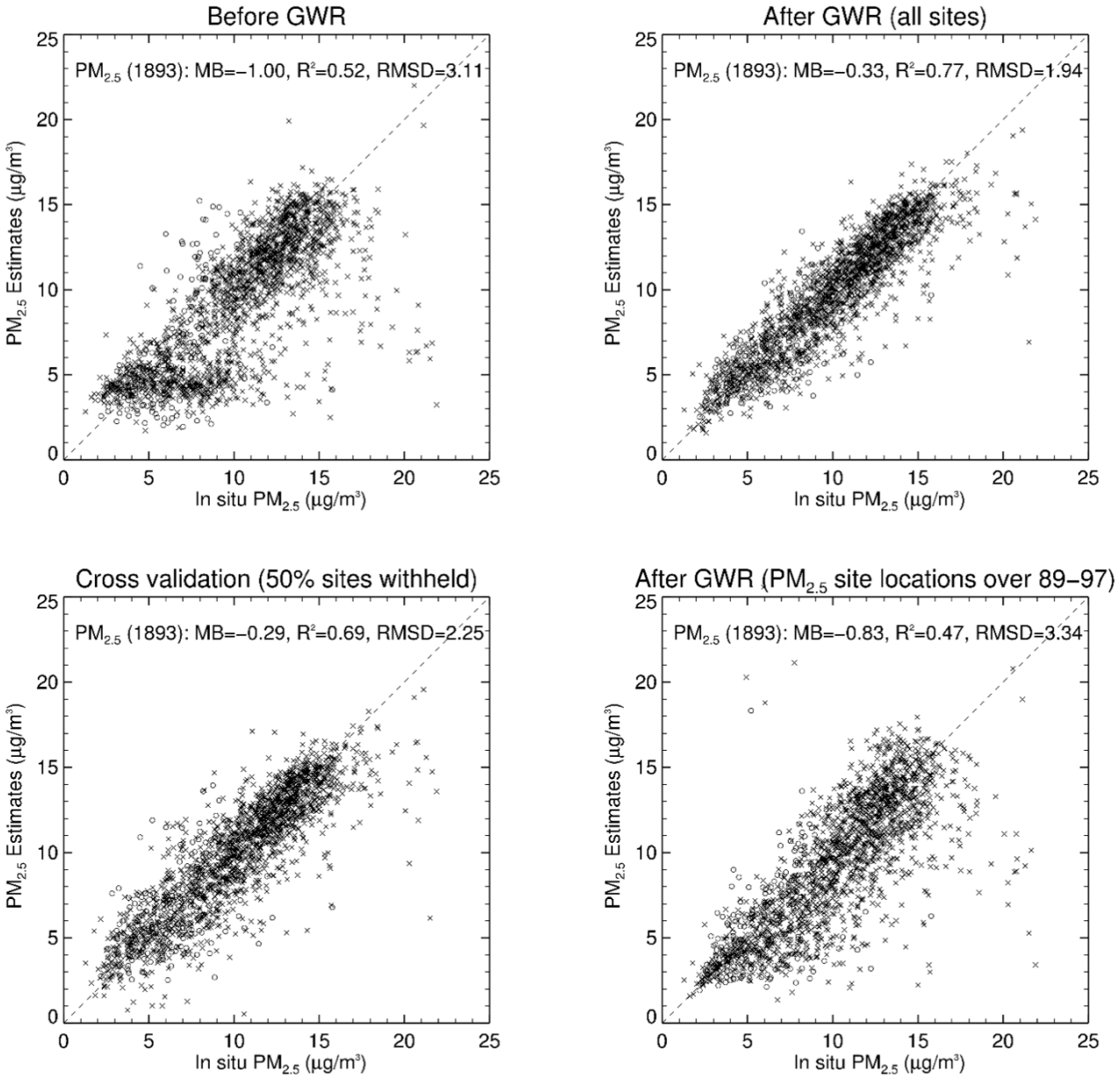

Figure 2-2. Comparison over 2004-2008 of mean $PM_{2.5}$ estimates with in situ measurements before (top left) and after GWR adjustment using all sites (top right), using cross validation sites using 50% random holdout (bottom left), and using $PM_{2.5}$ sites present over 1989-1997 (bottom right). Open circles are Canadian sites and crosses are US sites. Number of sites are shown in brackets. Statistics shown are mean bias (MB, in μg m^{-3}), coefficient of determination (R^2) and root mean square difference (RMSD, in μg m^{-3}).

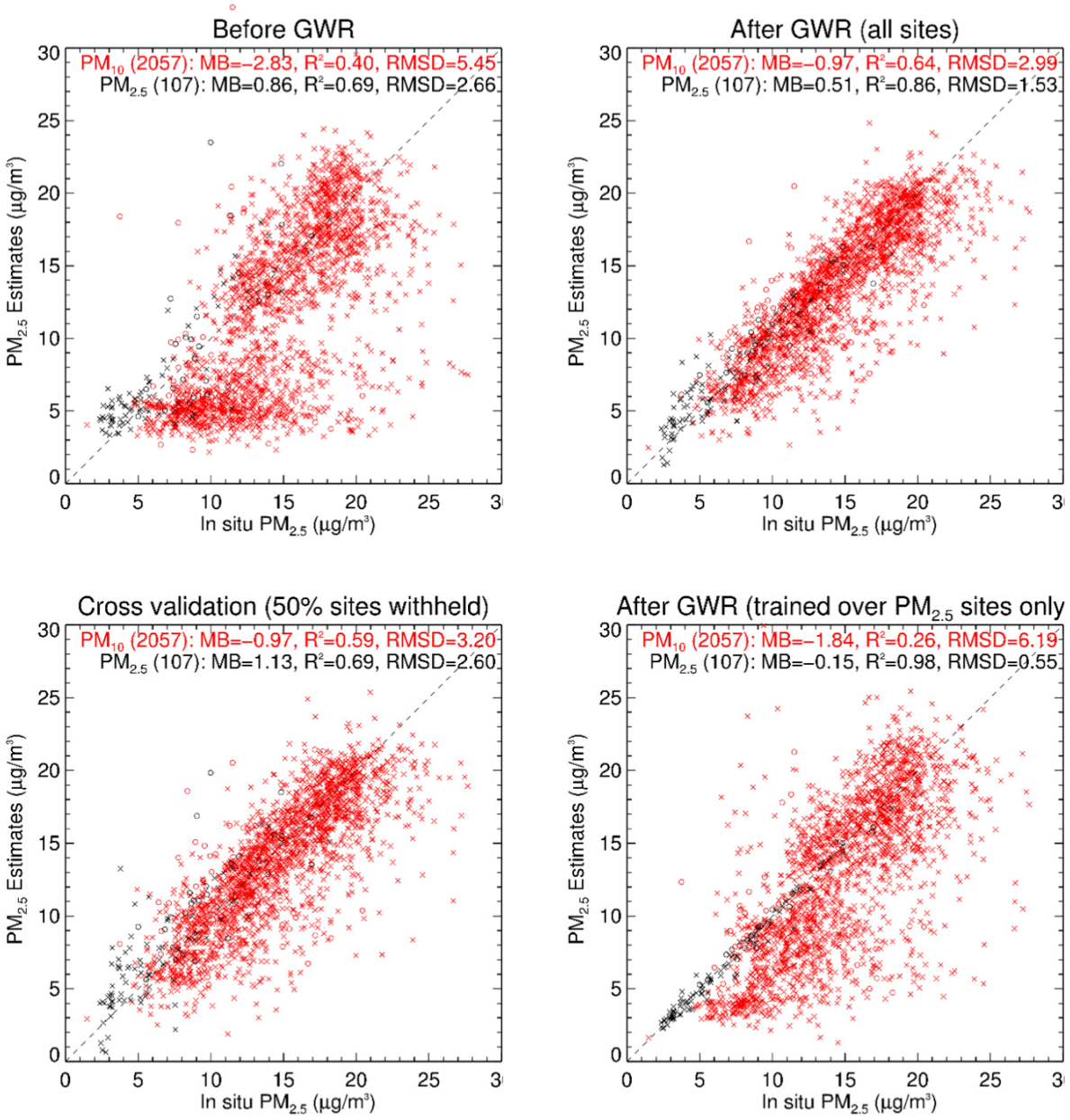

Figure 2-3. Comparison over 1992-1996 of mean $PM_{2.5}$ estimates with in situ measurements before (top left) and after GWR adjustment using all sites (top right), using

cross validation using 50% random holdout (bottom left), and using only $PM_{2.5}$ sites (bottom right). Open circles are Canadian sites and crosses are US sites. No. of sites are shown in brackets. Comparison for $PM_{2.5}$ (black) and PM_{10} (red) sites are shown separately. Statistics shown are mean bias (MB, in μg m^{-3}), coefficient of determination (R^2) and root mean square difference (RMSD, in μg m^{-3}).

Figure 2-3 shows scatter plots for the 1992-1996 time period to evaluate the performance of $PM_{2.5}$ inferred from PM_{10}. The top panels show that the performance of the scaled geophysical estimate is promising with an R^2 versus $PM_{2.5}$ monitors of 0.69 that increases to 0.86 after GWR adjustment. The RMSD decreases from 2.7 to 1.5 μg m^{-3} over ~100 $PM_{2.5}$ sites in the adjusted estimates. For ~2000 PM_{10} sites, significantly improved agreement is also found after GWR adjustment. Cross validation with 50% out-of-sample sites (bottom left) further confirms the overall robustness of the approach. As found in the 2004-2008 period, using only $PM_{2.5}$ sites for GWR modeling does not improve the overall representation of the estimates, especially for PM_{10} sites in urban areas.

Figure 2-4 shows the R^2 and RMSD for each year (1981-2016) of the estimates versus ground-based measurements to provide an overall assessment of uncertainty. Only $PM_{2.5}$ data are used over 1999-2016 since sufficient $PM_{2.5}$ measurements are available after 1999. Since the number of PM_{10} sites reduces significantly prior to 1989 (~1000 in 1989, ~600 in 1988, ~400 sites in 1986 and < 50 sites in 1984), the back-casting from 1985 to 1981 is based primarily on the trend information from TSP-based estimates, and expected to be more uncertain. The R^2 increases with the increase of PM_{10} sites for years 1985-1990. The R^2 is around 0.8 for years 1989-2005 compared to $PM_{2.5}$ sites. The relative RMSD at only $PM_{2.5}$ sites drops from 30% in the early 1990s to below 20% prior to 1999 when the $PM_{2.5}$ measurements became more widespread. The decrease in R^2 after 2008 reflects weaker spatial $PM_{2.5}$ gradients in recent years

as $PM_{2.5}$ levels decline across North America. Higher RMSD errors are expected before 1999 due to more uncertainties in emission inventories as well as larger uncertainties in the monitor data used in GWR adjustments. Overall, the GWR-adjusted $PM_{2.5}$ estimates yield an estimated error of less than 20% since 1999 and, less than 30% from 1981-1998.

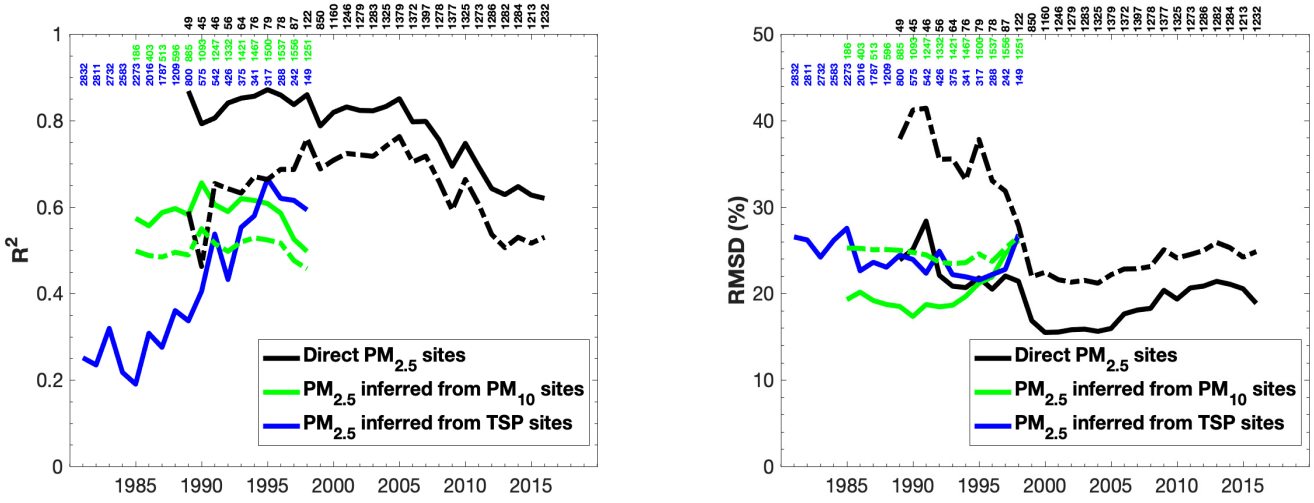

Figure 2-4. Statistics (R^2 and RMSD) of estimated $PM_{2.5}$ against ground-based measurements from year 1981 to 2016. Solid lines indicate performance of base estimates. Dashed lines indicate performance of sensitivity estimates that exclude satellite remote sensing information (no blue dashed line). Numbers at the top of each figure indicate the number of monitors of direct $PM_{2.5}$ (black), $PM_{2.5}$ inferred from PM_{10} (green) and $PM_{2.5}$ inferred from TSP (blue).

Figure 2-5 shows the distribution of $PM_{2.5}$ estimates and ground-based measurements for 1985, 1995, 2005 and 2015 from this study. Enhancements in both the GWR adjusted estimates and ground-based measurements are apparent across eastern US and California. The estimated $PM_{2.5}$ is generally consistent with ground-based measurements (Figure 2-4), especially with the direct $PM_{2.5}$ measurements. $PM_{2.5}$ concentrations decrease dramatically during the last three decades, especially in eastern United States.

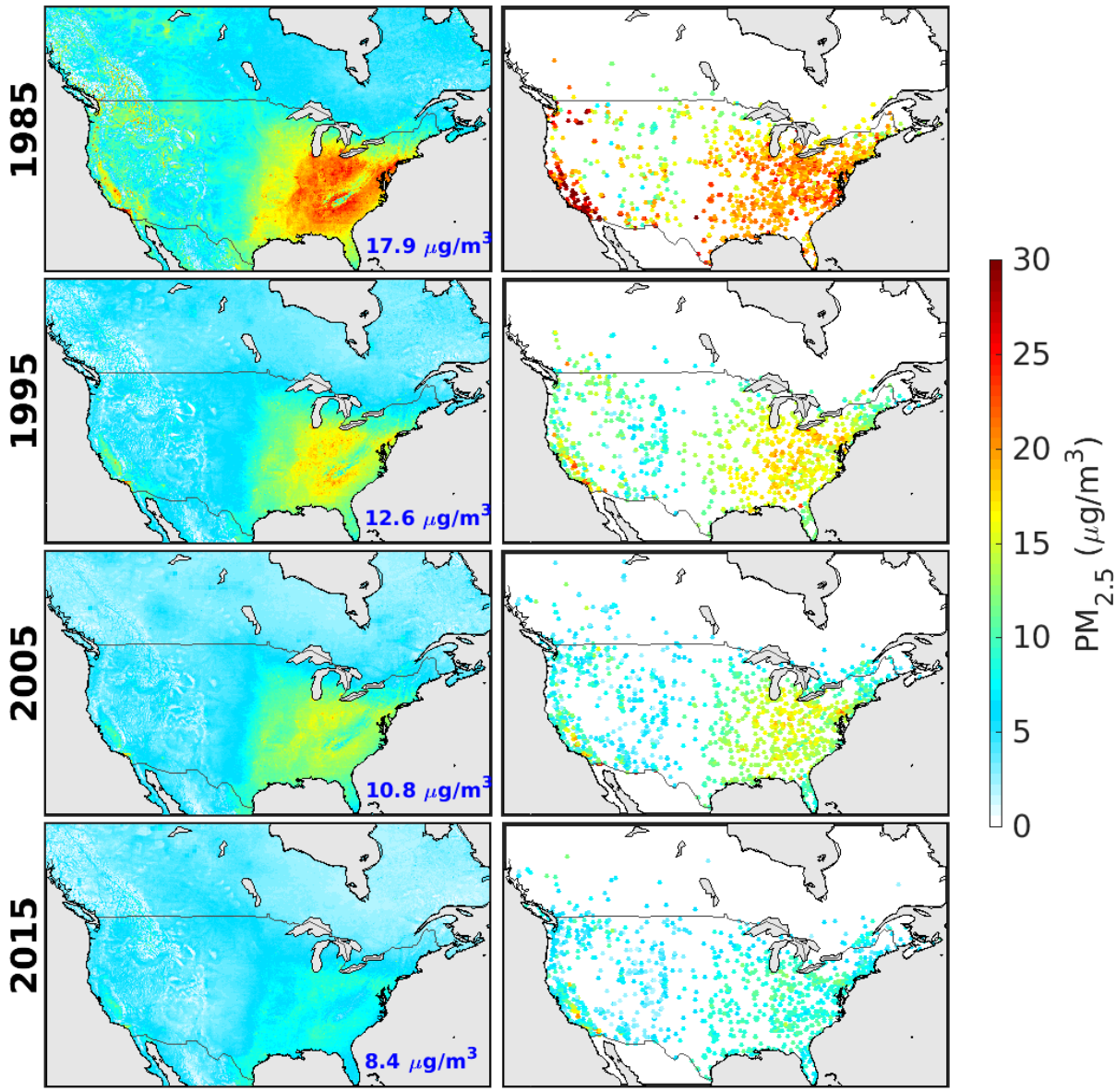

Figure 2-5. Estimated fine particulate matter annual means in 1985, 1995, 2005 and 2015 over North America. Left panels are estimated $PM_{2.5}$. Inset values in the left panel are the population-weighted average $PM_{2.5}$ mass. Right panels indicate $PM_{2.5}$ derived from ground-based measurements of $PM_{2.5}$, PM_{10} and TSP.

Figure 2-6 shows the time series of population-weighted annual average $PM_{2.5}$ concentrations across North America. We used gridded population estimates from the Socioeconomic Data and Applications Center ("Global Population Count Grid Time Series

Estimates, v1: Population Dynamics | SEDAC," n.d.; "Gridded Population of the World (GPW), v4, SEDAC," 2018) for calculating population-weighted average (section 2.7.3). The population-weighted annual average $PM_{2.5}$ over North America decreased from 22 ± 6.4 μg m^{-3} in the year 1981 to 7.9 ± 2.1 μg m^{-3} in the year 2016. The linear tendency over this period is -0.33 μg m^{-3} yr^{-1} ± 0.2 μg m^{-3} yr^{-1}. Both time series of the in-situ measurements and estimates of population-weighted annual mean $PM_{2.5}$ exhibit minor peaks in 2005 and 2007. The collocated comparison of the trends of population-weighted annual average $PM_{2.5}$ from our estimates and ground-based measurements are highly consistent (RMSD=0.66 μg m^{-3}) over 1985-1995. Population-weighted annual average $PM_{2.5}$ calculated from direct $PM_{2.5}$ sites is 20% lower than that calculated from all in-situ sites, illustrating the effects of changes in monitor placement over time when assessing long-term changes in ambient $PM_{2.5}$, and the value of spatiotemporally continuous $PM_{2.5}$ estimates from this work. Larger error bars prior to 1990 reflect greater uncertainty in the TSP dataset.

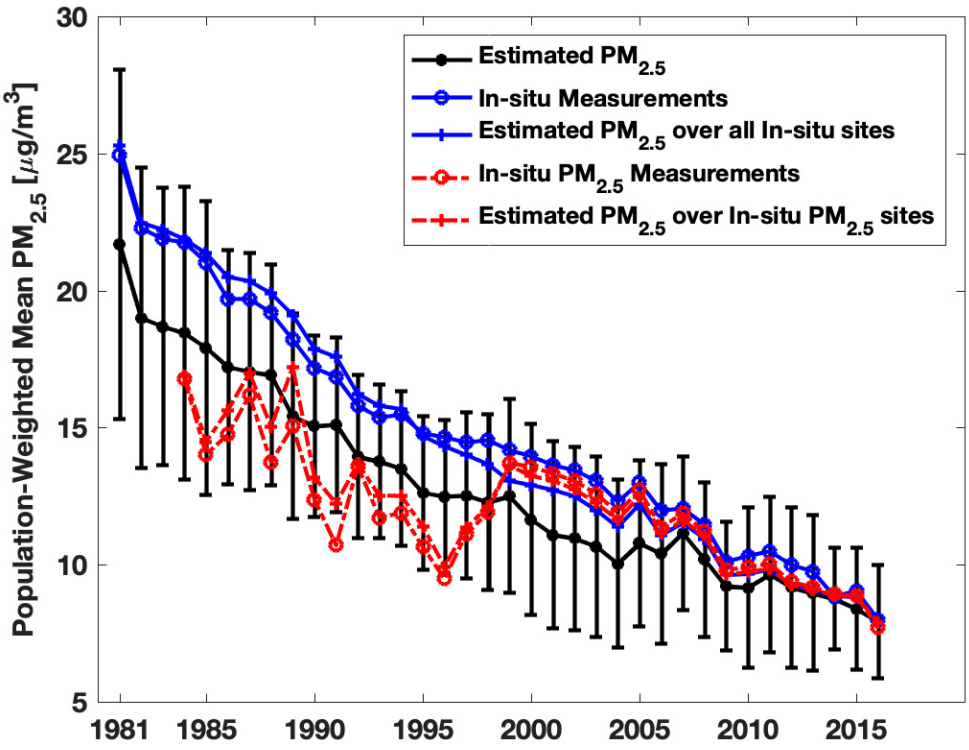

Figure 2-6. Time series of population-weighted average annual $PM_{2.5}$ concentrations across North America. Error bars are included for population-weighted annual mean estimated $PM_{2.5}$ concentrations.

Figure 2-S5 shows regional time series of population-weighted annual average $PM_{2.5}$. Figure 2-S6 shows regional time series of relative percentage change of population-weighted annual average $PM_{2.5}$ concentrations using 2016 as the reference year. Northwestern North America has the most dramatical decline for population-weighted average $PM_{2.5}$ concentrations with a factor of 2.7 decrease over 1981-2016, followed by southeastern and northeastern North America with a factor of 2.4 decrease over 1981-2016. The relative changes in northcentral, southcentral and southwestern North America are similar with a factor of 1.6–2.0 decrease in population-weighted $PM_{2.5}$ over 1981-2016. Overall the spatially resolved historical $PM_{2.5}$ data

set across North America reveals a factor of 1.7 decrease in population-weighted $PM_{2.5}$ over 1981-2016.

Comparison with previous estimates of historical $PM_{2.5}$ concentrations is instructive. Our estimated historical $PM_{2.5}$ concentrations during 1982-1991 in the southeastern US indicate a decrease of 3.9 $\mu g\ m^{-3}$, similar to the reported decline of 3-5 $\mu g\ m^{-3}$ found by Parkhurst et al. (1999). We find similar large-scale reductions in historical $PM_{2.5}$ concentrations during 1981-2000 as Lall et al. (2004), albeit with smoother temporal trends in the present study that are more consistent with Kim et al. (2017). The primary difference with our prior historical $PM_{2.5}$ estimates (Boys et al., 2014; van Donkelaar et al., 2015, 2019) is that our current study spans a time period (1981-2016) about twice as long as our prior work by including more trend information from our GEOS-Chem simulation, and includes historical ground-based measurements prior to 1999. Nonetheless the population-weighted trends from our current dataset remain within 0.03 $\mu g\ m^{-3}\ yr^{-1}$ of our prior work, indicating overall consistency as further discussed in section 2.7.4.

2.5 Data Availability

The annual mean estimated $PM_{2.5}$ for 1981-2016 across North America dataset has been deposited in the Zenodo Digital Repository (DOI: 10.5281/zenodo.2616769) (Meng et al., 2019b).

2.6 Acknowledgements

This research was supported by research agreement 4952-RFA14-3/16-3 with the Health Effects Institute (HEI), an organization jointly funded by the United States Environmental

Protection Agency (EPA) (Assistance Award No. R-82811201) and certain motor vehicle and engine manufacturers. The contents of this article do not necessarily reflect the views of HEI, or its sponsors, nor do they necessarily reflect the views and policies of the EPA or motor vehicle and engine manufacturers. We are grateful to the Atlantic Computational Excellence Network and Compute Canada for computing resources.

2.7 SUPPLEMENTAL INFORMATION

2.7.1 Description of Prediction of Historical $PM_{2.5}$ from Measured PM_{10} and TSP

We collect ground-based measurements over Canada and the United States. All Canadian PM data were downloaded from the NAPS website (http://maps-cartes.ec.gc.ca/rnspa-naps/data.aspx?lang=en). Data included all continuous PM measurement data, dichotomous sampler data and TSP data. Continuous $PM_{2.5}$ was measured using a range of monitoring methods and there are known biases with certain methods, which were corrected using the equations in Table 2-S2 (provided by NAPS). Once data were corrected the average of all continuous $PM_{2.5}$ data measured at a single site (if present) was calculated to represent the monitor average. PM data for the United States were downloaded from the US Air Quality System Data Mart using the pre-generated daily data files for PM_{10} and $PM_{2.5}$ (https://aqsdr1.epa.gov/aqsweb/aqstmp/airdata/download_files.html). For TSP, only annual files were available. In addition, data from the IPN (Hinton et al., 2002) was included, which consisted of $PM_{2.5}$ measurements in the early 1980's.

Historical estimates of monitoring $PM_{2.5}$ concentrations from the PM_{10} and TSP measurements were created using models developed from co-located $PM_{2.5}$, PM_{10} and TSP

measurements. Models were developed for pre-2000 concentrations when $PM_{2.5}$ measurement data were sparse. The unit of analysis was monthly concentrations for $PM_{2.5}$ and PM_{10} models and yearly concentrations for TSP models. Separate models were created using Canada and US data to maximize use of the Canadian specific data, which would be swamped by the larger numbers of US monitoring data if pooled together. Each model included monthly PM_{10} or yearly TSP measurements, year, month, region (Province or State), interactions terms for PM_{10} or TSP and month and region and a random intercept for monitoring station. A random effects model is used to account for station-specific effects when multiple monitors exist at a single station. Monthly PM_{10} models in Canada and the US were able to predict a large portion of measured $PM_{2.5}$. In Canada, 323 stations operating prior to the year 2000 were used to build the model, representing 2,706 monitor months. The fixed effects model alone predicted 75% of the measured $PM_{2.5}$ and when monitor random effects were included the model explained 95% of measured $PM_{2.5}$ (Figure 2-S1).

Table 2-S3 summarizes the model fixed effects contributions to the model. This increase in model performance is expected as most PM stations in Canada measure both PM_{10} and $PM_{2.5}$ using dichotomous samplers. In the United States, 3,403 stations were used to build the model, representing 10,802 monitor months. The fixed effects model predicted 62% of measured $PM_{2.5}$ variations and the random effects model explained 70%. (Figure 2-S1). Table 2-S4 summarizes the model fixed effects.

During the 1980's there were limited PM_{10} measurements. We therefore included TSP to further predict annual $PM_{2.5}$ concentrations. Annual models were created to predict $PM_{2.5}$ due to the annual TSP data availability in the United States. In Canada, the fixed effects model predicted 82% of the measured $PM_{2.5}$ annually and the RMSE improved when monitor random

effects were included the model (Figure 2-S2). In the United States, the fixed effects model predicted 76% of measured $PM_{2.5}$ variations and the random effects model explained 91% (Figure 2-S3).

The value of the random effects model reflects how many air monitor stations are used in the model building process (i.e. monitors that have both PM_{10} and $PM_{2.5}$ monitoring data at some point) and thus have best linear unbiased prediction (BLUP) of the random effects in the model prediction. In Figure 2-S1 (Canada), most monitors had some overlap between measured $PM_{2.5}$ and PM_{10}. While in the US, there were more monitors that had only PM_{10} measurements, which result in the random effects model not having as large of an influence on improving R^2. For the TSP and $PM_{2.5}$ models the opposite is true, where in Canada there are very few monitors (in total) and even less that had both TSP and $PM_{2.5}$ measures. In the US there were more co-located TSP and $PM_{2.5}$ monitors which leads to a better prediction with the random effects included.

2.7.2 Description of Estimated $PM_{2.5}$ Data without Satellite Remote Sensing Information

In order to test the effect of the satellite remote sensing information on our dataset, we generated a sensitivity dataset which does not contain satellite remote sensing information. Instead of downscaling the GEOS-Chem simulation with satellite-derived $PM_{2.5}$, we applied GWR directly to the GEOS-Chem simulation (1989-2016) following van Donkelaar et al. (2015) using available $PM_{2.5}$ observations, and $PM_{2.5}$ concentrations inferred from PM_{10} observation. For years 1981-1988, we used the information on inter-annual variation from ground-based measurements to back-cast the gridded $PM_{2.5}$ concentrations as described in section 2.3.

2.7.3 Description of Population Data

We downloaded population data from the National Aeronautics and Space Administration Socioeconomic Data and Application Center (SEDAC) for the years 1980, 1990, 2000, 2005, 2010 and 2015. Then we used linear interpolation and extrapolation to generate the population data in each year over 1980 to 2016.

2.7.4 Population-weighted $PM_{2.5}$ Trend Discussion

Figure 2-S7 shows the time series of population-weighted average $PM_{2.5}$ of this study and our most recent satellite-derived $PM_{2.5}$ (van Donkelaar et al., 2019). Our estimates are consistent with our most recent work with a RMSD of 0.4 $\mu g/m^3$ during 2000-2016. The trend over 2000-2016 of our estimate is -0.30 $\mu g/m^3$/yr (CI 95%: -0.33, -0.27), which is within the uncertainty of -0.27 $\mu g/m^3$/yr (CI 95%: -0.30, -0.25) reported in van Donkelaar et al. (2019). Our earlier work exhibits similar trends for North America (van Donkelaar et al., 2015) (-0.30 $\mu g/m^3$/yr (CI 95%: -0.34, -0.26)) using 1998-2012. Overall, the trend of $PM_{2.5}$ estimates in this study is consistent with our prior datasets during the same years.

2.7.5 AOD Representativeness

For insight into the representativeness of the 2004-2008 time period, Figure 2-S8 shows the spatial distribution of AOD for the time periods 2001-2005, 2004-2008 and 2012-2016 from the MODIS MAIAC product at 1km resolution (Lyapustin, Martonchik, et al., 2011; Lyapustin, Wang, et al., 2011). The spatial structure of the 2004-2008 dataset exhibits a high degree of consistency with the two time periods with an R^2 of 0.93 versus the 2001-2005 time period, and of 0.81 versus the 2012-2016 time period. Additional insight is offered by the spatial distribution

of a recent satellite derived $PM_{2.5}$ dataset (van Donkelaar et al., 2019) as shown in Figure 2-S9. The spatial structure of the 2004-2008 dataset is highly consistent with that for the 2001-2005 time period ($R^2 = 0.97$) and the 2012-2016 time period ($R^2 = 0.77$). The change in $PM_{2.5}$ across these time periods exhibits a large scale reduction over the eastern United States, driven by emission controls, and a large scale increase over northern Canada, driven by fire activity. These regional changes motivate our use of the GEOS-Chem model to represent the long-term evolution of the spatial distribution of $PM_{2.5}$.

Table 2–S1. Summary of available monitoring PM data for selected years during 1981 - 2016.

Country/Region	**Type**	**1981**	**1985**	**1990**	**1995**	**2000**	**2005**	**2010**	**2015**
Canada	TSP	117	90	78	50				
	PM_{10}		3	20	62	46	24	22	0
	$PM_{2.5}$ (dichot)		11	10	18	19	27	28	22
	$PM_{2.5}$ (continuous)				1	50	158	90	94
United States	TSP	325	2403	587	302	97	55	51	0
	PM_{10}		373	1363	1664	761	595	451	349
	$PM_{2.5}$			44	68	1212	1355	1329	1330

Table 2–S2. Transformation functions for Canadian monitoring methods by region.

Name	Season	Region	Slope	Intercept
TEOM_30	Cold	East	1.44	0.47
TEOM_30	Warm	East	0.98	1.24
TEOM_30	Cold	West	1.36	1.27
TEOM_30	Warm	West	1.01	1.42
TEOM_40	Cold	West	1.30	0.94
TEOM_40	Warm	West	0.94	1.72
BAM	Cold	East	0.88	0.00
BAM	Warm	East	0.88	0.15
FDMS	Cold	East	0.87	-0.48
FDMS	Warm	East	0.92	-0.09

*East= Provinces Ontario and East ; West= Provinces West of Ontario
** Cold=November-March; Warm=April-October

Table 2–S3. Predicting $PM_{2.5}$ from PM_{10} in Canada, summary of model predictors fixed effect contributions

Type III Tests of Fixed Effects

Effect	Num DF[1]	Den DF[2]	F-Value[3]	Pr > F[4]
PM_{10}	1	202	1188.75	<.0001
Years prior to 2000	1	202	58.76	<.0001
PM_{10}_avg*Years prior to 2000	1	202	18.36	<.0001
Month	11	202	1.86	0.0458
PM_{10}*Month	11	202	10.39	<.0001
Region	4	202	11.12	<.0001
PM_{10}*Region	4	202	90.97	<.0001
Years prior to 2000*Region	4	202	3.00	0.0195

[1]Numerator degrees of freedom
[2]Denominator degrees of freedom
[3]Observed value of the F statistic test
[4]Probability of the F statistic test

Table 2–S4. Predicting $PM_{2.5}$ from PM_{10} in the United States, summary of model predictors fixed effect contributions

Type III Tests of Fixed Effects				
Effect	**Num DF[1]**	**Den DF[2]**	**F-Value[3]**	**Pr > F[4]**
PM_{10}	1	10160	1290.16	<.0001
Years prior to 2000	1	10160	23.05	<.0001
State	50	10160	7.85	<.0001
PM_{10}*State	50	10160	17.19	<.0001
Month	11	10160	13.35	<.0001
PM_{10}*Month	11	10160	60.51	<.0001

[1]Numerator degrees of freedom
[2]Denominator degrees of freedom
[3]Observed value of the F statistic test
[4]Probability of the F statistic test

Table 2–S5. Statistics of back-casted $PM_{2.5}$ against estimated $PM_{2.5}$ in years 2001-2008

	2001	2002	2003	2004	2005	2006	2007	2008
R^2	0.94	0.92	0.93	0.81	0.87	0.82	0.86	0.85
RMSE($\mu g/m^3$)	0.82	0.84	0.83	1.3	1.2	1.4	1.3	1.1

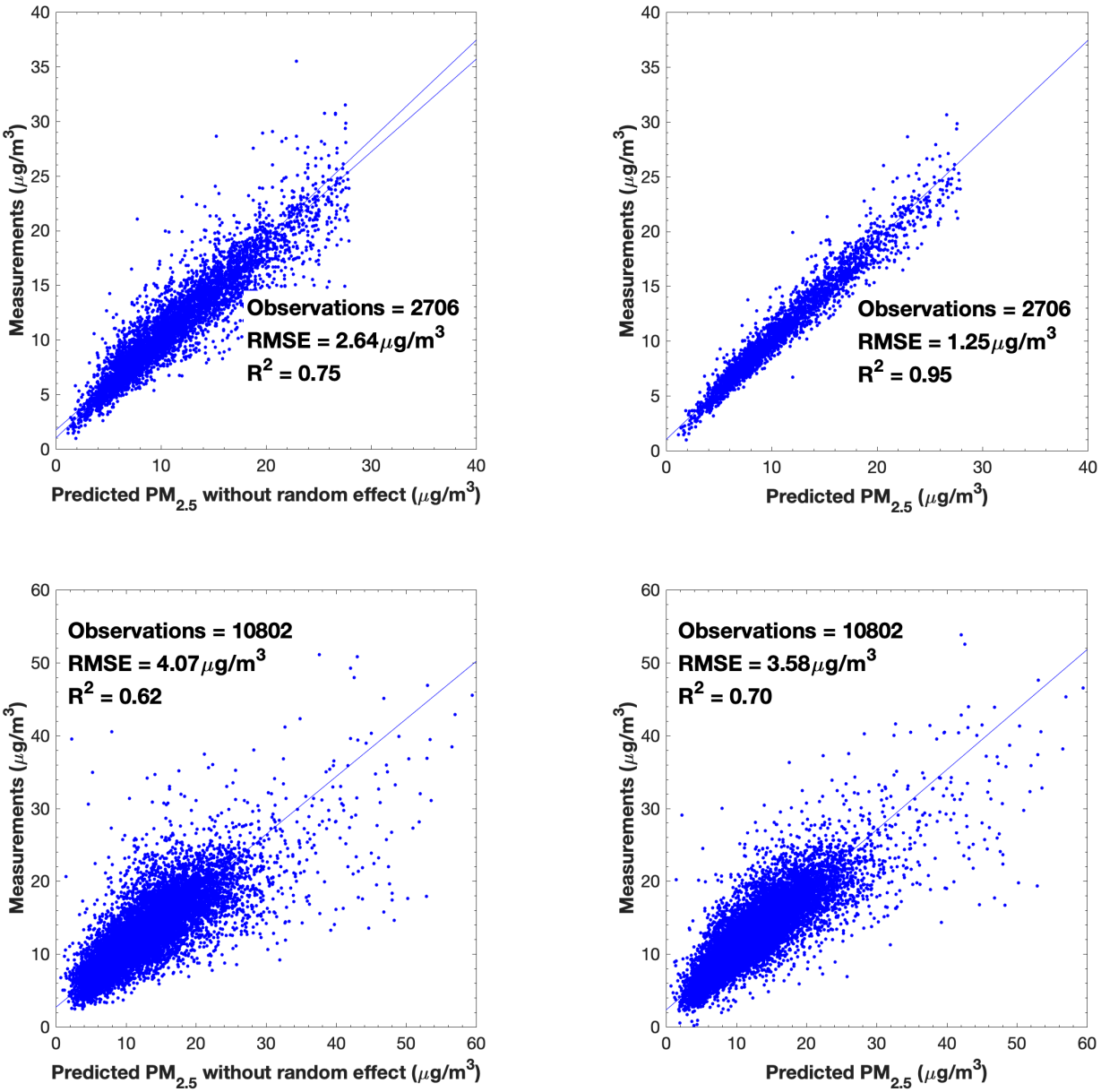

Figure 2-S1. Predictive models of monthly $PM_{2.5}$ from co-located PM_{10} measurements in Canada (top panels) and the United States (bottom panels). The left panels are models without random effects and the right panels are models with random effects.

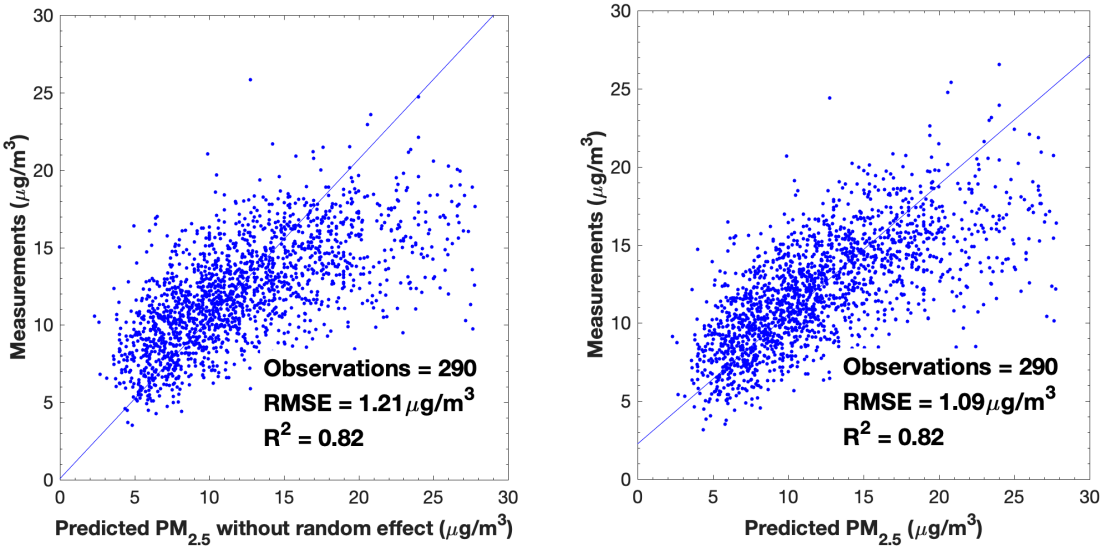

Figure 2-S2. Predictive models of annually $PM_{2.5}$ from co-located TSP measurements in Canada. The left panels are models without random effects and the right panels are models with random effects.

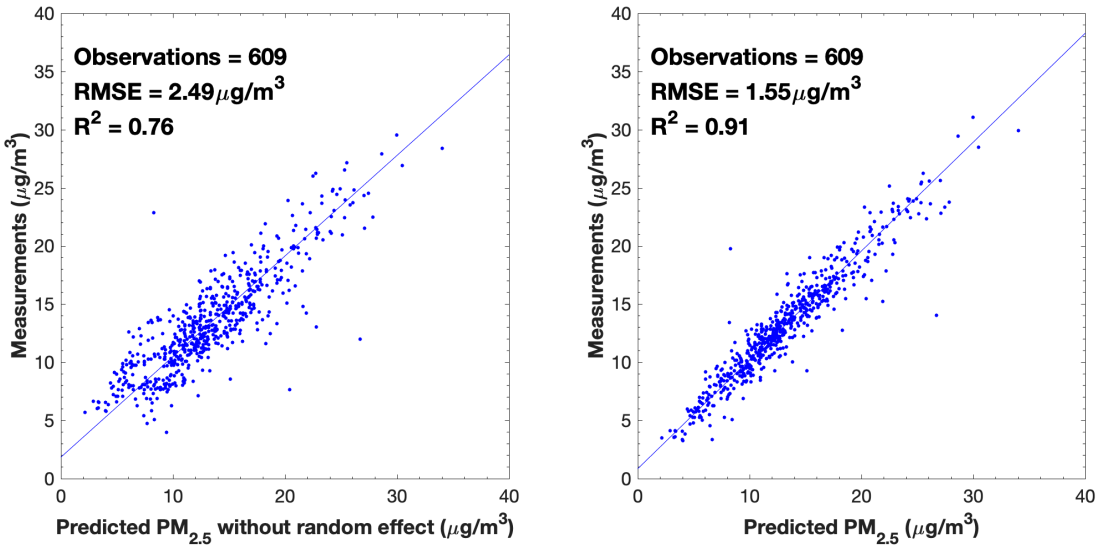

Figure 2-S3. Predictive models of annual $PM_{2.5}$ from co-located TSP measurements in the United States. The left panels are models without random effects and the right panels are models with random effects.

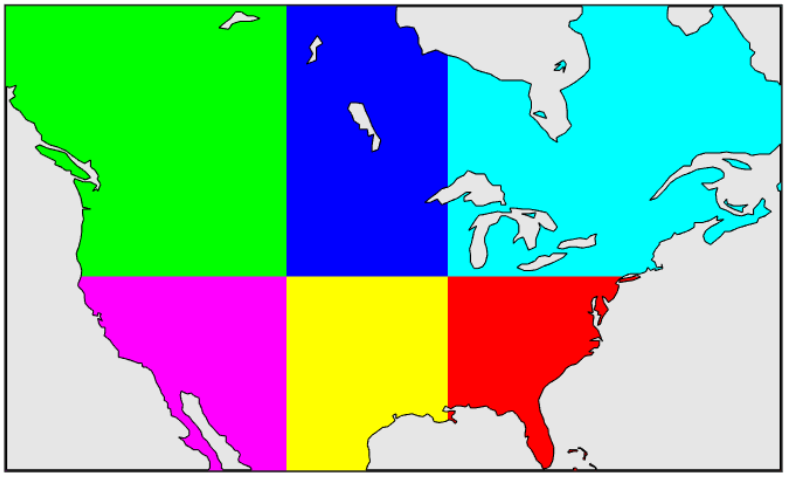

Figure 2-S4. Domain of six regions in North America (NA), including northeastern North America (NE-NA) (Cyan), southeastern North America (SE-NA) (Red), northcentral North America (NC-NA) (Blue), southcentral North America (SC-NA) (Yellow), northwestern North America (NW-NA) (Green) and southwestern North America (SW-NA) (Magenta).

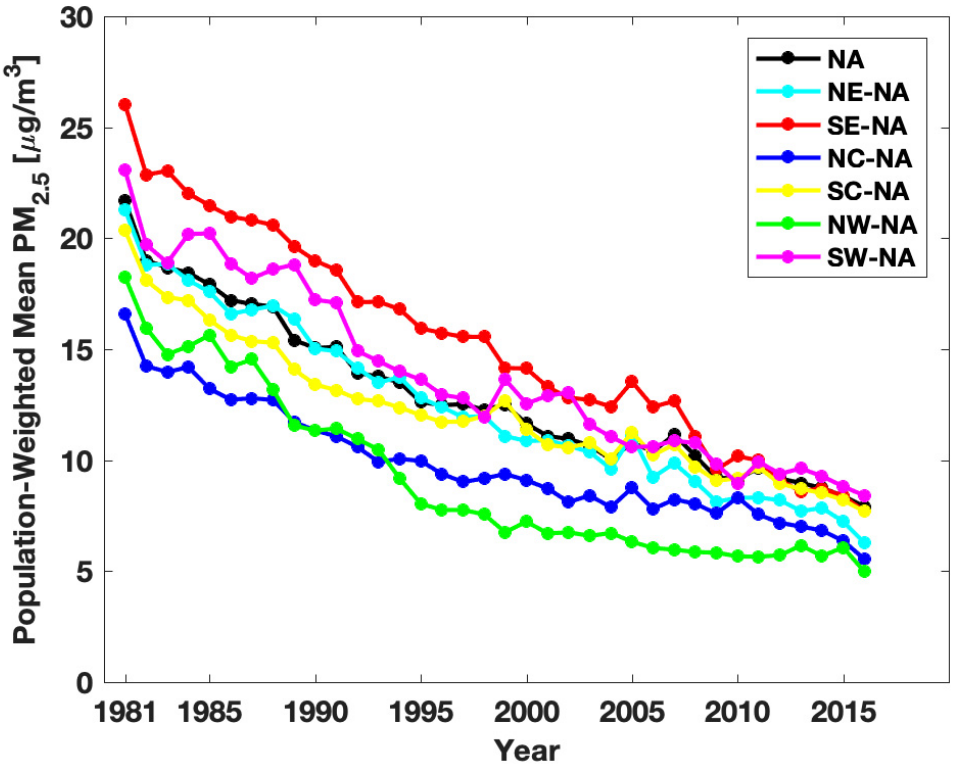

Figure 2-S5. Population-weighted annual mean $PM_{2.5}$ concentrations in different regions defined in Figure 2-S4.

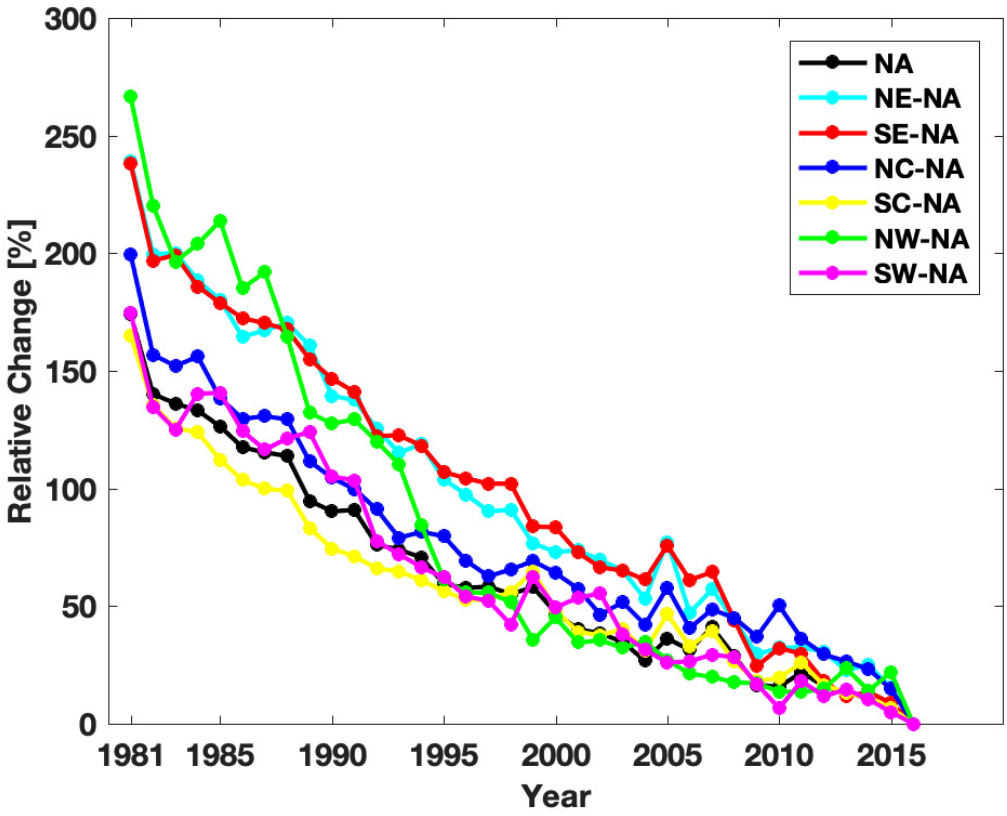

Figure 2-S6. Relative percentage change in population-weighted $PM_{2.5}$ using 2016 as the reference year. Regions are defined in Figure 2-S4.

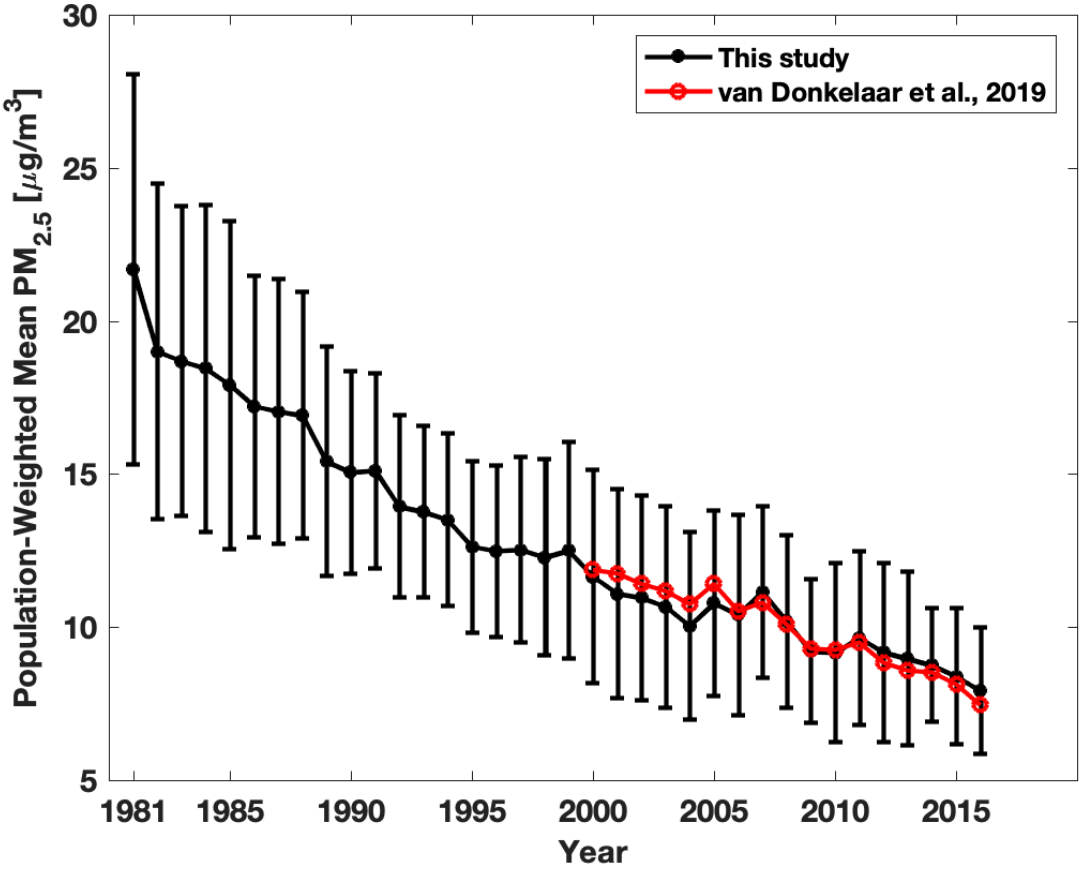

Figure 2-S7. Time series of population-weighted average $PM_{2.5}$ in this study and our most recent dataset (van Donkelaar et al., 2019).

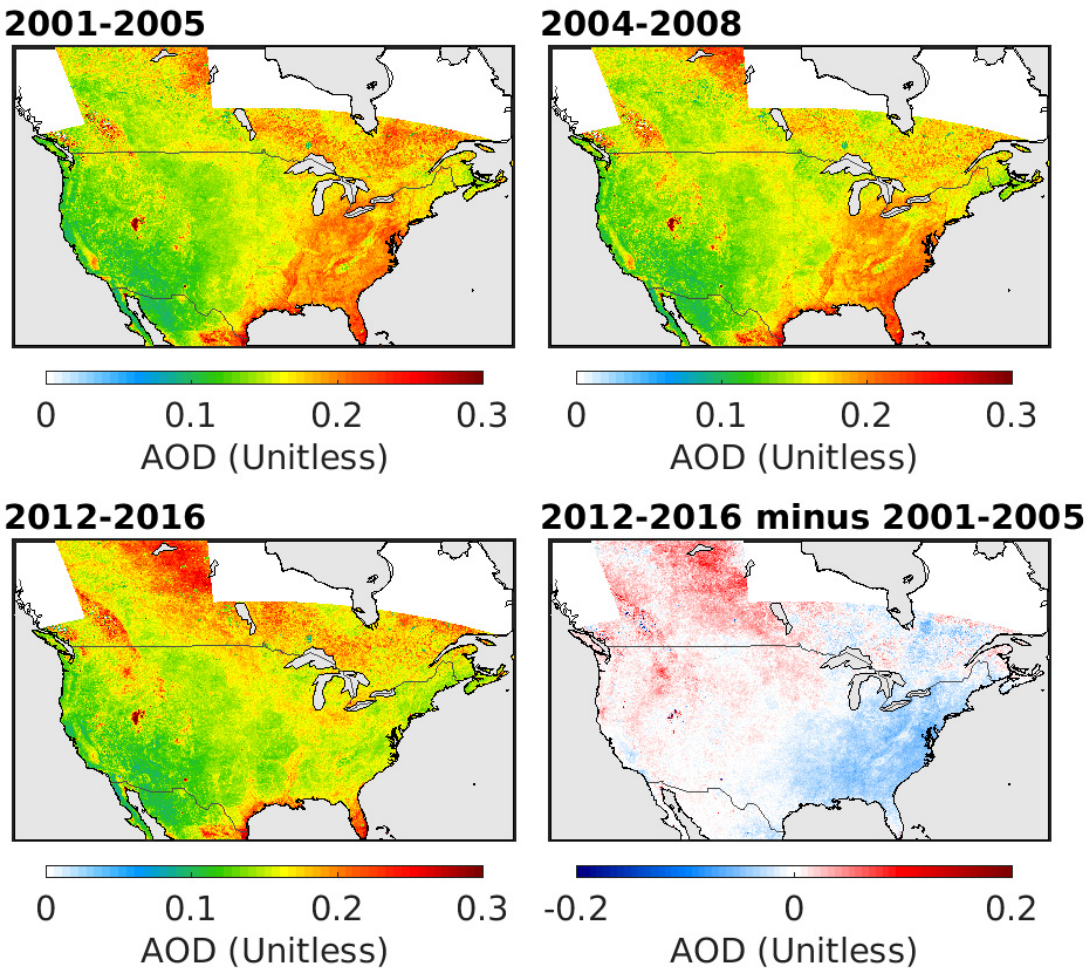

Figure 2-S8. Aerosol optical depth (AOD) for different time periods from the MODIS MAIAC product. White indicates gaps in the availability of the regional MODIS MAIAC product.

CHAPTER 3 SOURCE CONTRIBUTIONS TO AMBIENT FINE PARTICULATE MATTER FOR CANADA

Authors: Jun Meng[1], Randall V. Martin[1,2,3], Chi Li[1], Aaron van Donkelaar[1], Zitely A. Tzompa-Sosa[4], Xu Yue[5], Jun-Wei Xu[1], Crystal L. Weagle[1], Richard T. Burnett[6]

[1]Department of Physics and Atmospheric Science, Dalhousie University, Halifax, Nova Scotia, B3H 4R2, Canada

[2]Smithsonian Astrophysical Observatory, Harvard-Smithsonian Center for Astrophysics, Cambridge, MA 02138, USA

[3]Department of Energy, Environmental & Chemical Engineering, Washington University in St. Louis, St. Louis, Missouri, 63130, USA

[4]Department of Atmospheric Science, Colorado State University, Fort Collins, Colorado, 80523, USA

[5]School of Environmental Science and Engineering, Nanjing University of Information Science & Technology, Nanjing, 210044, China

[6]Health Canada, Ottawa, Ontario, K1A 0k9, Canada

Adapted with permission from "Meng, J., R. V. Martin, C. Li, A. van Donkelaar, Z. A. Tzompa-Sosa, X. Yue, J.-W. Xu, C. L. Weagle, R. T. Burnett, Source Contributions to Ambient Fine Particulate Matter for Canada, Environmental Science & Technology, 2019, 53, 17, 10269-10278. doi: 10.1021/acs.est.9b02461". Copyright (2019) by American Chemical Society. https://pubs.acs.org/doi/10.1021/acs.est.9b02461.

3.1 Abstract

Understanding the sectoral contribution of emissions to $PM_{2.5}$ offers information for air quality management, and for investigation of association with health outcomes. This study evaluates the contribution of different emission sectors to $PM_{2.5}$ in 2013 for Canada using the GEOS-Chem chemical transport model, downscaled with satellite-based $PM_{2.5}$. Despite the low population-weighted $PM_{2.5}$ concentrations of 5.5 μg m^{-3} across Canada, we find that over 70% of population-weighted $PM_{2.5}$ originates from Canadian sources followed by 30% from the contiguous United States. The three leading sectoral contributors to population weighted $PM_{2.5}$ over Canada are wildfires with 1.0 μg m-3 (17%), transportation with 0.96 μg m-3 (16%) and residential combustion with 0.91 μg m-3 (15%). The relative contribution to population-weighted $PM_{2.5}$ of different sectors varies regionally with residential combustion as the leading contributor in Central Canada (19%); while wildfires dominate over Northern Canada (59%), Atlantic Canada (34%) and Western Canada (18%). The contribution from U.S. sources is larger over Central Canada (33%) than over Western Canada (17%), Atlantic Canada (17%) and Northern Canada (< 2%). Sectoral trend analysis showed that the contribution from anthropogenic sources to population-weighted $PM_{2.5}$ decreased from 7.1 μg/m^3 to 3.4 μg/m^3 over the last two decades.

3.2 Introduction

$PM_{2.5}$ adversely affects human health (Baccarelli et al., 2009; R. D. Brook et al., 2010; Hamra et al., 2014; Krewski et al., 2009; Lepeule et al., 2012). $PM_{2.5}$ is recognized as the leading environmental risk factor for the global burden of disease (Gakidou et al., 2017) with recent estimates of annual attributable deaths worldwide of 4 million (Cohen et al., 2017) to 9 million

(Burnett et al., 2018). Air quality in North America has improved dramatically during the last three decades by reducing emissions (Environment and Climate Change Canada, 2018; U.S. EPA, 2018) with national mean $PM_{2.5}$ concentrations across Canada below the WHO air quality guideline (10 $\mu g/m^3$) (van Donkelaar et al., 2015; Pinault et al., 2017). Thus Canada is attractive to study the health effects of low-level $PM_{2.5}$. Several studies report adverse effects of long-term exposure to the low-level $PM_{2.5}$ concentration environment (Crouse et al., 2012; Hales et al., 2012; Pinault et al., 2016; Shi et al., 2016), but none have examined the relationship with specific sources. A better understanding of the sources contributing to $PM_{2.5}$ could inform national air quality management, and inform studies on the association of health outcomes with $PM_{2.5}$ concentrations at low levels (Pinault et al., 2016, 2017).

A number of studies have investigated the relative contribution of multiple sectors to $PM_{2.5}$ globally (Lelieveld et al., 2015; Silva et al., 2016; Weagle et al., 2018). Most previous studies on sectoral contributions to ambient $PM_{2.5}$ over Canada either focused on a single emission sector or a specific regional area. Additionally, most of those studies used a top-down source attribution method based on statistical analyses of measured chemical composition, including studies on the contribution of regional transport in southeast Canada and urban areas (J. R. Brook et al., 2002; J. R. Brook, Graham, et al., 2007; J. R. Brook, Poirot, et al., 2007), dust in British Columbia (Hong et al., 2017), industry in Ontario (Barker, 2012), coal-fired power plants (Goodarzi, 2006), wildfires (Landis et al., 2018; Sofowote & Dempsey, 2015) and biomass burning (Jeong et al., 2008; Weichenthal et al., 2017). A few studies have used a bottom-up approach based on emission inventories and chemical transport modeling to study the sector contributions to gas phase pollutants or to specific regions of Canada. For example, Pappin & Hakami (2013) examined the source attribution to nitrogen oxides and volatile organic compounds across North

America. Cho et al. (2012) investigated the contribution of oil sands development to $PM_{2.5}$ and ozone using an air quality model.

In this study, we used the GEOS-Chem chemical transport model at its finest resolution of 0.25° x 0.31° to investigate the contributions of different emission sectors to $PM_{2.5}$ across Canada from both Canada and the United States sources. We evaluated the performance of the baseline simulation and examine the contributions of different sectors to $PM_{2.5}$ concentrations across Canada. We also investigated the trend of the sectoral contribution to $PM_{2.5}$ concentrations across Canada over the last two decades.

3.3 Materials and Methods

3.3.1 GEOS-Chem Simulations

GEOS-Chem (http://www.geos-chem.org) includes detailed aerosol-oxidant chemistry (Bey et al., 2001; Park et al., 2004; Parrella et al., 2012). Gas-aerosol partitioning is performed by the ISORROPIA II thermodynamic scheme (Fountoukis & Nenes, 2007) as implemented into GEOS-Chem by Pye et al. (2009). The interaction between aerosols and gas-phase chemistry includes the effects of aerosol extinction on photolysis rates (Martin et al., 2003), brown carbon (Hammer et al., 2016), heterogeneous chemistry (Jacob, 2000) with dinitrogen pentoxide (N_2O_5) uptake by aerosol (Evans & Jacob, 2005) and hydroperoxyl radical (HO_2) uptake by aerosol (Mao et al., 2013).

The GEOS-Chem aerosol simulation includes the sulfate-nitrate-ammonium (SNA) aerosol system (Fountoukis & Nenes, 2007; Park et al., 2004), mineral dust (Fairlie et al., 2007), sea salt (Jaeglé et al., 2011), and carbonaceous aerosol (Park et al., 2003) with updates to black carbon (Q. Wang et al., 2014), semi-volatile SOA formation from isoprene (Pye et al., 2010) and

SOA formed from isoprene with an irreversible aqueous scheme (Marais et al., 2016). The ratio between organic mass and organic carbon (OM/OC) is spatially resolved (Philip et al., 2014). Nitric acid concentrations are reduced following Heald et al. (2012). The mineral dust simulation includes updates to the aerosol size distribution (L. Zhang et al., 2013) and dust optics (Ridley et al., 2012). We include recent updates in dry and wet deposition (Amos et al., 2012; Fisher et al., 2011; Q. Wang et al., 2011; Q. Wang et al., 2014).

GEOS-Chem uses assimilated meteorological data from the Goddard Earth Observation System (GEOS) of NASA's Global Modeling and Assimilation Office (GMAO). We used GEOS Forward Processing (GEOS-FP) meteorological data archived at a native horizontal resolution of 0.25° x 0.3125°, roughly 25km x 25km, with 72 vertical levels.

We used the nested-grid capability (P. S. Kim et al., 2015; Y. X. Wang et al., 2004) of the GEOS-Chem chemical transport model (version 11-02c) at 0.25° x 0.3125°, to simulate $PM_{2.5}$ concentrations across North America. We first conducted global simulations at coarse resolution of 2° x 2.5° to archive boundary conditions. Then, we conducted regional (nested-grid) simulations at fine resolution of 0.25° x 0.31° over North America. The operator time steps in the simulation followed previous recommendations (Philip et al., 2016). We used a 1-month spin up to remove the effects of initial conditions. We used the lowest layer of the model to represent the ground-level aerosol concentrations. We calculated simulated $PM_{2.5}$ concentrations at 35% relative humidity (RH) and chemical composition at dry conditions for consistency with the measurement protocols over North America. We downscaled our simulations to better represent spatial variation of population density using satellite-derived $PM_{2.5}$ gridded at 1 km resolution across North America (van Donkelaar et al., 2019). We calculated the ratio between the annual mean satellite-derived $PM_{2.5}$ and baseline simulated $PM_{2.5}$. We applied this ratio to both the

baseline simulation and sector sensitivity simulations to downscale all simulations to 1 km resolution.

We used population data from the National Aeronautics and Space Administration Socioeconomic Data and Application Center (SEDAC, version4) ("Gridded Population of the World (GPW), v4, SEDAC," 2018) to calculate population weighted average $PM_{2.5}$ concentrations regionally and provincially in Canada.

3.3.2 North American Emissions for Baseline Simulation

GEOS-Chem emissions were configured via the HEMCO module (Keller et al., 2014). Anthropogenic emissions were provided by regional emission inventories. We used the Criteria Air Contaminants (CAC) over Canada (http://www.ec.gc.ca/inrp-npri/), the 2011 U.S. National Emissions Inventory (NEI2011, http://ww.epa.gov/air-emissions-inventories) over the United States and the Big Band Regional Aerosol and Visibility Observational study (BRAVO) over Mexico (Kuhns et al., 2005). We used annual scale factors obtained from other available datasets to scale the emission inventories to our simulation year. For CAC, we calculated annual scale factors over 1990 to 2016 from Canada's Air Pollutant Emission Inventory (APEI) (Environment and Climate Change Canada, 2015). For NEI2011, we calculated annual scale factors for 2013 from the national annual total trends from EPA (http://www.epa.gov/ttnchie1/trends/). We calculated BC and OC emissions by applying the sector-specific OC and BC to $PM_{2.5}$ emission ratios reported in the EPA SPECIATE database (Reff et al., 2009) following recent studies (C. Li et al., 2017; Ridley et al., 2018).

Other emissions were default in GEOS-Chem. Wildfire emissions at 3-hour resolution were from the fourth-generation global fire emissions database (GFED-4) (Giglio et al., 2013).

Aircraft emissions were from the AEIC inventory (Stettler et al., 2011). Ship emissions were from ICOADS (Lee et al., 2011). Lighting NOx emissions were also included (Murray et al., 2012). Biogenic VOC emissions were from the MEGAN v2.1 inventory (Guenther et al., 2012; Tai et al., 2013). Biogenic soil NOx emissions were from Hudman et al. (2012). Volcano emissions were implemented by Fisher et al. (2011). Marine DMS emissions were from Breider et al. (2017).

3.3.3 Sector Sensitivity Analyses

We conducted a baseline simulation for the year 2013 using the emissions described above over North America. We quantified the impact of individual sectors by conducting sensitivity simulations that individually exclude each emission sector from the baseline simulation. This method had been extensively used in previous studies to evaluate the contribution of different sectors or regions to $PM_{2.5}$ concentrations or health impacts (Caiazzo et al., 2013; Lelieveld et al., 2015; Y. Li et al., 2016; Silva et al., 2016; Weagle et al., 2018). This method may lead to uncertainty due to the non-linear response to emission changes. We studied five anthropogenic emission sectors (Power Generation, Agriculture, Transportation, Industry and Residential Combustion), as well as wildfires, sea salt, and other sources (mineral dust, biogenic secondary organic aerosol, DMS, volcanos, and long-range transport). We also investigated the diesel sector, which is a sub-sector of the transportation sector.

The sectoral emissions for our sensitivity simulations were from APEI for Canada and from the U.S. NEI 2011 v6.3 (Tzompa-Sosa et al., 2019) for the United States. The power generation sector included coal burning for electric power generation. The agriculture sector primarily included ammonia from livestock and agricultural soils. The transportation sector

contained mobile sources and dust from paved and unpaved roads. The diesel sector, which included emissions from diesel engine vehicles and trucks and off-road use of diesel, was a sub-sector of the transportation sector. The industry sector contained multiple industrial sources including the petroleum industry, chemical industry, mineral product industry, pulp and paper industry, and aluminum industry. The residential combustion sector included residential fuel and wood combustion emissions.

We individually excluded each sectoral emission from the baseline simulation by applying the sectoral scale factor from APEI and the U.S. NEI 2011 v6.3 to baseline emission inventories (CAC and NEI2011) respectively. For the five major anthropogenic sectors, we also further separated the contribution from U.S emissions by performing five extra sensitivity simulations that only exclude the emissions from the Canadian sources.

3.3.4 Sectoral Contribution Trend Analysis

We conducted sectoral sensitivity analyses for selected years (1990, 2000 and 2010) over the last two decades to investigate trends in the sectoral contributions across Canada. We conducted GEOS-Chem baseline and sectoral sensitivity simulations for the years 1990, 2000 and 2010, driven by assimilated meteorology data from the Modern-Era Retrospective analysis for Research and Application, version 2 (MERRA-2), which included updates in both the Goddard Earth Observing System Model and the assimilation system back to 1980 (Molod et al., 2015). We first conducted global simulations at coarse resolution of 2° x 2.5° to archive boundary conditions. Then, we conducted regional (nested-grid) simulations at the finest resolution available for MERRA-2 (0.5° x 0.625°) over North America.

For baseline simulations, we used the Criteria Air Contaminants (CAC) over Canada (http://www.ec.gc.ca/inrp-npri/) and the Community Emissions Data System (CEDS) (Hoesly et al., 2018) historical emission inventory over the United States. We used annual scale factors obtained from other available datasets to scale the emission inventories to our simulation year. For CAC, we calculated annual scale factors from Canada's Air Pollutant Emission Inventory (APEI) (Environment and Climate Change Canada, 2015), which had a time span from 1990 to 2016. We used the 3-hour resolution of GFED4 (Giglio et al., 2013) for wildfire emissions for 2000 and 2010 simulations. We implemented a ground-based North America fire emission database (Yue et al., 2013) into GEOS-Chem for wildfire emissions in the 1990 simulation.

For sectoral sensitivity simulations, we quantified the impact of individual sectors by conducting simulations that individually exclude each sectoral emission from the baseline simulation for each year (1990, 2000 and 2010). We grouped APEI into 5 sectors, which include the agricultural, power generation, surface transport, industrial and residential combustion sectors. CEDS had eight sectors, which included agricultural, energy transformation and extraction, industrial combustion and process, surface transport, residential combustion, solvents, waste disposal and handling, and international shipping sectors. We individually excluded each sector emission from the baseline simulations.

3.3.5 Ground-based Measurements of $PM_{2.5}$ and Its Chemical Components

We collected ground-based measurements of $PM_{2.5}$ concentrations and its chemical components from several networks across North America in 2013 to evaluate our baseline simulation. Detailed information on network selection and data processing are provided in the Supporting Information. Monitor locations are in Figure 3-S1. Numerous studies have described

and evaluated these ground-based measurements (Dabek-Zlotorzynska et al., 2011; Hand et al., 2012). We treated these ground-based measurements as "truth" to evaluate model performance, even though these datasets do have uncertainties (Hand et al., 2012).

We compared the baseline simulated $PM_{2.5}$ and its chemical components with ground-based measurements using reduced major axis linear regression. We reported root mean square error (RMSE), correlation (r), intercept as well as slopes. Details about the performance of the baseline simulation in 2013 are provided in section 3.6.2.

3.4 Results and Discussion

3.4.1 Sectoral Contributions of Emissions to $PM_{2.5}$ Concentrations over Canada

Figure 3-1 shows the annual mean contributions of individual emission sectors to $PM_{2.5}$ concentrations. For Canada, the wildfires sector is the leading contributor, responsible for 1.0 μg m^{-3} of the total population-weighted $PM_{2.5}$ with the largest influences across northern Canada. The transportation sector (0.96 μg m^{-3}) follows closely with large contributions across populated regions of southern Canada. The residential combustion sector (0.91 μg m^{-3}), the third largest contributor, is most important in rural British Columbia and southern Quebec where wood is used for residential heating. The industry (0.86 μg m^{-3}) and agriculture (0.63 μg m^{-3}) sectors are most important in Alberta. The biogenic SOA sector (0.54 μg m^{-3}) most influences Ontario and southern Quebec reflecting both isoprene and terpene sources. The power generation sector (0.44 μg m^{-3}) is most important along the southern border of central Canada where advection from US sources is prevalent.

The relative contribution of different emission sectors varies seasonally across Canada. In winter (Figure 3-S4), residential combustion (1.6 μg m^{-3}) is the leading contributor due to home heating. Both of the transportation (1.4 μg m^{-3}) and agriculture (1.2 μg m^{-3}) sectors are important in winter due to the seasonal increase in ammonium nitrate. In summer (Figure 3-S5), the importance of the wildfires and biogenic SOA sectors increases across both Canada and the United States. The contribution from the agriculture sector in summer is negative due to nonlinearities in which there is enhanced $PM_{2.5}$ formation with decreasing aerosol acidity as ammonia emissions increase (Q. Ma et al., 2017; Marais et al., 2016; Silva et al., 2016; Weagle et al., 2018).

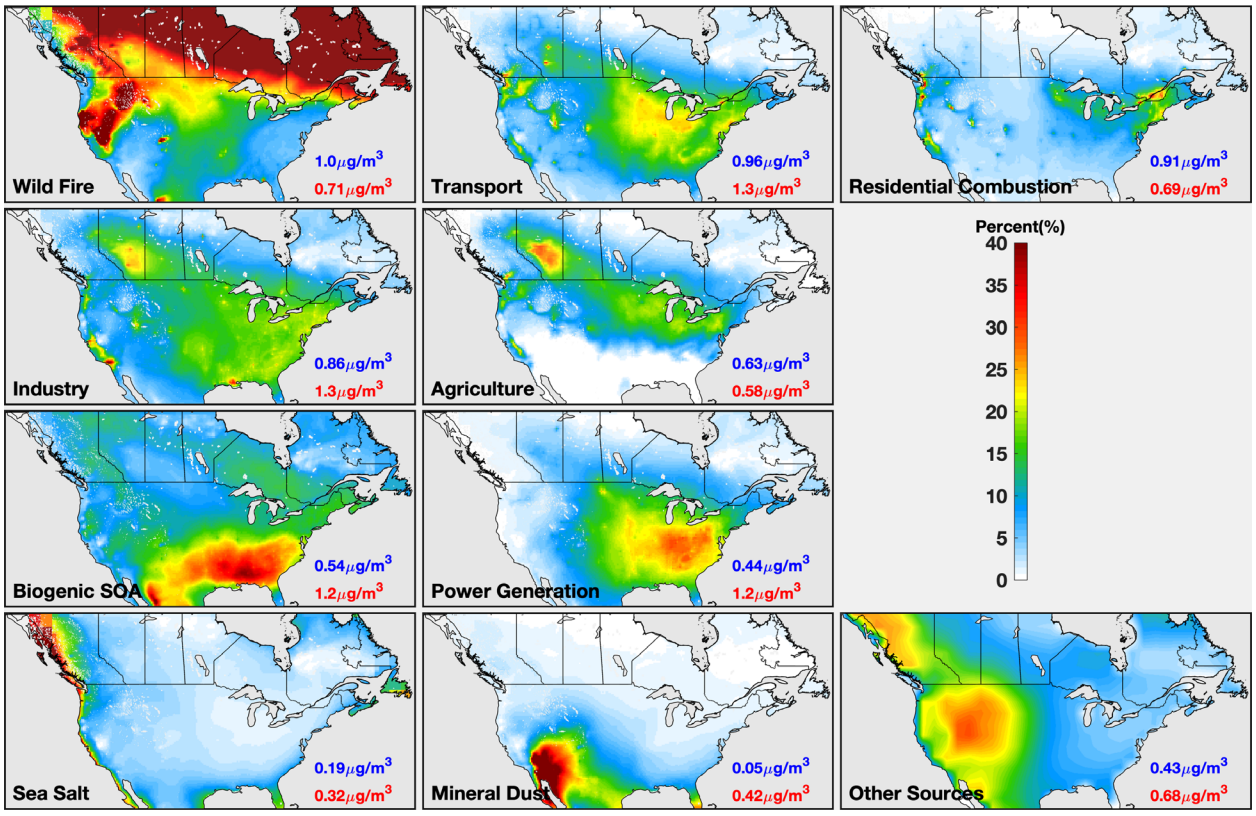

Figure 3-1. Contribution of emission sectors to $PM_{2.5}$ concentrations for 2013. Other Sources include volcano, dimethyl sulfide (DMS), and long-range transport (LRT) from Asia, Europe and Alaska. Inset values are population-weighted annual mean $PM_{2.5}$ concentrations attributable to each sector across the U.S. (red) and Canada (blue).

Figure 3-2 shows the fractional contribution of different sectors to population weighted annual mean $PM_{2.5}$ concentrations over different regions (defined in Figure 3-S6) of Canada. Over 80% of the population-weighted $PM_{2.5}$ of 5.5 μg m^{-3} across Canada arises from the five anthropogenic sectors and the wildfires sector. The wildfires sector is the largest contributor across Canada, responsible for 17% of population-weighted $PM_{2.5}$, followed closely by the transportation sector (16%), the residential combustion sector (15%) and the industry sector (14%). The agriculture and power generation sectors account for 10% and 7% of population-weighted $PM_{2.5}$ respectively. Other sources, including sea salt, dust, DMS, volcanos, biogenic secondary organic aerosol and long-range transport, explain the remaining contribution. The leading anthropogenic contribution of the transportation sector in Canada is consistent with recent findings for the United States (Caiazzo et al., 2013) however, differs from regions such as India where residential burning dominates (Venkataraman et al., 2018), China where coal burning dominates (Q. Ma et al., 2017), and globally where residential burning dominates (Philip et al., 2014; Weagle et al., 2018).

The diesel sector is a specified subsector of the transportation sector, which is the leading anthropogenic contributor across Canada in 2013 (Figure 3-2). Table 3-S1 in section 3.6 shows the fractional annual contribution of diesel to the transportation sector from Canadian sources across different Canadian regions in 2013. The diesel sector accounts for 35% of population-weighted mean $PM_{2.5}$ attributed to transportation sector with little variation (± 2%) regionally.

The relative contribution of different emission sectors varies regionally across Canada. In Central Canada, with the highest population-weighted $PM_{2.5}$ (5.9 μg m^{-3}) among all the Canadian regions, about 70% of population-weighted $PM_{2.5}$ arises from five anthropogenic sectors. The residential sector is the leading contributor (19%) followed closely by the transportation sector

(17%). In Western Canada, the wildfires sector is the largest contributor accounting for 18% of population-weighted $PM_{2.5}$ followed by the agriculture (15%) and transportation (15%) sectors. In the Atlantic Canada region with low population-weighted $PM_{2.5}$ (3.3 μg m^{-3}), the wildfires sector accounts for 34% of total population-weighted $PM_{2.5}$ followed by secondary organic aerosol (13%) and then the transportation, industry, power generation and residential combustion sectors (~7% - 9%). Northern Canada has the lowest level of $PM_{2.5}$ concentration with population-weighted $PM_{2.5}$ of 1.4 μg m^{-3} of which over half (59%) arises from the wildfires sector.

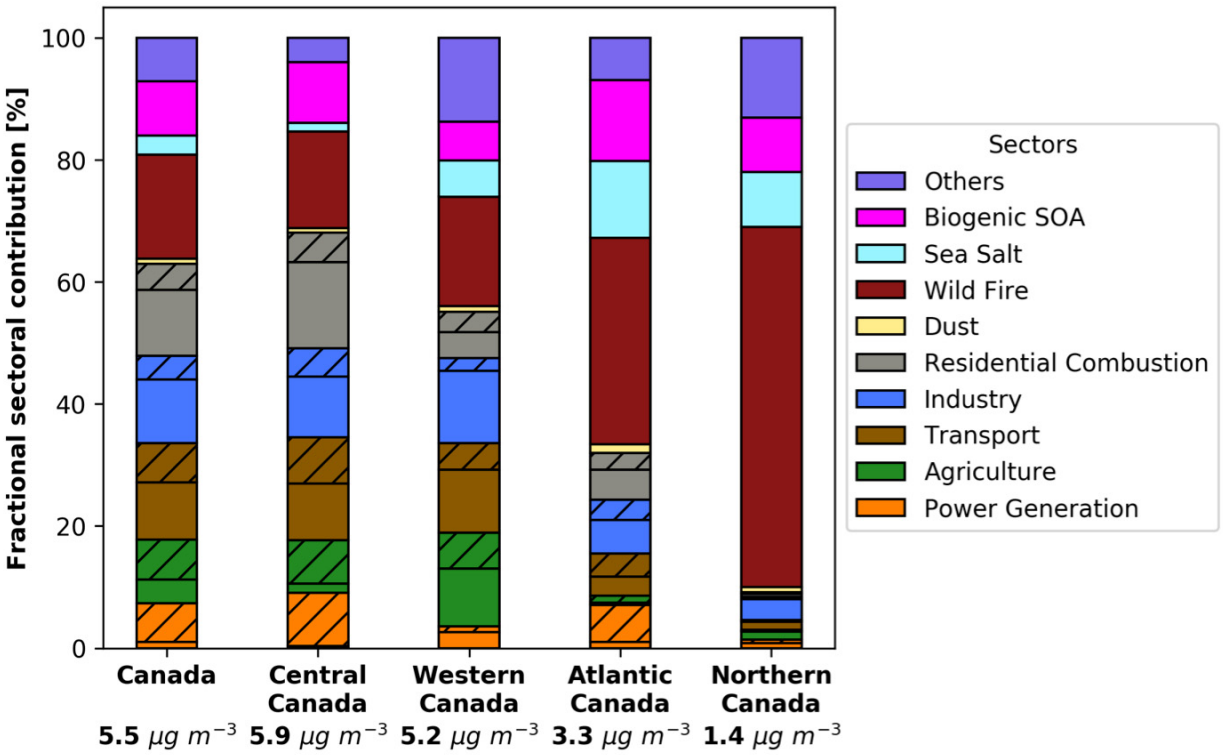

Figure 3-2. Fractional contribution of different sectors to population-weighted average $PM_{2.5}$ concentrations over different regions in Canada for 2013. The number under each bar represents the total population-weighted annual mean $PM_{2.5}$ concentrations over that region. The hatched part in each sector represents the fractional contribution from the United States. Others include dimethyl sulfide (DMS), volcano, and long-range transport (LRT) from Asia, Europe and Alaska.

The relative contribution of different emission sectors over each region in Canada also varies seasonally as shown in Figure 3-S7 for winter and Figure 3-S8 for summer. The percentage contribution from the five anthropogenic emission sectors increases in winter to 95% for Central Canada, 78% for Western Canada, 70% for Atlantic Canada and 30% for Northern Canada. In summer, the percentage contribution from wildfires is the largest over all regions (78% over Northern Canada, 55% over Atlantic Canada, 38% over Western Canada and 36% over Central Canada). The seasonality of dominant sources (i.e. anthropogenic emissions in winter vs. wildfires in summer) is similar across provinces (Figure 3-S9 – 3-S11).

We separate the contributions from the United States out of the five primary anthropogenic emission sectors as shown in the hatched bars in Figure 3-2. We find that 27% of population-weighted $PM_{2.5}$ in Canada is from anthropogenic U.S. sources. The U.S. agriculture, transportation and power generation sectors each account for 6% of population-weighted $PM_{2.5}$ across Canada followed by the U.S. residential combustion (4%) and industry (4%) sectors. The fractional contribution from the U.S. sources varies regionally. In Central Canada, 33% of population-weighted $PM_{2.5}$ is from the U.S. with the U.S. power generation source accounting for 9% of $PM_{2.5}$ followed closely by the U.S. transportation sector (8%). In western Canada, 17% of population-weighted $PM_{2.5}$ is from the U.S. with the U.S. agriculture sector as the largest contributor (6%). In Atlantic Canada, 17% of population-weighted $PM_{2.5}$ is from U.S. sources with the power generation sector as the largest contributor among U.S. sectors accounting for 6% of $PM_{2.5}$. The effects of U.S. emissions to $PM_{2.5}$ in northern Canada is less than 2%. The fractional contribution from the U.S. sources also varies seasonally with 46% from the U.S. sources in winter and only 12% from the U.S. sources in summer.

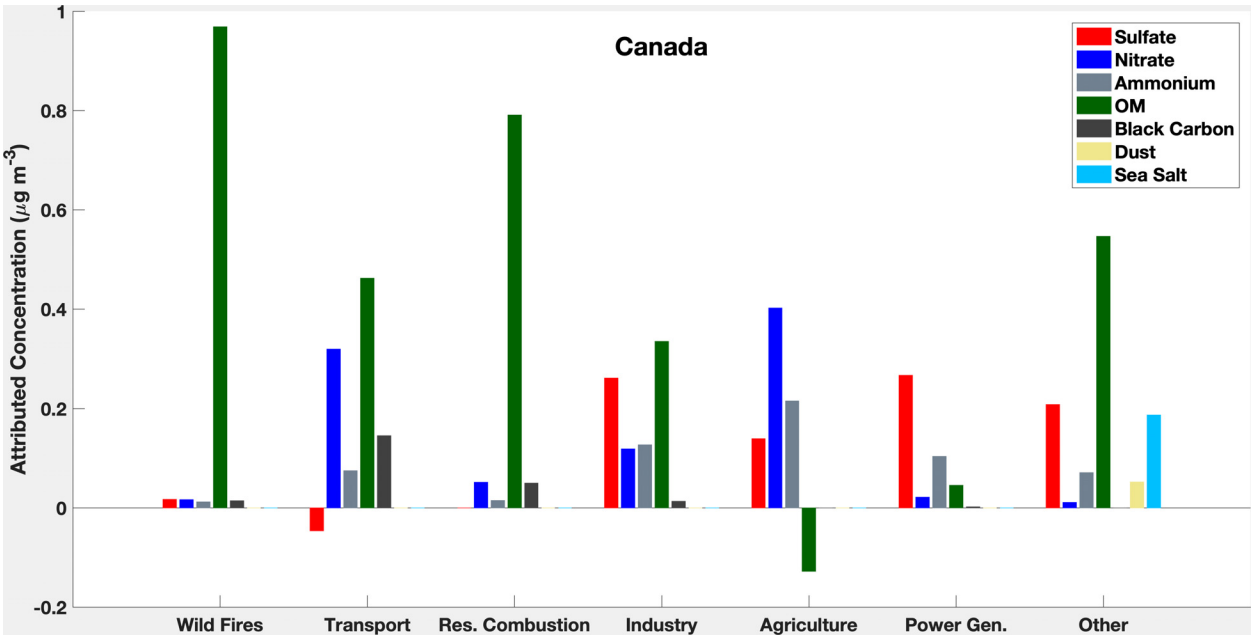

Figure 3-3. Population-weighted annual mean concentrations of chemical components (μg m^{-3}) attributed to different sectors (including the contribution from U.S.) across Canada for 2013. Other includes dimethyl sulfide (DMS), volcano, biogenic secondary organic aerosol (SOA) and long-range transport (LRT) from Asia, Europe and Alaska. Figure was created using MATLAB_R2016b.

Figure 3-3 shows the Canadian population-weighted annual mean concentration of chemical components attributable to different sectors. $PM_{2.5}$ from the wildfires sector is dominated by OM (94%). The main components of $PM_{2.5}$ mass arising from the transportation sector are OM (0.46 μg m^{-3}) and nitrate (0.32 μg m^{-3}), reflecting the NO_x and VOC emissions from traffic (Environment and Climate Change Canada, 2015). The contribution of sulfate attributable to the transportation sector is slightly negative due to nonlinear chemistry because the oxidation efficiency of SO_2 to sulfate increases as the emission of NOx significantly decreases (Holt et al., 2015; Shah et al., 2018) when eliminating the transportation sector. The residential combustion population-weighted mean $PM_{2.5}$ concentration of 0.91 μg m^{-3} is driven by OM (87%). $PM_{2.5}$ from the industry sector includes contributions from OM (39%) and sulfate (31%). $PM_{2.5}$ from the power generation sector is driven by sulfate (61%) followed by

ammonium (24%). The population-weighted $PM_{2.5}$ from the agriculture sector is dominated by nitrate (64%) and ammonium (34%). The concentration of organic matter increases when emissions from the agriculture sector are excluded due to the increase of aerosol acidity (Fisher et al., 2011; Marais et al., 2016; Weagle et al., 2018). The remaining other sectors include biogenic SOA, sulfate from DMS and volcanos, and sea salt. Figure 3-S12 shows the population weighted annual mean concentration of chemical components attributed to different sectors over different regions in Canada. The relative contributions of different chemical components remain similar across regions as the source magnitude varies.

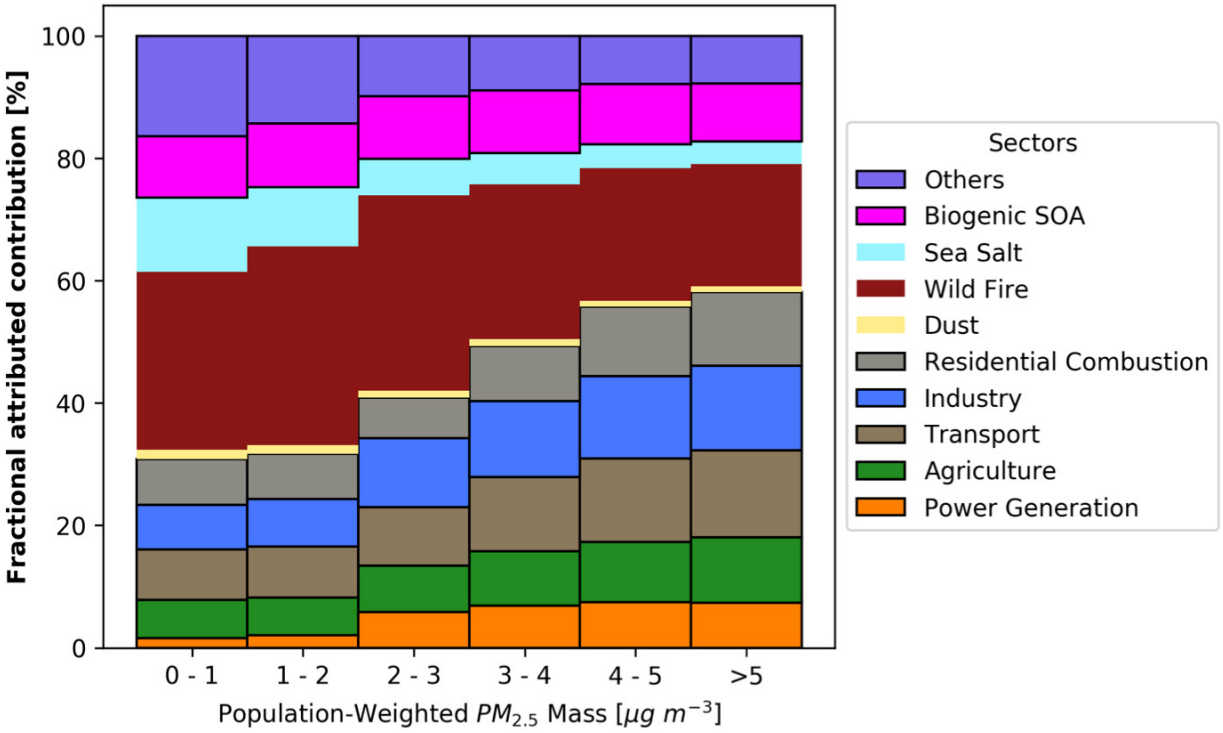

Figure 3-4. Population-weighted sectoral fractional contribution versus population-weighted $PM_{2.5}$ over Canada for 2013. Stacked bar plots show percentage of each sector in different $PM_{2.5}$ levels. Other includes dimethyl sulfide (DMS), volcano, and long-range transport (LRT) from Asia, Europe and Alaska.

Figure 3-4 shows the sectoral contribution to population weighted average $PM_{2.5}$ as a function of $PM_{2.5}$ concentration levels in Canada. The importance of different sectors remains

similar for different $PM_{2.5}$ concentration levels. Wildfires have a larger fractional contribution at locations with smaller annual population weighted average $PM_{2.5}$ concentrations. The percentage contribution from the five primary anthropogenic emission sectors increases with the ambient annual population weighted average $PM_{2.5}$ concentrations. The sectoral contribution to $PM_{2.5}$ in the U.S. is similar to that in Canada albeit with a weaker wildfire contribution and a stronger anthropogenic contribution in the US (Figure 3-S13).

3.4.2 The Trend of Sectoral Contribution in the Last Two Decades across Canada

Figure 3-5 shows the contributions of different sectors to population-weighted average $PM_{2.5}$ concentrations across Canada in 1990, 2000 and 2010. The population-weighted average $PM_{2.5}$ concentration across Canada decreased from 8.9 $\mu g\ m^{-3}$ in 1990 to 7.4 $\mu g\ m^{-3}$ in 2000, and to 7.0 $\mu g\ m^{-3}$ in 2010. These values are close (within 16%) to observational constrained estimates for these years (Meng et al., 2019a), supporting the $PM_{2.5}$ trends from the simulations. The power generation sector was the largest contributor to population-weighted average $PM_{2.5}$ concentrations in 1990 (2.4 $\mu g\ m^{-3}$) and 2000 (1.9 $\mu g\ m^{-3}$); while the wildfires sector has the largest contribution in 2010 (1.6 $\mu g\ m^{-3}$) followed by the power generation sector (1.3 $\mu g\ m^{-3}$). The total contribution from the five anthropogenic sectors decreased from 7.1 $\mu g\ m^{-3}$ in 1990 to 3.4 $\mu g\ m^{-3}$ in 2013, reflecting the success of air quality control over the last three decades across North America. The contribution from the power generation sector decreased from 2.4 $\mu g\ m^{-3}$ in 1990 to 1.3 $\mu g\ m^{-3}$ in 2010, while the contribution from industry sector decreased from 1.4 $\mu g\ m^{-3}$ in 1990 to 0.7 $\mu g\ m^{-3}$ in 2010, both of which reflect the successful controls on emissions (Environment and Climate Change Canada, 2015; U.S. EPA, 2018) reductions in coal burning.

$PM_{2.5}$ from the power generation sector continues to decrease dramatically after 2010 (Figure 3-2) driven by a decrease in total SO_2 emissions over 2010 to 2013 of 20% for Canada and of 42% for the United States nationally. The relative sectoral contribution from the U.S. sources remains similar during the last two decades, with the largest fraction from U.S. source from power generation followed by agriculture.

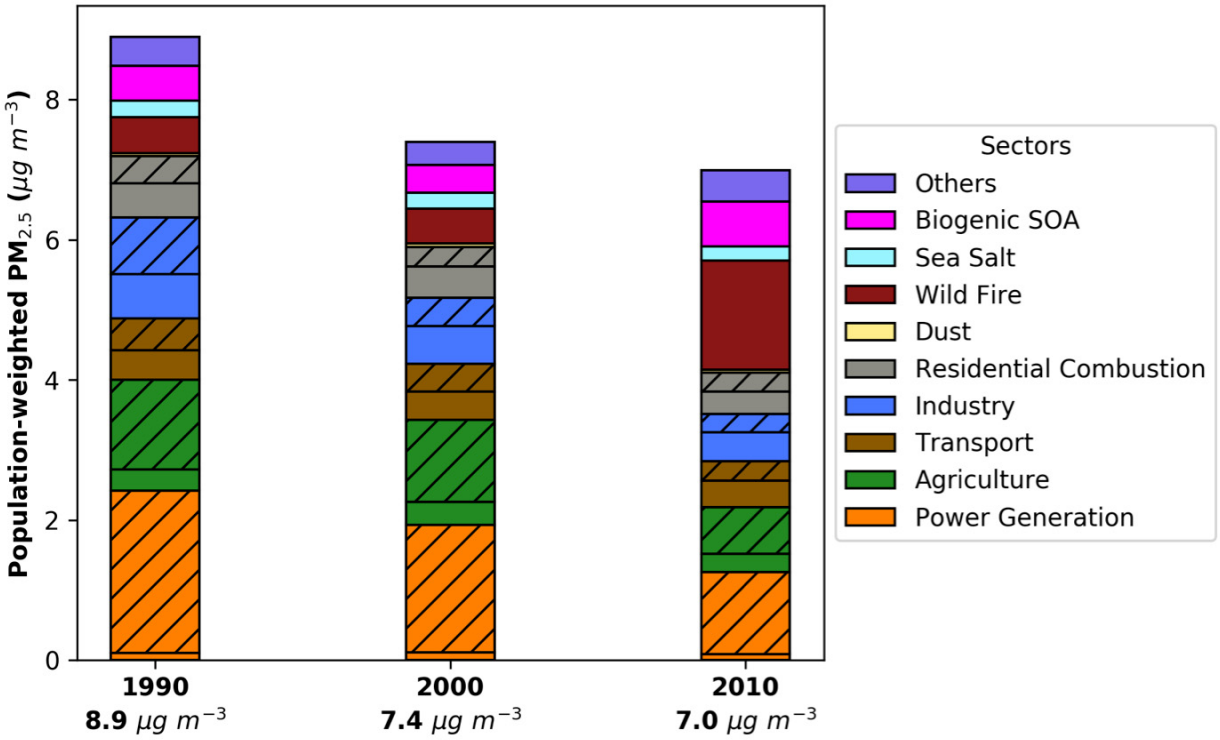

Figure 3-5. Contribution of different sectors to population-weighted average $PM_{2.5}$ concentrations over Canada in 1990, 2000 and 2010. The number under each bar represents the total population-weighted annual mean $PM_{2.5}$ concentrations in that year. The hatched part in each sector represents the fractional contribution from the United States. Others include dimethyl sulfide (DMS), volcano, and long-range transport (LRT) from Asia, Europe and Alaska.

3.4.3 Variability in Wildfires Contribution

We examined how wildfire variability could affect the trends in section 3.4.2. Figure 3-S14 shows the annual total dry matter time series from 1990 to 2015 in our wildfires emission inventories across Canada. The total dry matter emitted in 2013 is 25 Tg, which is about the average during 1990 to 2015, while lower than average in recent years given that the total dry matter burnt time series from 1990 to 2015. Thus wildfires may play a proportionally larger role in other years, or in a warmer climate in the future (Hurteau et al., 2014; Randerson et al., 2012).

3.4.4 Perspective

This assessment found that the contributions to $PM_{2.5}$ at the low population-weighted $PM_{2.5}$ concentrations across Canada of 5.5 μg m^{-3} is primarily (81%) from five major anthropogenic sectors and the wildfires sector. The regionally-varying relative contribution of different emission sectors across Canada implies that mitigation strategies will benefit from regional policies. For example, across Central Canada, around 70% population-weighted $PM_{2.5}$ arises from five major anthropogenic sectors with the residential combustion sector as the leading contributor (19%) followed closely by the transportation sector (17%). The notable $PM_{2.5}$ contributions from the contiguous United States (~30%) implies benefits from international coordination. The leading U.S. contributors of the agricultural, transportation and power generation sectors are also important contributors to $PM_{2.5}$ in the United States implying mutual benefits from reducing the emissions from these sources. The increasing contributions of anthropogenic sectors with increasing $PM_{2.5}$ found here may have implications for the shape of the concentration-response function.

3.5 Acknowledgement

This work was supported by Health Canada contract #4500358772. Jun Meng was partially supported a Nova Scotia Research and Innovation Graduate Scholarship. We are grateful to the Atlantic Computational Excellence Network and Compute Canada for computing resources. We thank four anonymous reviewers for invaluable comments and suggestions.

3.6 Supporting Information

3.6.1 Description of Ground-based Measurements of $PM_{2.5}$ and Its Chemical Components

We collected ground-based measurements of $PM_{2.5}$ concentrations and its chemical components from several networks across North America in 2013. The $PM_{2.5}$ mass measurements included the Canadian National Air Pollution Surveillance Network (NAPS, http://www.ec.gc.ca/rnspa-naps/), the U.S. Environmental Protection Agency (EPA) federal reference method (EPA-FRM, http://www.epa.gov/outdoor-air-quality-data/) and the Interagency Monitoring of Protected Visual Environments (IMPROVE, http://views.cira.colostate.edu/fed/DataWizard/). The networks for ground-based measurements of chemical composition included the EPA chemical speciation network (EPA-CSN, http://www.epa.gov/ttn/airs/airaqs/), IMPROVE, NAPS and the Clean Air Status and Trends Network (CASTNET, http://www.epa.gov/castnet/). The NAPS network provided 24-hr average composition data every third day across Canada (Dabek-Zlotorzynska et al., 2011). The IMPROVE network provided 24-hr average composition data every third day over the national parks in the United States. The EPA-CSN network located sites mainly in urban or suburban areas, with reported 24-hr average composition data every three or six days. The CASTNET network provided weekly average inorganic ion measurements. We calculated ammonium

concentrations from sulfate and nitrate measurements of the IMPROVE network by assuming the aerosol is in neutral state. We calculated OM from measured OC using a spatially and seasonally varying OM/OC ratio (Philip et al., 2014).

3.6.2 Description of Simulated $PM_{2.5}$ and Chemical Components

Both the measurements and the downscaled simulation exhibited enhanced $PM_{2.5}$ concentrations across the eastern United States extending into southern Ontario. Regional enhancements across northern Canada reflect wildfire influence as discussed further below. We found a high degree of consistency of the downscaled simulation with in situ $PM_{2.5}$ concentrations, with a RMSE of 1.79 μg m^{-3} and r of 0.77 over North America (Figure 3-S1).

The downscaled simulation was most consistent with measured chemical components for sulfate (r=0.76, slope=0.88), ammonium (r=0.74, slope=1.12), nitrate (r=0.69, slope=0.75) and to a lesser extent OM (r=0.68, slope=0.88). The enhanced concentrations of sulfate-nitrate-ammonium aerosols south of the Great Lakes were reproduced by the simulation, albeit with a slight underestimate of sulfate and nitrate. The measured enhancement of OM over the southeastern U.S. was well represented in the simulation. The simulation exhibited hotspots of BC concentration associated with major urban areas (Figure 3-S2).

Figure 3-S3 showed the fractional contribution of different chemical components to total annual mean $PM_{2.5}$ concentrations. OM accounts for more than 40% of the total $PM_{2.5}$ concentrations over many regions in North America. SNA were major components of total $PM_{2.5}$ over North America contributing 44% of population-weighted $PM_{2.5}$ over Canada and 51% over the United States. Sulfate had a major influence on population-weighted $PM_{2.5}$, accounting for 22% over Canada and 25% over the United States. Nitrate and ammonium contribute similarly

over Canada and the United States, accounting for roughly 12% of population-weighted $PM_{2.5}$ mass respectively. BC, dust and sea salt typically accounted for a small fraction (less than 5%) of total $PM_{2.5}$ concentrations over North America, with the exception of mineral dust in the southwest.

Table 3–S1. Percentage contribution of diesel sector to the Canadian transport sector

	Canada	Atlantic Canada	Northern Canada	Western Canada	Central Canada
Percentage	35%	37%	37%	36%	35%

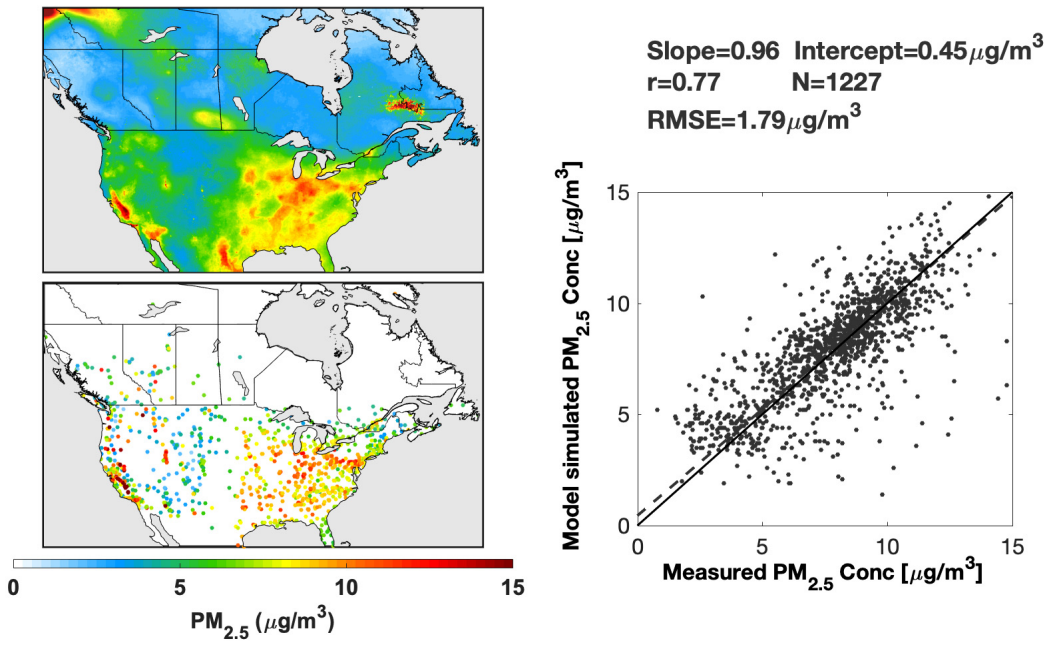

Figure 3-S1. Annual mean $PM_{2.5}$ concentrations for 2013. The top-left panel shows the baseline downscaled simulation. The bottom-left panel shows ground-based measurements. The right panel shows the corresponding scatter plot with root mean square error (RMSE), correlation coefficient(r) and slope calculated with reduced major axis linear regression. N is the number of valid ground-based monitoring records. The best fit line is dashed. The 1:1 line is solid. Figure was created using MATLAB_R2016b.

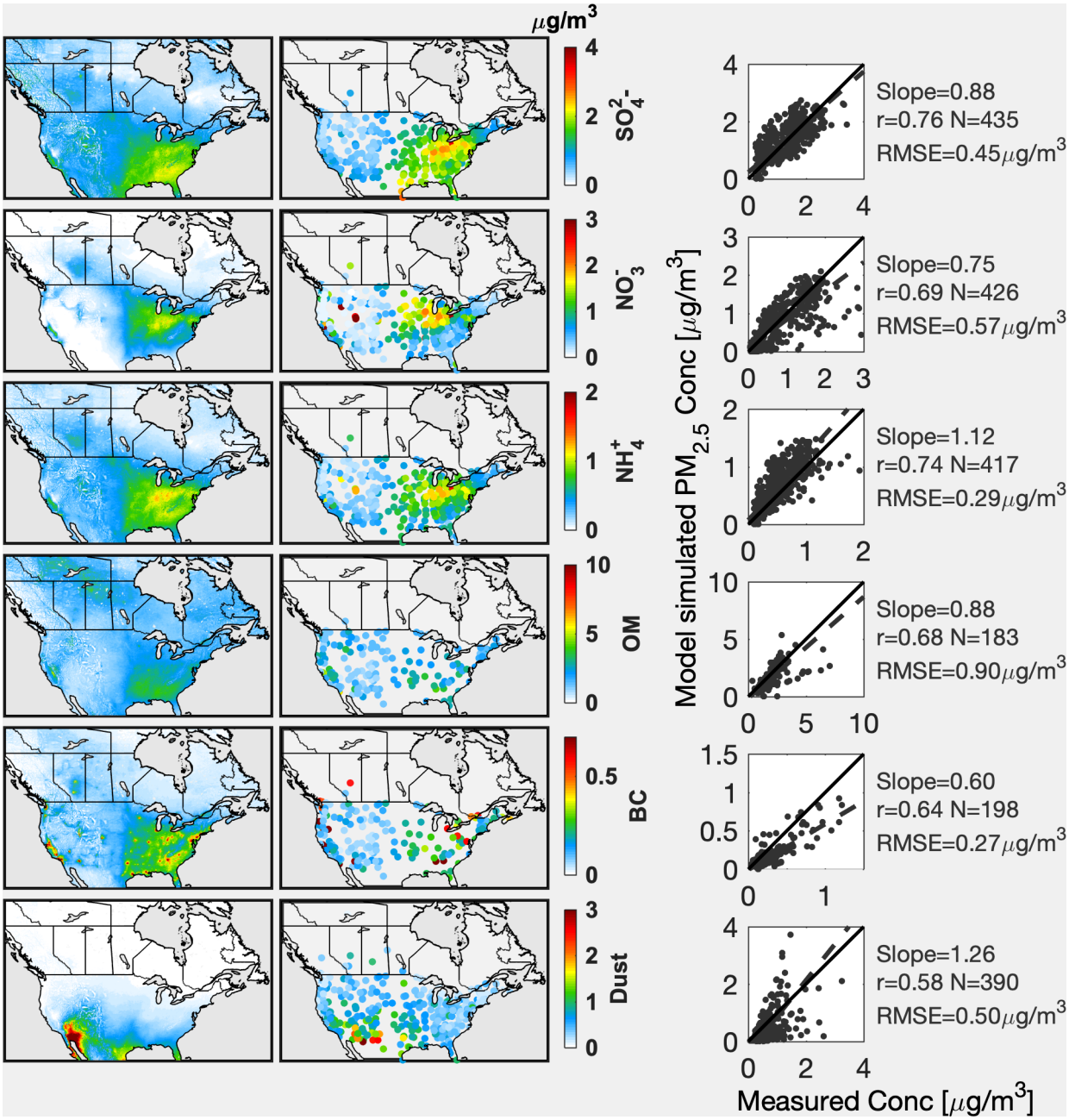

Figure 3-S2. Annual mean chemical components in baseline downscaled simulation (left) and ground-based measurements (middle). The right column contains scatter plots between simulated and observed species concentrations using reduced major axis linear regression. Slope, root mean square error (RMSE) and correlation coefficient (r) are reported. The best fit line is dashed. The 1:1 line is solid. Figure was created using MATLAB_R2016b.

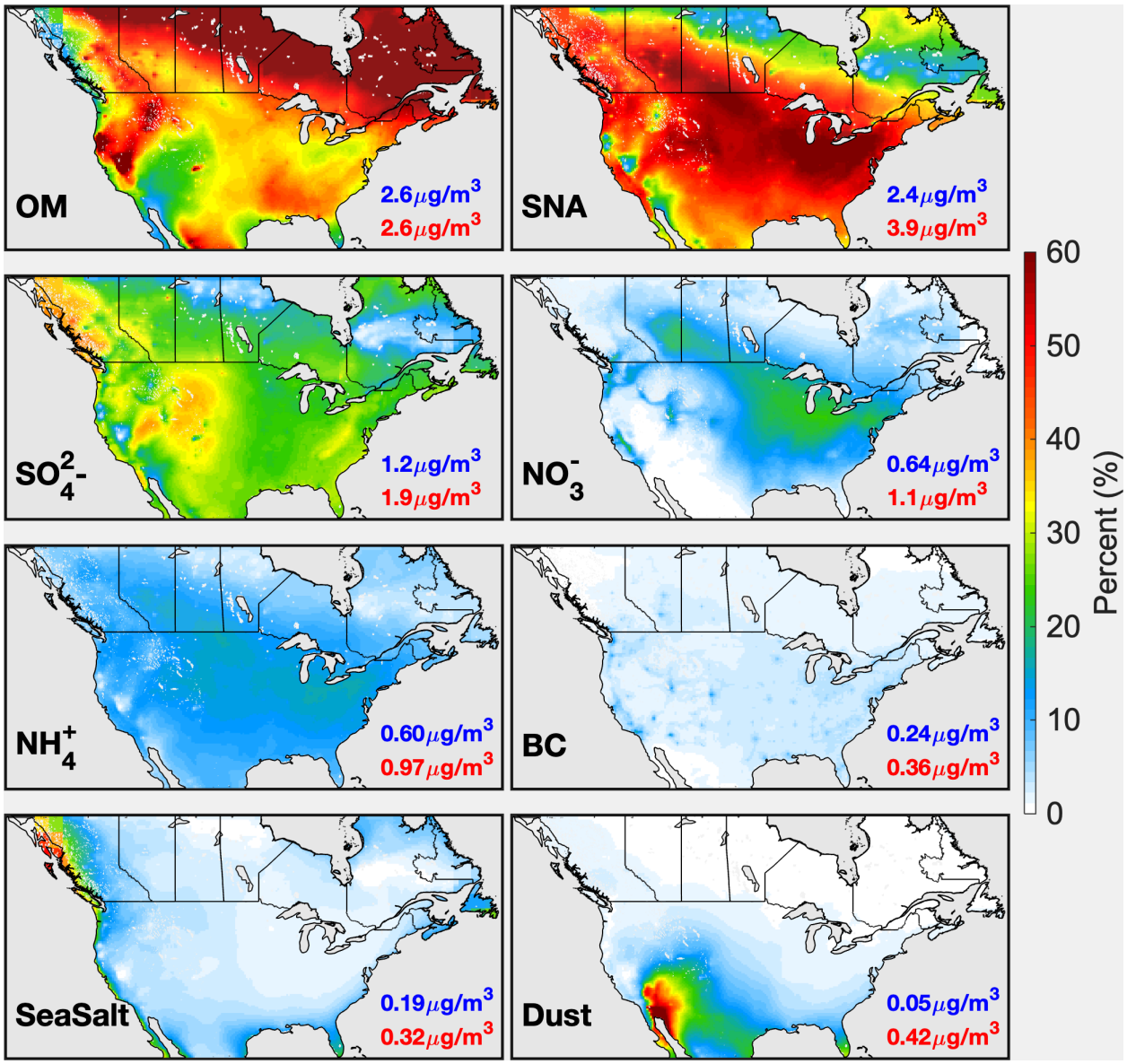

Figure 3-S3. Fractional contribution of different chemical components to total annual mean $PM_{2.5}$ concentrations. Aerosol water is associated with each chemical component at 35% RH. Abbreviations are sulfate-nitrate-ammonium (SNA), organic mass (OM) and black carbon (BC). Inset values are population-weighted annual mean $PM_{2.5}$ concentrations resulting from each chemical component over the U.S. (red) and Canada (blue). Figure was created using MATLAB_R2016b.

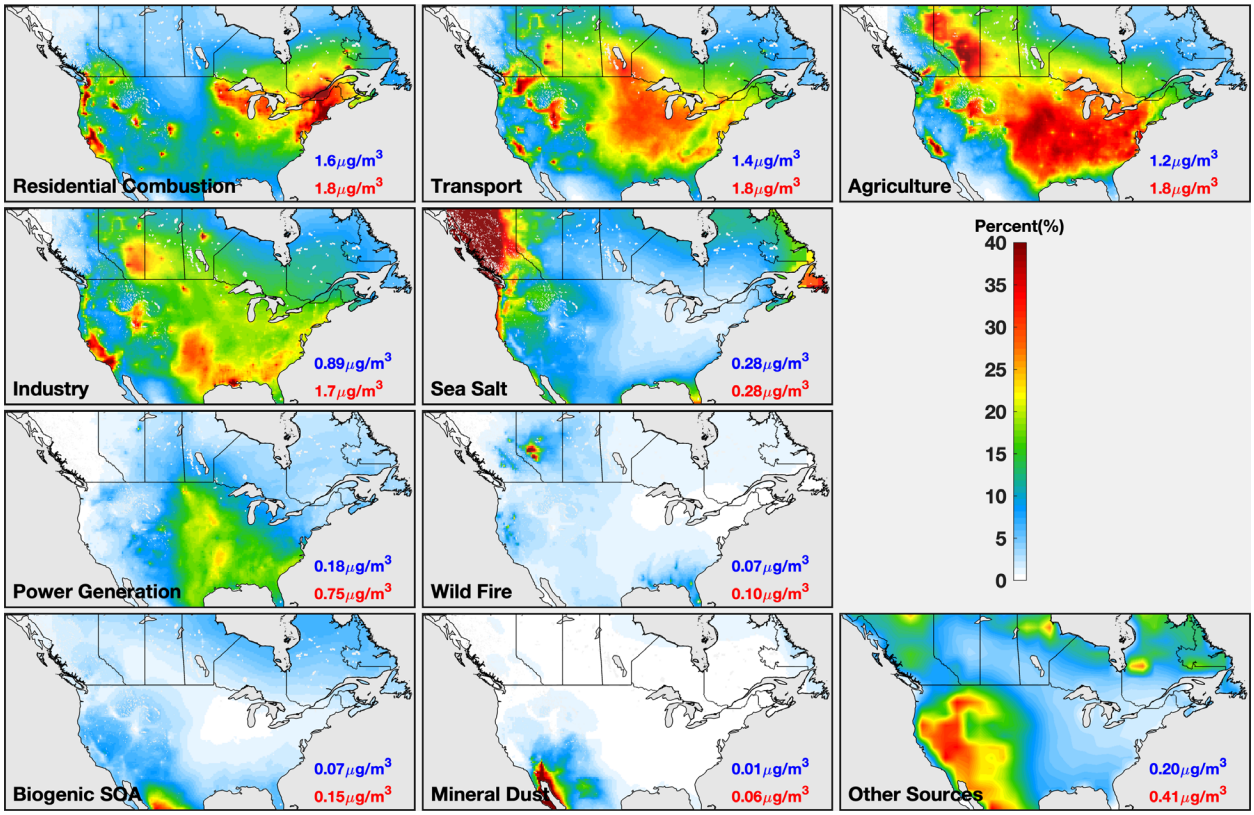

Figure 3-S4. Contribution of individual emission sector to $PM_{2.5}$ concentrations in winter (December, January, February). Other Sources includes volcano, dimethyl sulfide (DMS), and long-range transport (LRT) from Asia, Europe and Alaska. Inset values are population-weighted annual mean $PM_{2.5}$ concentrations attributing to each sector over the U.S. (red) and Canada (blue). Figure was created using MATLAB_R2016b.

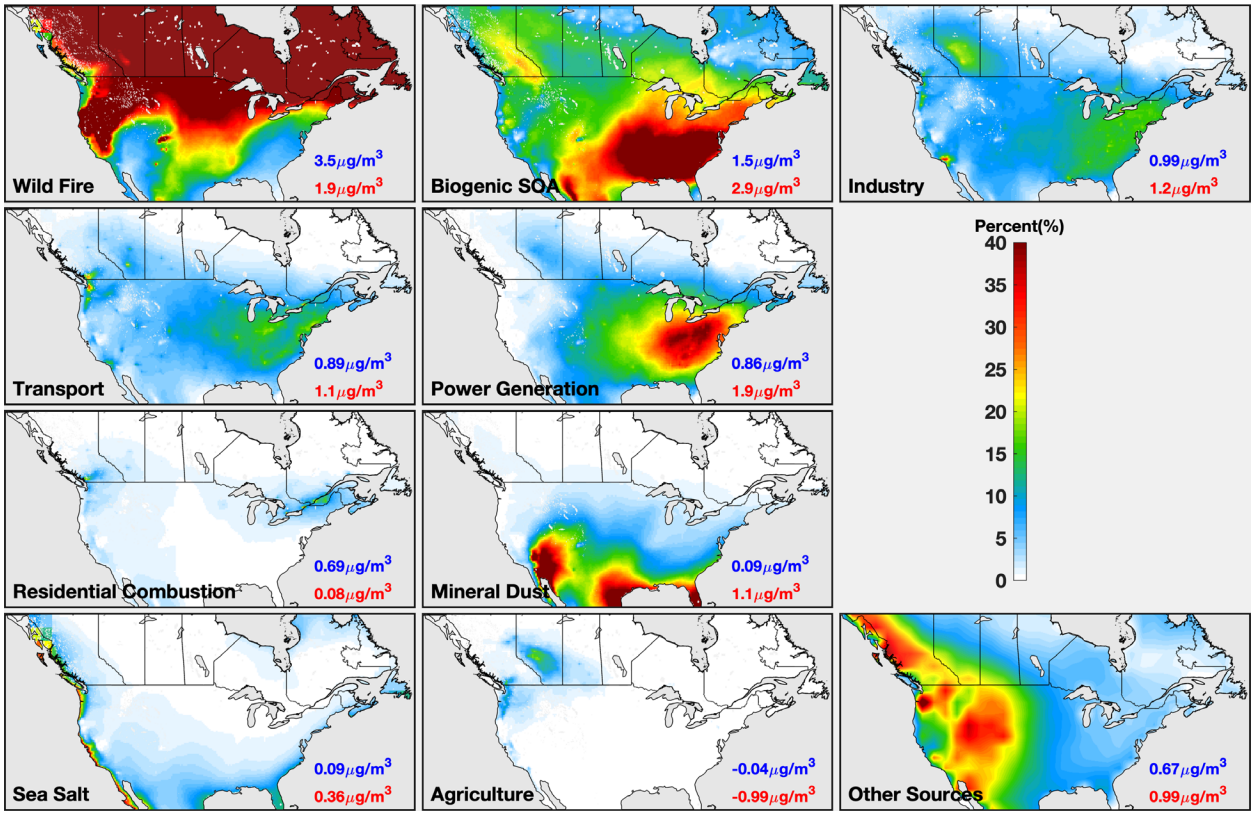

Figure 3-S5. As in Figure 3-S4 but in summer (June, July, August). Figure was created using MATLAB_R2016b.

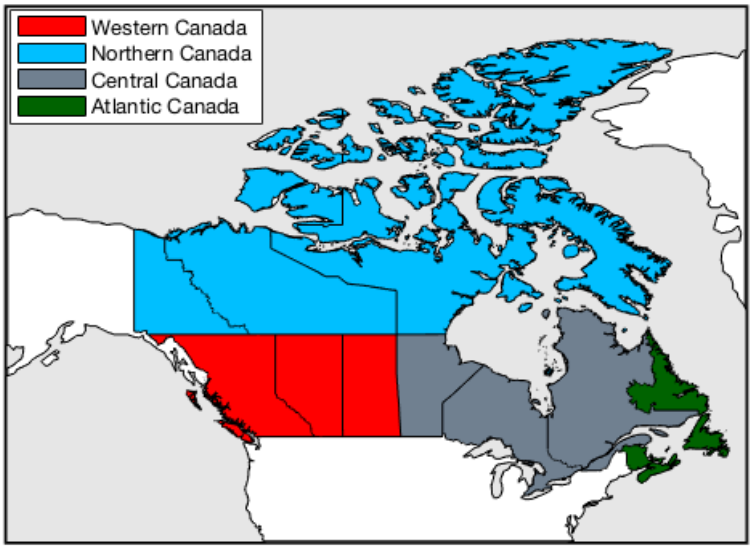

Figure 3-S6. Domain of regions in Canada. Figure was created using MATLAB_R2016b.

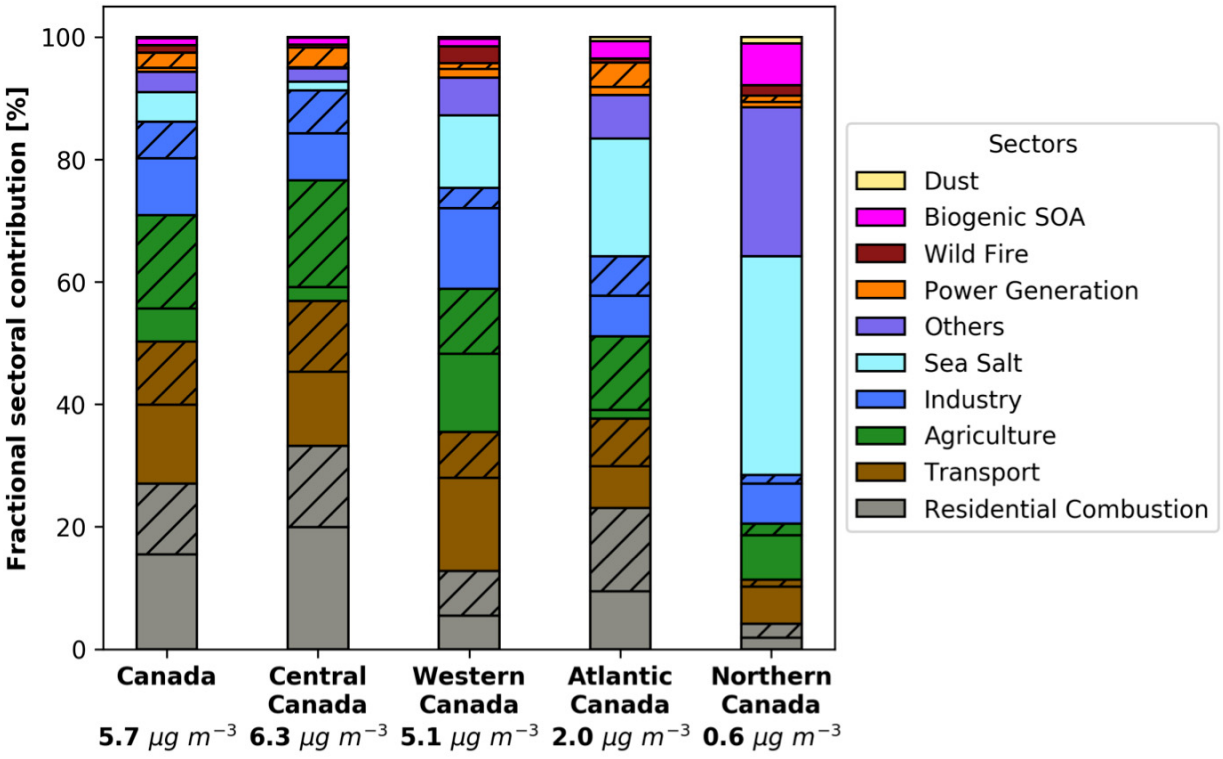

Figure 3-S7. Fractional contribution of different sectors to population-weighted average $PM_{2.5}$ concentrations over different regions in Canada in winter (December, January, February). The number under each bar represents the total population-weighted annual mean $PM_{2.5}$ concentrations over that region. The hatched part in each sector represents the fractional contribution from the United States. Others include dimethyl sulfide (DMS), volcano, and long-range transport (LRT) from Asia, Europe and Alaska.

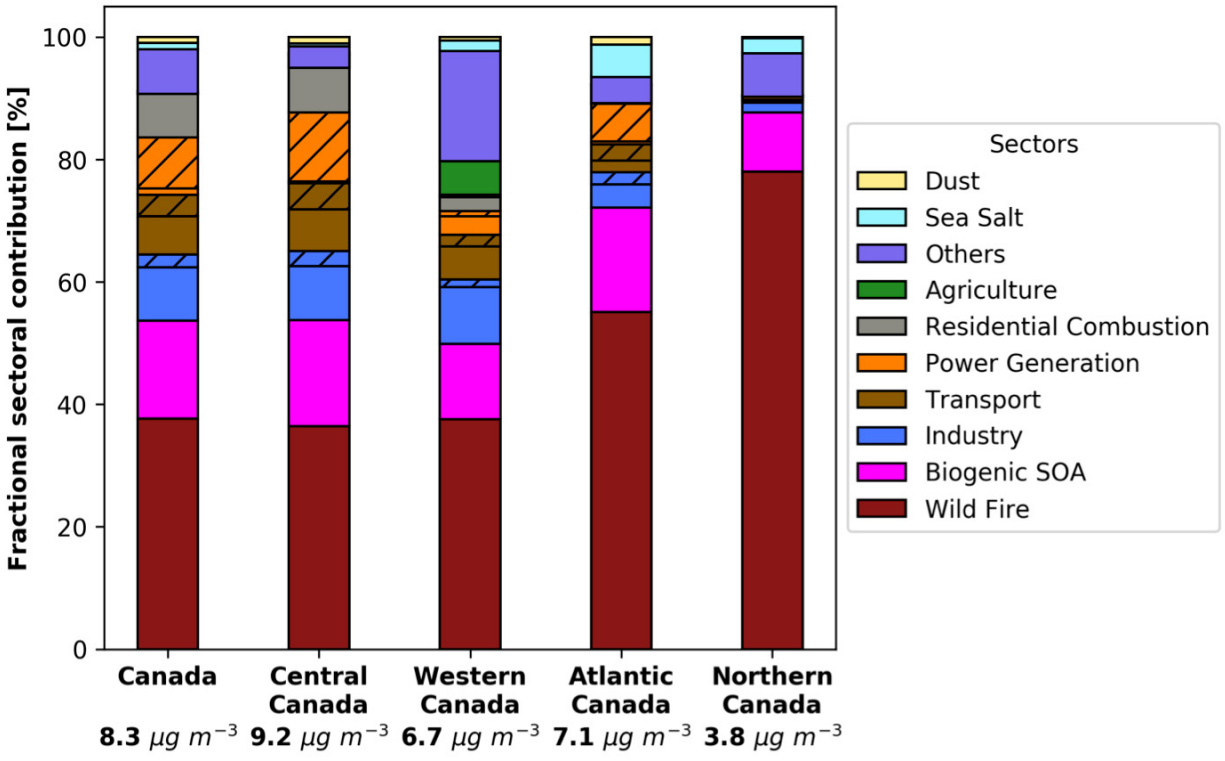

Figure 3-S8. As in Figure 3-S7 but in summer (June, July, August).

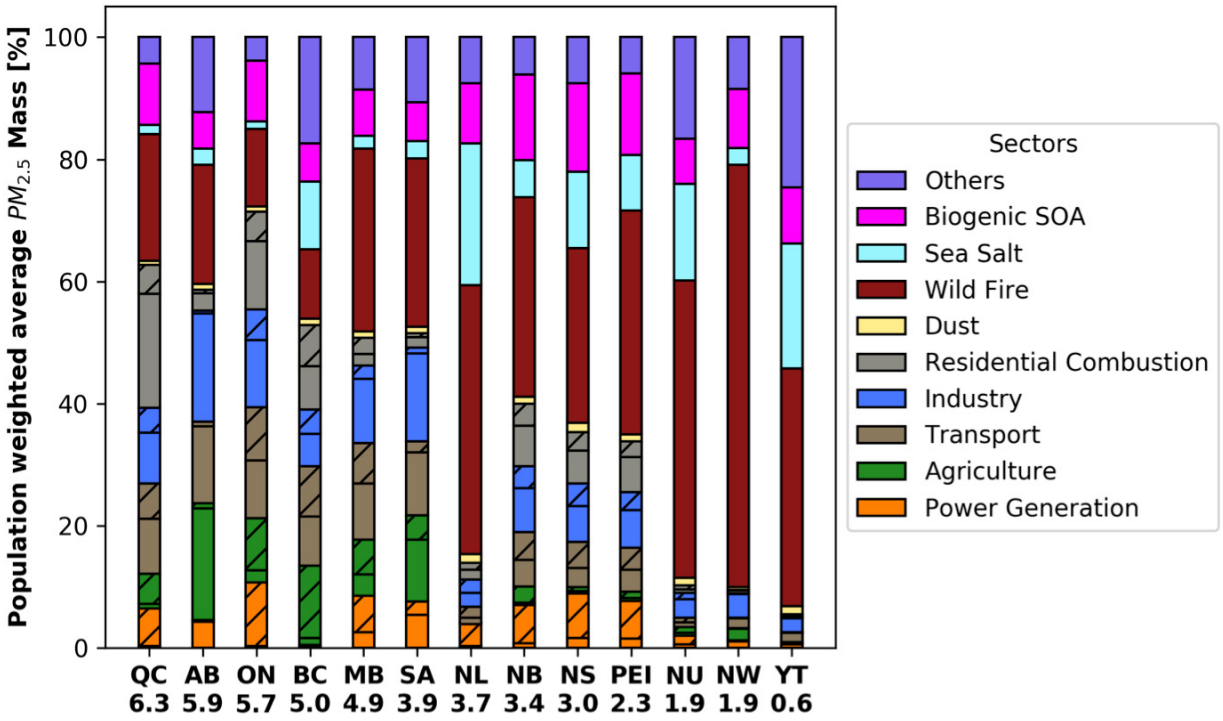

Figure 3-S9. Fractional contribution of different sectors to population-weighted average $PM_{2.5}$ concentrations over different provinces in Canada. The number under each bar represents the total population-weighted annual mean $PM_{2.5}$ concentrations over that region. The hatched part in each sector represents the fractional contribution from the United States. Others include dimethyl sulfide (DMS), volcano, and long-range transport (LRT) from Asia, Europe and Alaska.

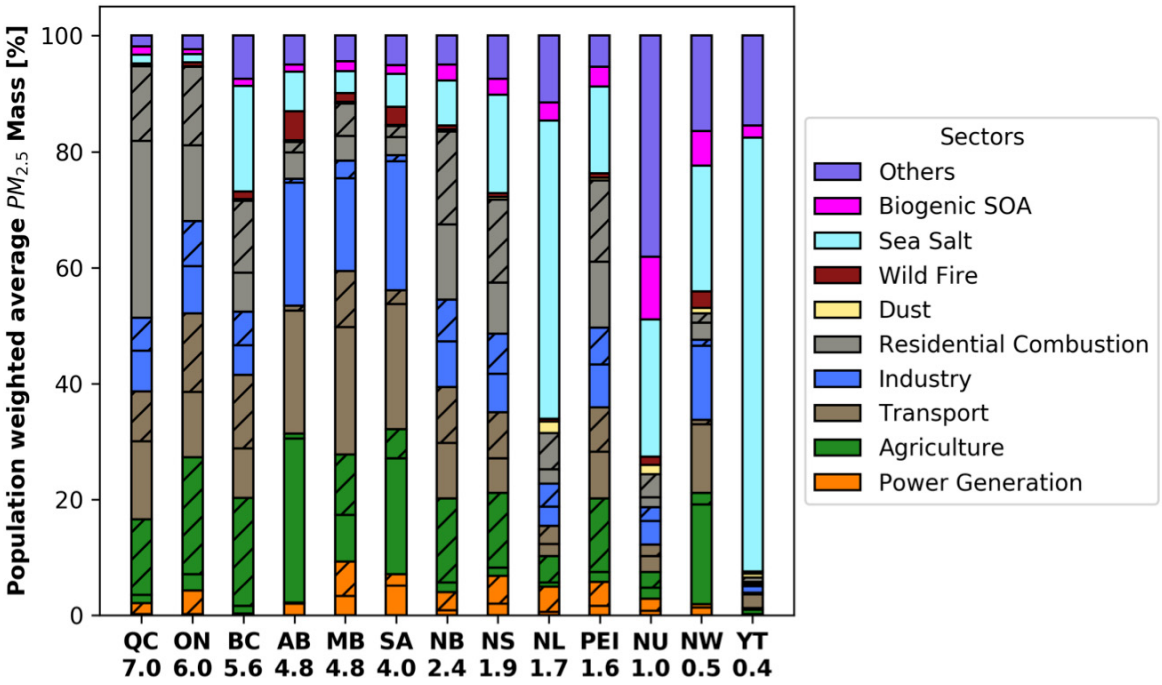

Figure 3-S10. As in Figure 3-S9 but averaged over winter (December, January, February).

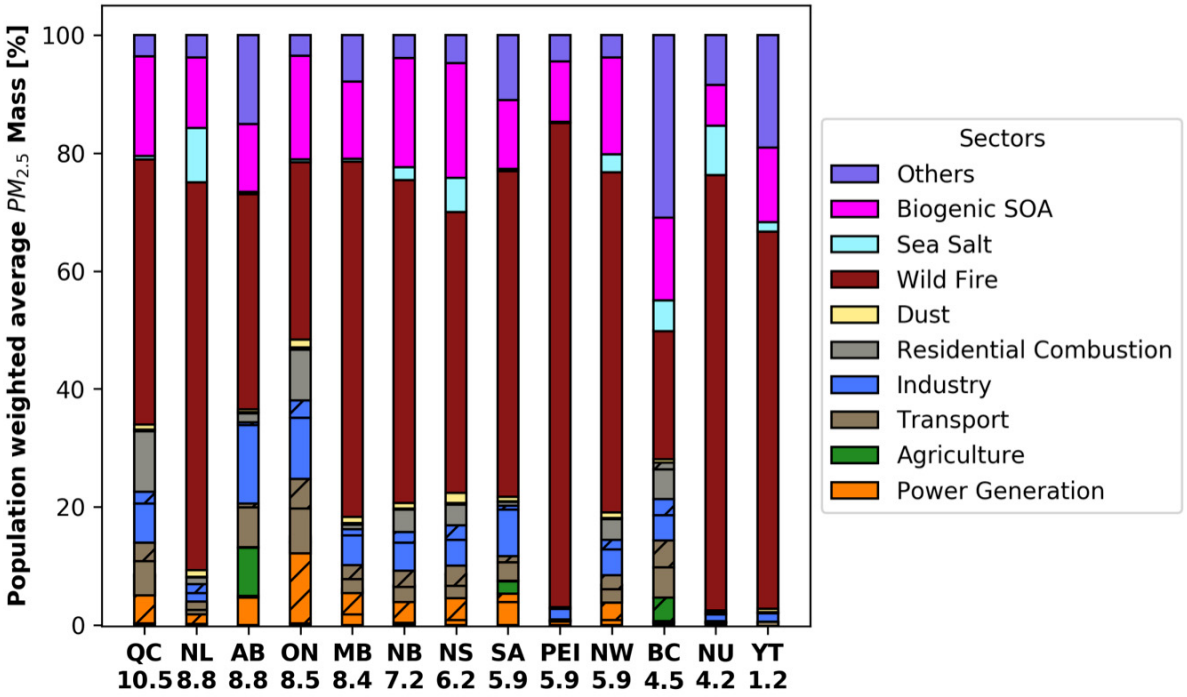

Figure 3-S11. As in Figure 3-S9 but averaged over summer (June, July, August).

(a)

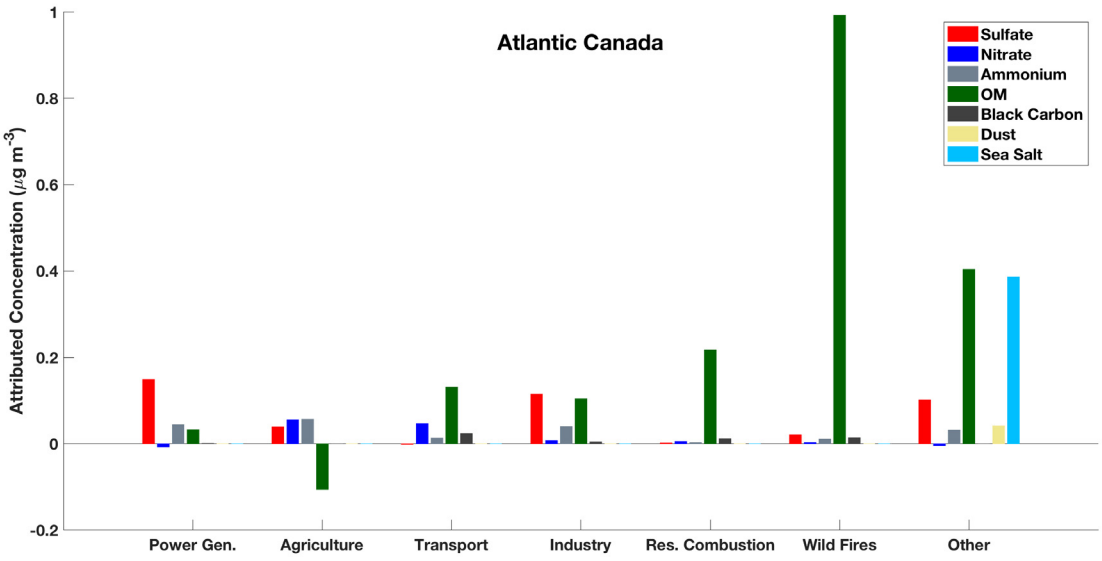
Atlantic Canada
Attributed Concentration (μg m^{-3})
1
0.8
0.6
0.4
0.2
0
-0.2
Sulfate
Nitrate
Ammonium
OM
Black Carbon
Dust
Sea Salt
Power Gen.
Agriculture
Transport
Industry
Res. Combustion
Wild Fires
Other

(b)

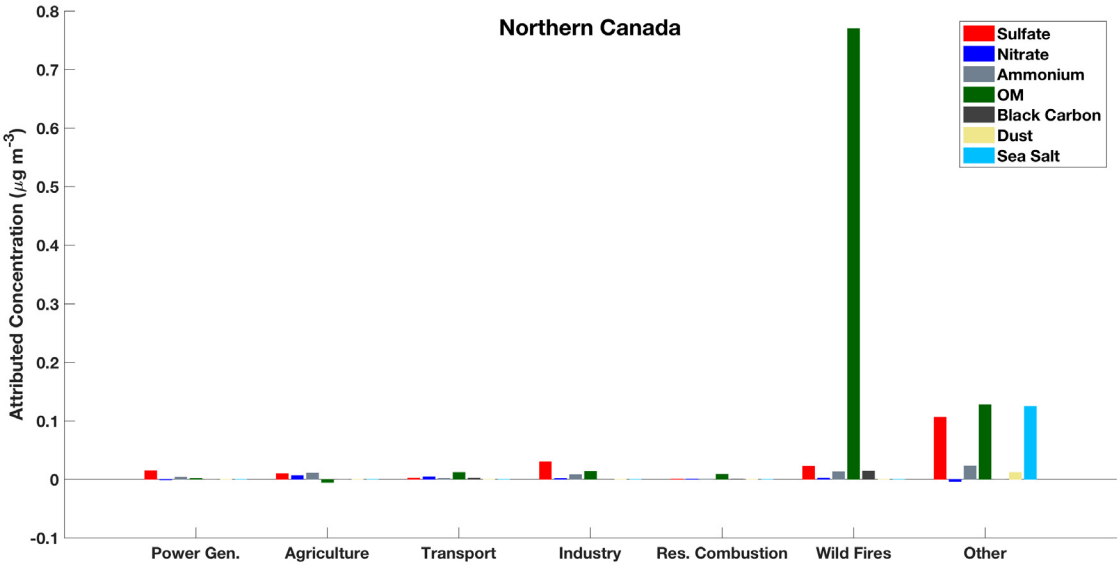
Northern Canada
Attributed Concentration (μg m^{-3})
0.8
0.7
0.6
0.5
0.4
0.3
0.2
0.1
0
-0.1
Sulfate
Nitrate
Ammonium
OM
Black Carbon
Dust
Sea Salt
Power Gen.
Agriculture
Transport
Industry
Res. Combustion
Wild Fires
Other

(c)

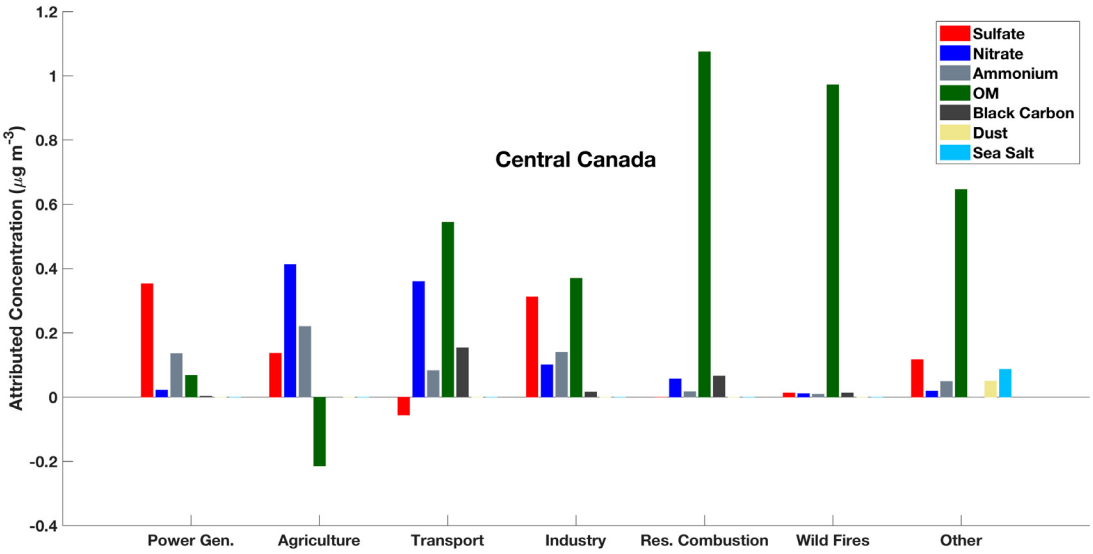

(d)

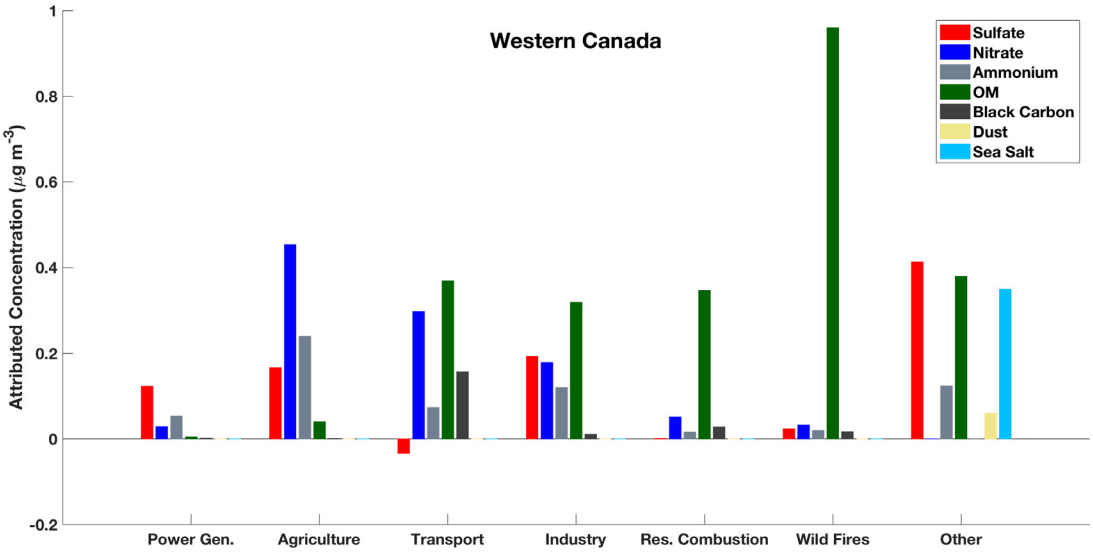

Figure 3-S12. Population-weighted annual mean concentration of chemical components (μg m^{-3}) attributed to different sectors over Atlantic, Northern, Central and Western Canada. Other includes dimethyl sulfide (DMS), volcano, biogenic secondary organic aerosol (SOA) and long-range transport (LRT) from Asia, Europe and Alaska. Figure was created using MATLAB_R2016b.

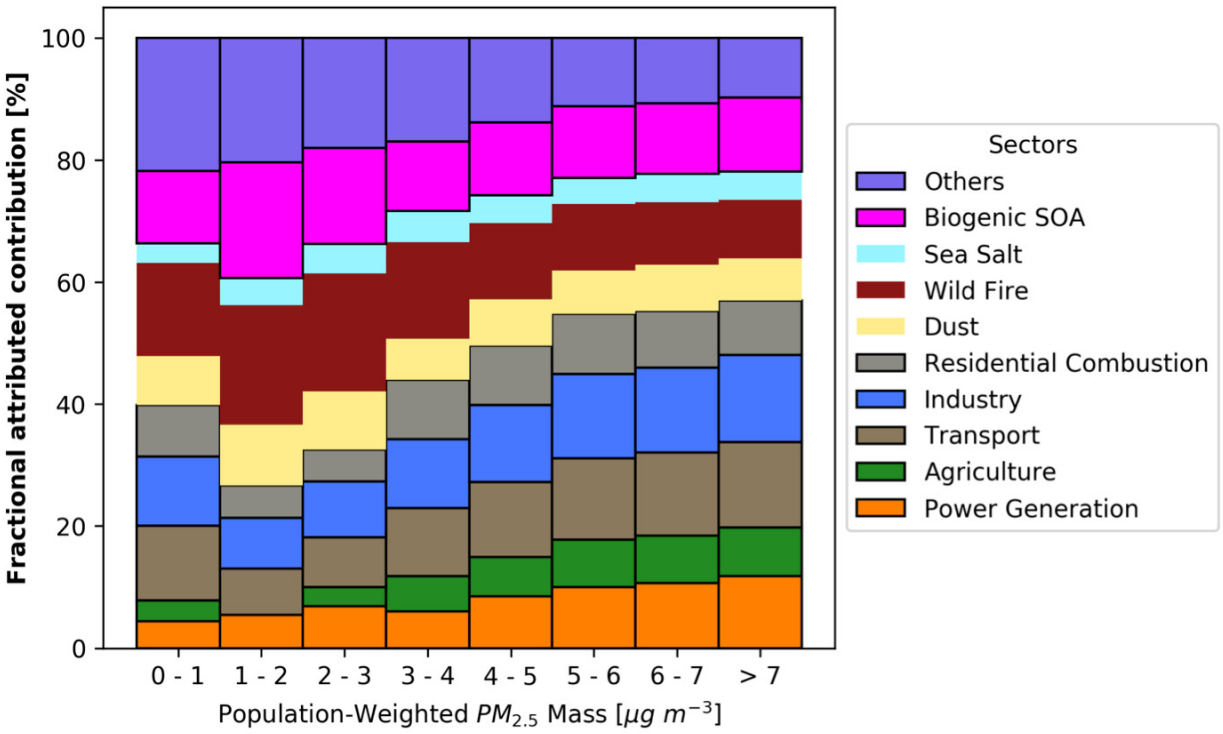

Figure 3-S13. Population-weighted sectoral fractional contribution versus population-weighted $PM_{2.5}$ mass over the United States. Stacked bar plots show percentage of each sector in different $PM_{2.5}$ levels. Other includes dimethyl sulfide (DMS), volcano, and long-range transport (LRT) from Asia, Europe and Alaska.

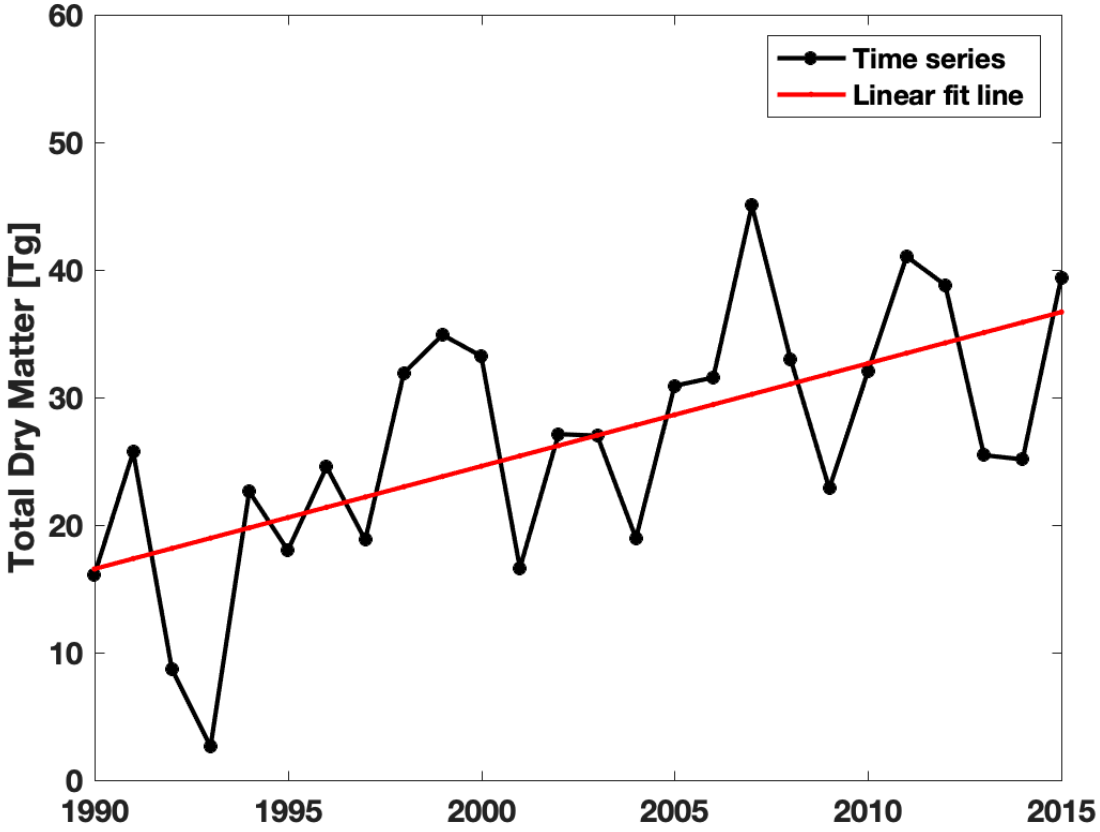

Figure 3-S14. Annually total dry matter over Canada from wildfire emission inventories in the simulation (1990 to 1996 from ground-based North America fire emission database;1997 to 2015 from GFED). Figure was created using MATLAB_R2016b.

CHAPTER 4 Grid-independent high resolution dust emissions for chemical transport models: application to GEOS-Chem

Authors: Jun Meng[1,2,*], Randall V. Martin[2,1,3], Paul Ginoux[4], Melanie Hammer[2,1], Melissa S. Payer[5], David A. Ridley[6], Aaron van Donkelaar[1,2]

Affiliations:
[1]Department of Physics and Atmospheric Science, Dalhousie University, Halifax, Nova Scotia, B3H 4R2, Canada
[2] Department of Energy, Environmental & Chemical Engineering, Washington University in St. Louis, St. Louis, Missouri 63130, United States
[3]Smithsonian Astrophysical Observatory, Harvard-Smithsonian Center for Astrophysics, Cambridge, MA 02138, USA
[4]NOAA Geophysical Fluid Dynamics Laboratory, Princeton, New Jersey 08540, USA
[5]School of Engineering and Applied Science, Harvard University, Cambridge, MA 02138, USA
[6]California Environmental Protection Agency, Sacramento, CA 95814, USA

The material in this chapter will be submitted to Earth System Science Data journal.

4.1 ABSTRACT

The nonlinear dependence of the dust saltation process on wind speed poses a challenge for models of varying resolutions. This challenge is of particular relevance for the next generation of chemical transport models with nimble capability for multiple resolutions. We develop and apply a method to harmonize dust emissions across simulations of different resolutions by generating offline grid independent dust emissions driven by native high resolution meteorological fields.

We implement into the GEOS-Chem chemical transport model a high resolution dust source function to generate updated offline dust emissions. These updated offline dust emissions based on high resolution meteorological fields can better resolve weak dust source regions, such as in southern South America, southern Africa and the southwestern United States. Identification of an appropriate dust emission strength is facilitated by the resolution independence of offline emissions. We find that the performance of simulated AOD versus measurements from the AERONET network and satellite remote sensing improves significantly when using the updated offline dust emissions with the total global annual dust emission strength of 2,000 Tg yr^{-1}rather than the standard online emissions in GEOS-Chem. The offline high resolution dust emissions are easily implemented in chemical transport models, with potential to promote module model development and evaluation.

4.2 Introduction

Mineral dust, as one of the most important natural aerosols in the atmosphere, has significant impacts on weather and climate by absorbing and scattering solar radiation (Bergin et al., 2017; Kosmopoulos et al., 2017), on atmospheric chemistry by providing surfaces for heterogeneous reaction of trace gases (Chen et al., 2011; Tang et al., 2017), on the biosphere by fertilizing the tropical forest (Bristow et al., 2010; H. Yu et al., 2015), and on human health by increasing surface $PM_{2.5}$ concentrations (De Longueville et al., 2010; Fairlie et al., 2007). Dust emissions are primarily controlled by surface wind speed, vegetation cover and soil water content. The principal mechanism for natural dust emissions is saltation bombardment (Gillette & Passi, 1988; Shao et al., 1993), in which sand-sized particles creep forward and initiate the suspension of smaller dust particles when the surface wind exceeds a threshold. The nonlinearity

of this process introduces an artificial dependence of simulations upon model resolution (Ridley et al., 2013). For example, dust emissions in most numerical models are parameterized with an empirical method (e.g. Ginoux et al., 2001; Zender et al., 2003), which requires a critical wind threshold to emit dust particles. Methods are needed to address the artificial dependence of simulations upon model resolution that arises from this nonlinearity in dust emissions.

Addressing this nonlinearity is especially important for the next generation of chemistry transport models that is emerging with nimble capability for a variety of resolutions at the global scale. For example, the high performance version of GEOS-Chem (GCHP) (Eastham et al., 2018) currently offers simulation resolutions from C24 (~ 4°x5°) to C360 (~0.25°), with progress toward even finer resolution and toward a variable stretched grid capability. Resolution-dependent mineral dust emissions would vary by a factor of 3 from C360 to C24, and inhibit interpretation (Ridley et al., 2013). Grid-independent high resolution dust emissions offer a potential solution to this concern.

An important capability in global dust evaluation is ground-based and satellite remote sensing. AERONET, a global ground-based remote sensing aerosol monitoring network of Sun photometers (Holben et al., 1998), has been widely used to evaluate dust simulations. Satellite remote sensing provides additional crucial information across arid regions where in-situ observations are sparse (Hsu et al., 2013). Satellite aerosol retrievals have been used extensively in previous studies to either evaluate the dust simulation (Ridley et al., 2012, 2016) or constrain the dust emission budget (Zender et al., 2004). Satellite aerosol products have been used to identify dust sources worldwide (Ginoux et al., 2012; K. Schepanski et al., 2012; Y. Yu et al., 2018), especially for small-scale sources (Gillette, 1999).

The objective of this study is to develop a method to mitigate the inconsistency of total dust emissions across different resolution of simulations by generating and archiving an offline dust emissions using native high resolution meteorological fields. We apply this method to GEOS-Chem chemical transport model. As part of this effort, we implement an updated high resolution satellite-identified dust source function into the dust mobilization module of GEOS-Chem to better represent the spatial structure of dust sources. We apply this new capability to assess the source strength that best represents observations.

4.3 Materials and Methods

4.3.1 Description of Observations

We use both ground-based and satellite observations to evaluate our GEOS-Chem simulations. AERONET is a global ground-based remote sensing aerosol monitoring network of Sun photometers with direct sun measurements every 15 minutes (Holben et al., 1998). We use Level 2.0 Version 3 data that has improved cloud screening algorithms (Giles et al., 2019). AOD at 550 nm is interpolated based on the local angstrom exponent at the 440 nm and 670 nm channels.

Twin Moderate-Resolution Imaging Spectroradiometer (MODIS) instruments were launched aboard both on the Terra and Aqua NASA satellite platforms and provide near daily measurements globally. We use the AOD at 550 nm retrieved from Collection 6.1 (C6) of MODIS product (Sayer et al., 2014). We use AOD from the Deep Blue (DB) retrieval algorithm (Hsu et al., 2013; Sayer et al., 2014) designed for bright surfaces, and the Multi-Angle Implementation of Atmospheric Correction (MAIAC) algorithm (Lyapustin et al., 2018), which

provides global AOD retrieved from MODIS C6 radiances at a resolution of 1 km. The MAIAC AOD used in this study is interpolated to the AOD value at 550 nm.

We compare the simulated fine AOD with measurements using reduced major axis linear regression. We report root mean square error (E), correlation (R) and slope (M).

4.3.2 Dust Mobilization Module

We use the dust detrainment and deposition (DEAD) scheme (Zender et al., 2003) in the GEOS-Chem model to calculate dust emissions. The saltation process is dependent on the critical threshold wind speed, which is determined by surface roughness, soil type and soil moisture. We use a fixed soil clay fraction of 0.2 as suggested in Zender et al. (2003). Dust aerosol is transported in four size bins (0.1-1.0, 1.0-1.8, 1.8-3.0, and 3.0-6.0 μm radius). Detailed description of the dust emission parameterization is in section 4.7.

The fractional area of land with erodible dust is represented by a source function. The dust source function used in the dust emission module plays an important role in determining the spatial distribution of dust emissions. The standard GEOS-Chem model (version 12.5.0) uses a source function at 2° x 2.5° resolution from Ginoux et al. (2001) as implemented by Fairlie et al. (2007). We implement an updated high resolution version of the dust source function in this study at 0.25° x 0.25° resolution. Figure 4-S1 shows a map of the original and updated version of the dust source function. The updated source function exhibits more spatially resolved information due to its finer spatial resolution resulting in a higher fraction of erodible dust over in the eastern Arabian Peninsula, the Bodélé depression, and the central Asian deserts. The dust module dynamically applies this source function, together with information on soil moisture, vegetation, and land use to calculate hourly emissions using the HEMCO module described below.

4.3.3 Offline Dust Emissions at Native Meteorological Resolution

HEMCO (Keller et al., 2014) is a stand-alone software module for computing emissions in global atmospheric models. We run the HEMCO standalone version using native meteorological resolution (0.25° x 0.3125°) data to archive the offline dust emissions at the same resolution as the meteorological data. In this study, we generate two offline dust emission datasets at 0.25° x 0.3125° resolution. One, referred to as the default offline dust emissions, uses the existing dust source function in the dust module; the other, referred to as the updated offline dust emissions, uses the updated dust source function implemented here. Both datasets are at the hourly resolution of the parent meteorological fields. The archived native resolution offline dust emissions can be an input emission inventory for chemical transport models with scalable dust source strengths. We use the GEOS-Chem model to evaluate the dust simulations and the emission strength.

4.3.4 GEOS-Chem Chemical Transport Model and Simulation Configurations

GEOS-Chem (The International GEOS-Chem User Community, 2019) is a three-dimensional chemical transport model driven by assimilated meteorological data from the Goddard Earth Observation System (GEOS) of the NASA Global Modelling and Assimilation Office (GMAO). The GEOS-Chem aerosol simulation includes the sulfate-nitrate-ammonium (SNA) aerosol system (Fountoukis & Nenes, 2007; Park et al., 2004), carbonaceous aerosol (Hammer et al., 2016; Park et al., 2003; Q. Wang et al., 2014), secondary organic aerosols (Marais et al., 2016; Pye et al., 2010), sea salt (Jaeglé et al., 2011) and mineral dust (Fairlie et al., 2007) with updates to aerosol size distribution (Ridley et al., 2012; L. Zhang et al., 2013). We

include dry and wet deposition (Liu et al., 2001) processes in the model. Gravitational settling for dust is from Fairlie et al. (2007).

The original GEOS-Chem simulation used online dust emissions by coupling the dust mobilization module online. We develop the capability to use offline dust emissions based on the archived fields described in Section 4.3.3 as input emission inventory. We conduct global simulations with GEOS-Chem (version 12.5.0) at a horizontal resolution of 2° by 2.5° for the year 2016. Simulations using the online and offline dust emissions are conducted to evaluate the offline dust emissions. We conduct two simulations using online dust emissions with different dust source functions. The first is with the original version of dust source function. The other one is with the updated version of source function. The annual total emissions for the online dust emissions are at the original value of 909 Tg yr^{-1}. We conduct another two sets of simulations using offline dust emissions. The first uses the default offline dust emissions with the annual total dust emissions of 909 Tg yr^{-1}. The second uses the updated offline dust emissions with the annual total dust emissions scaled to 2,000 Tg yr^{-1}, which is in the range of the current dust emission estimates of over 426 - 2726 Tg yr^{-1} (Huneeus et al., 2011) and better represents observations as will be shown below.

We calculate AOD at 550 nm in the model with the assumption of lognormal size distributions of externally mixed aerosols as a function of local relative humidity. Aerosol optical properties are based on the Global Aerosol Data Set (GADS) as implemented by Martin et al. (2003) with updates based on measurements (Drury et al., 2010; Latimer & Martin, 2019).

4.4 Results and Discussion

4.4.1 The Spatial and Seasonal Variation of Offline Dust Emissions

Figure 4-1 shows the spatial distribution of the annual and seasonal dust emission flux rate for the updated offline dust emissions. The annual dust emission flux rate is high over major deserts, such as the northwestern Sahara, the Bodélé Depression in northern Chad, eastern Arabian Peninsula and central Asian Taklimakan and Gobi deserts. There are also hotspots of dust emission flux rate over relatively smaller deserts, such as the Mojave Desert of the southwestern United States, the Atacama Desert of southern South America, the Kalahari Desert on the west coast of southern Africa and the deserts in central Australia. Those features reflect the fine resolution of the updated dust source function and of the offline dust emissions. Seasonally, the dust emission flux rate resembles the annual distribution, however, with a lower dust emission flux rate over the Bodélé Depression in northern Chad in summer and higher dust emission flux rate over the Middle East and central Asian deserts in spring and summer.

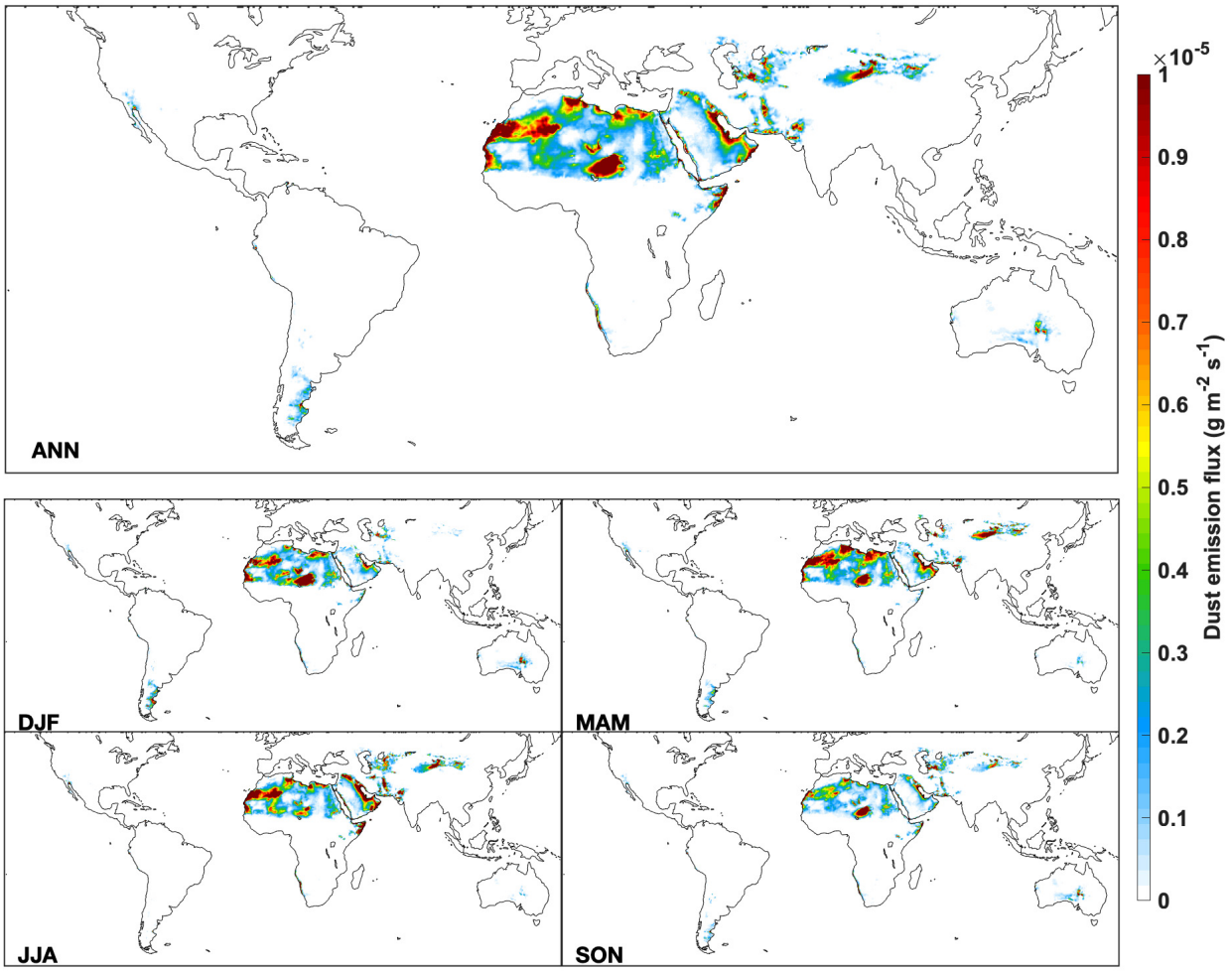

Figure 4-1. Annual and seasonal mean dust emission flux rate for the offline high resolution dust emissions with updated dust source function and updated annual total dust emissions of 2,000 Tg.

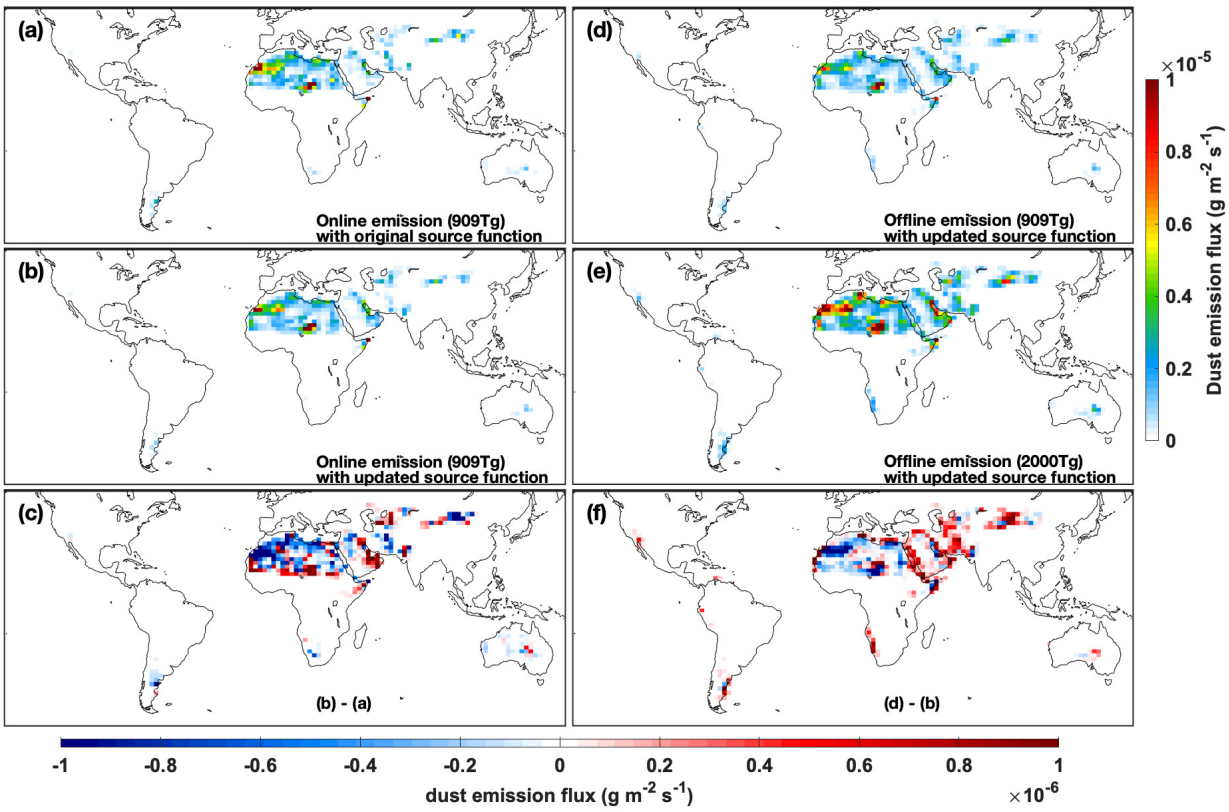

Figure 4-2. Annual mean dust emission flux rate for 2016. (a), The original online dust emissions with original dust source function and annual total dust emissions of 909 Tg. (b), Online dust emissions with updated dust source function. (c), Difference of flux rate between online dust emissions using original and updated dust source functions. (d), Offline dust emissions with updated dust source function. (e), Offline dust emissions with updated dust source function and updated annual total dust emissions of 2,000 Tg. (f), Difference of flux rate between offline and online dust emissions. The online dust emissions are in 2° x 2.5° resolution. The offline dust emissions shown in (b), (d), (f) are regridded from 0.25° x 0.3125° resolution for comparison with online dust emissions.

Figure 4-2 shows the spatial distribution of the annual dust emission flux rate for the online and offline dust emissions with the original and updated dust source functions with original and updated global total dust source strengths. All simulations exhibit high dust emission flux rate over major desert regions, such as the Sahara, Middle East and Central Asian deserts, with local enhancements over the western Sahara and northern Chad. The simulation

with the updated source function exhibits stronger emissions in the Sahara and Persian Gulf regions (Figure 4-2c). The difference between the online and offline dust emissions, shown in Figure 4-2f, indicates that the offline dust emissions based on native resolution meteorological fields have lower dust emission flux rates over northwest Africa, but higher dust emission flux rates over the Middle East and Central Asia. Higher annual dust emission flux rates over the southwestern United States, southern South America, west coast of southern Africa and central Australia in the offline dust emissions reflect that the native resolution offline dust emissions are strengthened over relatively weaker dust emission regions. Generally, coastal and minor desert regions emit more dust when calculating emissions at the native meteorological resolution.

Figures 4-S2 – S5 show the seasonal variations of dust emission flux rates for online and offline emissions. The offline dust emissions have lower emission flux rates than the online dust emissions during spring (March, April and May) (MAM) and winter (December, January and February) (DJF) over the Sahara Desert. The offline dust emission flux rate is higher than the online dust emission flux rate over the Middle East and Central Asian deserts during spring and summer (June, July and August) (JJA). Emission flux rates are low over Central Asian deserts during winter. The strengthening of offline dust emissions over weaker dust emitting regions persists throughout all seasons.

4.4.2 The Performance of AOD Simulations over Desert Regions

Figure 4-3 shows simulated AOD using the original online and updated offline dust emissions. We select for evaluation the AERONET sites where the ratio of simulated dust optical depth (DOD) to simulated total AOD exceeds 0.5 in the simulation using the updated offline dust emissions. Annually, the simulated DOD has the highest value over the Bodélé Depression. This

feature persists in all seasons except summer when DOD has the highest values over the western Sahara and eastern Arabian Peninsula. The scatter plots show that annually the simulated AOD from both simulations are highly correlated with AERONET measurements across the dust regions (R= 0.86 – 0.88). The simulation with updated offline dust emissions has an improved slope and smaller root mean square error than the simulation using the original online dust emissions. AOD from the simulation with updated offline dust emissions are also more consistent with the measurements in different seasons, especially in the spring (MAM) and fall (SON) with slopes close to unity and R exceeding 0.9.

We further evaluate the performance of simulated AOD over major desert regions using the MODIS DB and MAIAC AOD products. Figure 4-4 shows annual and seasonal scatter plots comparing GEOS-Chem simulated AOD using original online dust emissions and updated offline dust emissions against retrieved AOD from MODIS DB and MAIAC satellite products over the three major desert regions outlined in Figure 4-3. Figure 4-S6 shows the annual and seasonal AOD distribution from MODIS DB and MAIAC. Annually, the simulation using updated offline dust emissions exhibits greater consistency with satellite AOD than does the simulation using original online dust emissions across all three desert regions. The simulation using updated offline dust emissions performs better across all three desert regions and in all four seasons except for the Sahara in summer, during which AOD is overestimated. Both simulations underestimate AOD over central Asian deserts during winter when dust emissions are low and other sources may be more important. Overall, the simulation using original online dust emissions underestimates AOD over all three major desert regions, especially over the Middle East and central Asian deserts. The simulation using updated offline dust emissions exhibits greater consistency with satellite observations with higher slopes and correlations.

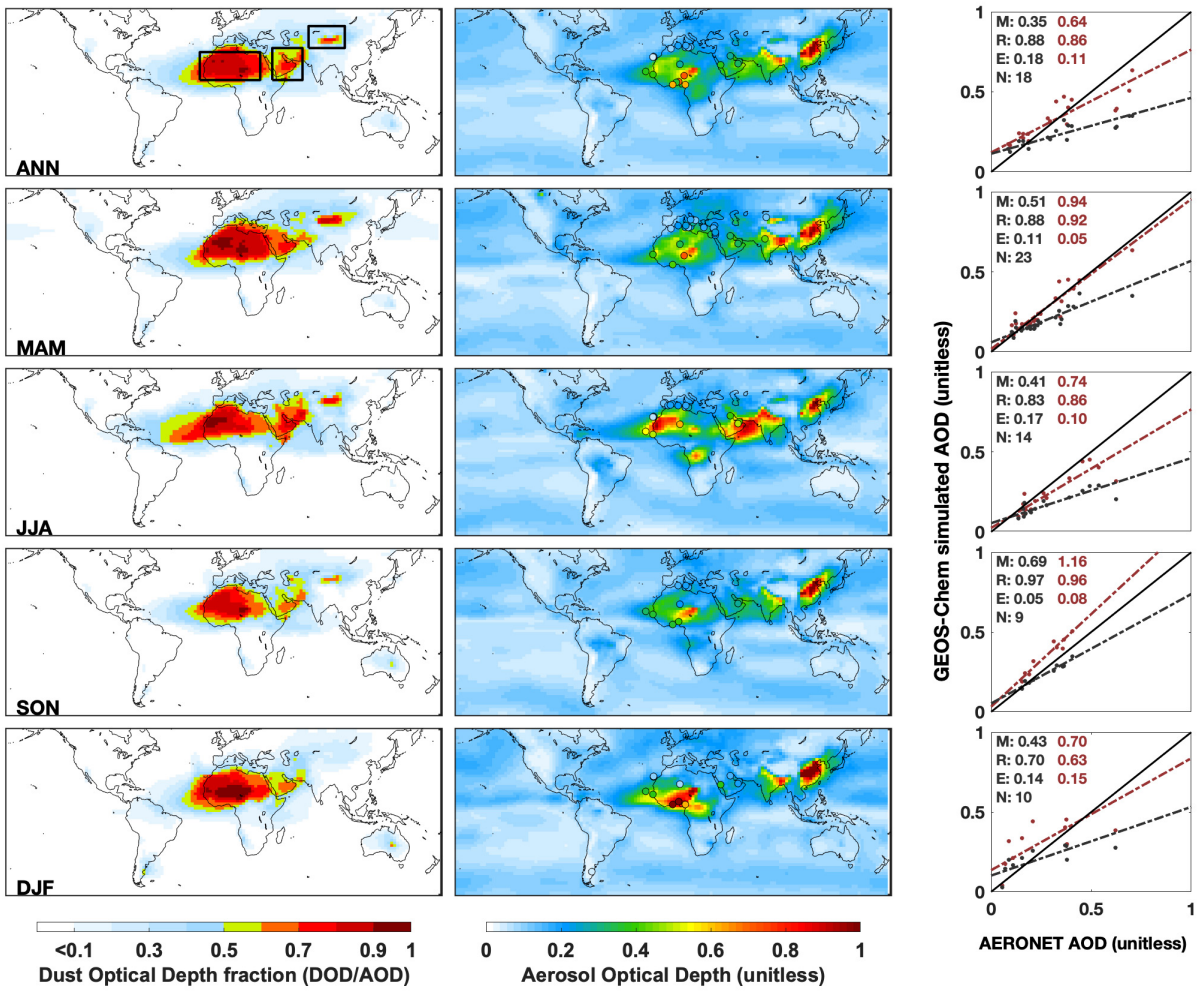

Figure 4-3. Annual and seasonal mean simulated dust optical depth (DOD) fraction (left column) and aerosol optical depth (AOD) (middle column) from GEOS-Chem simulations for 2016, and AERONET measured AOD at sites where the ratio of simulated DOD and AOD exceeds 0.5, which are shown as filled circles in the middle column. Boxes in the left top panel outline the three major deserts examined in Figure 4-4. The right column shows the corresponding scatter plot with root mean square error (E), correlation coefficient(R) and slope (M) calculated with reduced major axis linear regression. N is the number of valid ground-based monitoring records. The results for the simulation using the original dust emissions are shown in black; the results for the simulation using updated dust emissions are shown in red. The best fit lines are dashed. The 1:1 line is solid.

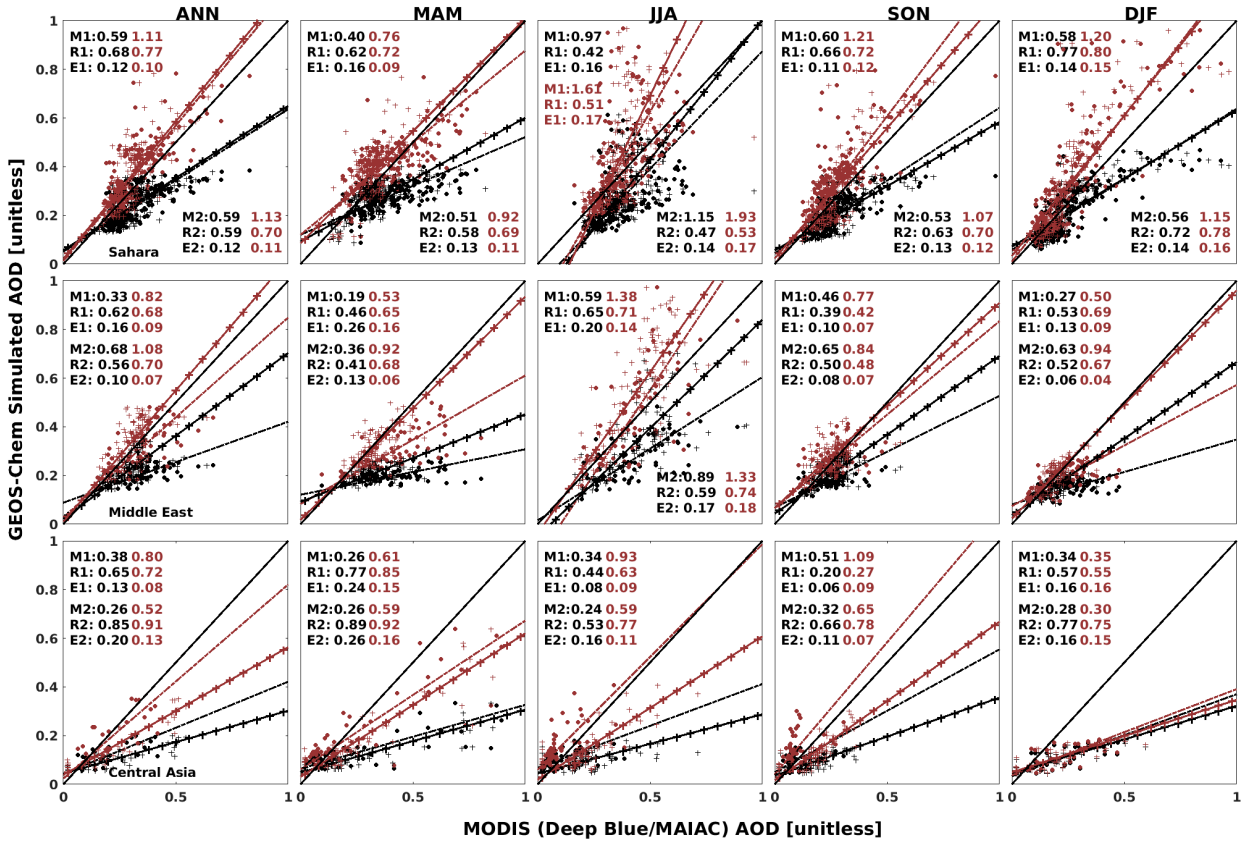

Figure 4-4. Scatter plots and statistics of comparing GEOS-Chem simulated AOD with satellite AOD over desert regions annually (the first column) and seasonally (the right four columns). The results for Sahara, Middle East and Central Asia deserts are shown in the top, middle and bottom rows respectively. The results for the simulation using the original dust emissions are shown in black; the results for the simulation using updated dust emissions are shown in red. Dots represent the comparison with MODIS Deep Blue (DB) AOD; the plus signs represent the comparison with MAIAC AOD. Correlation coefficient(R), root mean square error (E), and Slope (M) are reported, in which R1, E1 and M1 show the results of the comparison with MODIS DB AOD; R2, E2 and M2 show the results of the comparison with MAIAC AOD. The best fit lines are dashed lines with corresponding marker signs and colors. The 1:1 line is solid black line.

4.4.3 Discussion of the Dust Source Strength

One of the advantages of the offline dust emissions is that the dust source strengths are scalable. We have found that the simulation with global total annual dust emissions scaled to 2,000 Tg better represents observations than does the default simulation with global total annual

dust emissions of 909 Tg. We also evaluate simulations with global total annual dust emissions scaled to 1,500 Tg and 2,500 Tg. Figure 4-S7 indicates that the simulation with global total annual dust emissions scaled to 2,000 Tg is more consistent with satellite observations over the Sahara and Middle East. Although the central Asian deserts and regions with AERONET observations (Figure 4-S8) are better represented by the simulation with global total annual dust emissions scaled to 2,500 Tg, since the Sahara has highest dust emissions (Huneeus et al., 2011), and AOD over the Sahara is most likely dominated by dust, we scale global total annual dust emissions to best match this source region. Additional development and evaluation should be conducted to further narrow the uncertainty of dust emissions, especially at the regional scale.

4.4.4 Advantages of High Resolution Offline Dust Emissions for Model Development

Uncertainty remains in the estimated global annual total dust emissions. Direct dust emission flux observations are few. Current atmospheric and chemical transport models apply a global scale factor to optimize with a specific set of ground observations. Because of the non-linear dependence on resolution of the dust emissions, the source strength has historically depended upon model resolution, which inhibits general evaluation. The native resolution offline dust emissions facilitate consistent evaluation and application across all model resolutions.

4.5 Summary and Conclusion

The nonlinear dependence of dust emission parameterizations upon model resolution poses a challenge for the next generation of chemical transport models with nimble capability for multiple resolutions. In this paper we have developed and tested a method to calculate offline

dust emissions at the native meteorological resolution to promote consistency of dust emissions across different model resolutions. We take advantage of the capability of HEMCO standalone module to calculate dust emission offline at native meteorological resolution using DEAD dust emission scheme combined with an updated high resolution dust source function. We evaluate the performance of the simulation with native resolution offline dust emissions and an updated dust source function with source strength of 2,000 Tg/yr. We find better agreement with measurements, including satellite and AERONET AOD. The offline fine resolution dust emissions better resolve smaller desert regions. The independence of source strength from simulation resolution facilitates evaluation with observations. Further work should continue to develop and evaluate the representation of dust emissions.

Code availability: Codes calculating offline dust emissions can be obtained by contacting the leading author.

Data availability: The offline dust emissions dataset with updated dust source function can be accessed freely from (http://geoschemdata.computecanada.ca/Transfers/OFFLINE_DUST/v2020-05/0.25x0.3125).

4.6 Acknowledgement

This work was supported by the Natural Science and Engineering Research Council of Canada. Jun Meng was partially supported by a Nova Scotia Research and Innovation Graduate Scholarship. We are grateful to Compute Canada and Research Infrastructure Services in Washington University in St. Louis for computing resources. All figures are produced with the MATLAB 2019a software.

4.7 SUPPLEMENTAL MATERIALS

This section includes the description of DEAD dust emission scheme and supplemental figures described in the main text.

The dust detrainment and deposition (DEAD) scheme (Zender et al., 2003) is based on a theory studying the transport of dust by winds on Mars to calculate horizontal dust saltation flux H:

$$H = C\frac{\rho}{g}U^{*3}\left(1-\frac{U_t^*}{U^*}\right)\left(1+\frac{U_t^*}{U^*}\right)^2 \quad (1)$$

where C is a global tuning factor determining the total dust strength, ρ is the air density, g is the acceleration of gravity, U^* is the friction velocity and U_t^* is the threshold friction velocity. The vertical dust flux, F, is proportional to the horizontal saltation flux. F is parameterized as:

$$F = A_m S \alpha H, \quad (2)$$

where α is the sandblasting mass efficiency, which is a function of the clay fraction in the soil. We use a fixed soil clay fraction of 0.2 as suggested in Zender et al. (2003). S is dust source function, which is an effective factor that favors emissions from specific geographic features. We updated S with a fine resolution dataset without vegetation mask (Ginoux et al., 2001). A_m is a factor that suppresses dust emission from snow covered land (A_s), wetlands (A_i) and water bodies (A_w) and vegetated area (A_v),

$$A_m = (1-A_s)(1-A_i-A_w)(1-A_v) \quad (3)$$

The vegetation effect A_v is represented by monthly mean leaf plus stem area index (LAI) following Zender et al. (2003). This feature enables seasonal dust mobilization in the dust emisison scheme. We have not investigated the annual vegetation variation in this study.

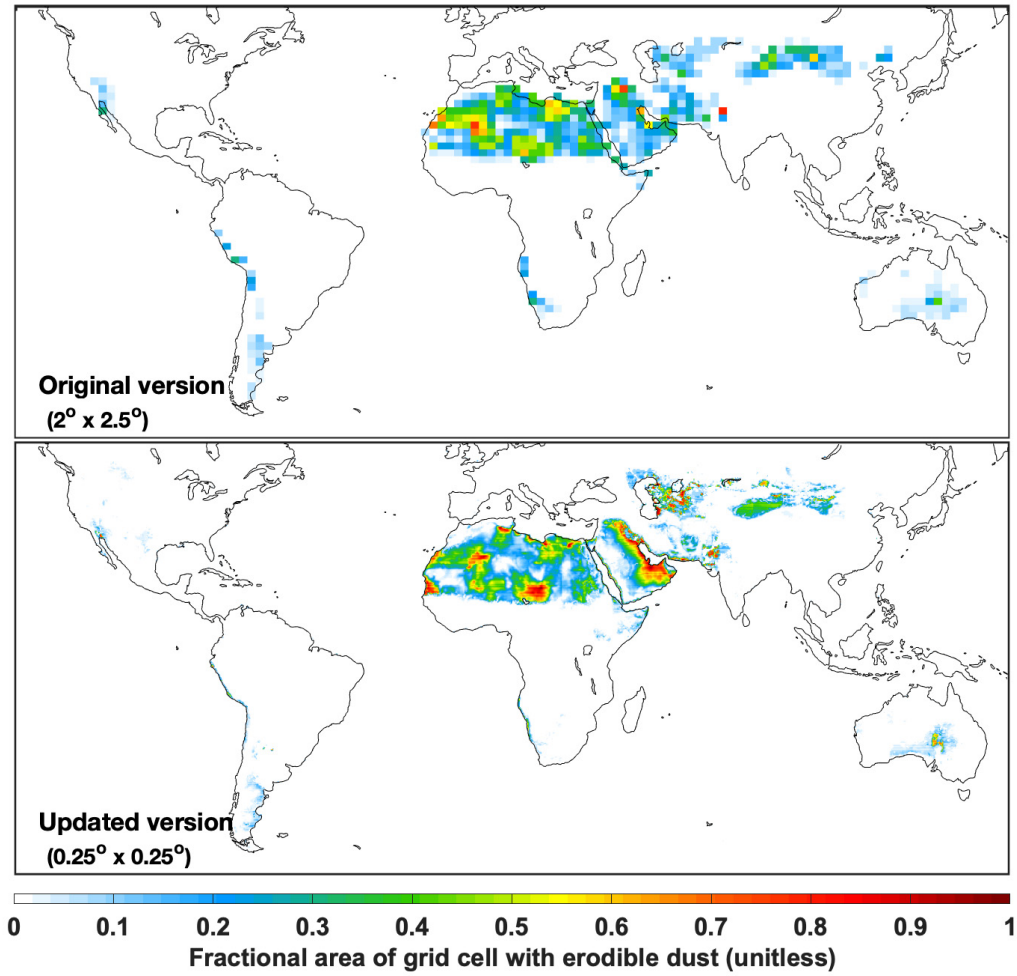

Figure 4-S1. The original and updated versions of the dust source function.

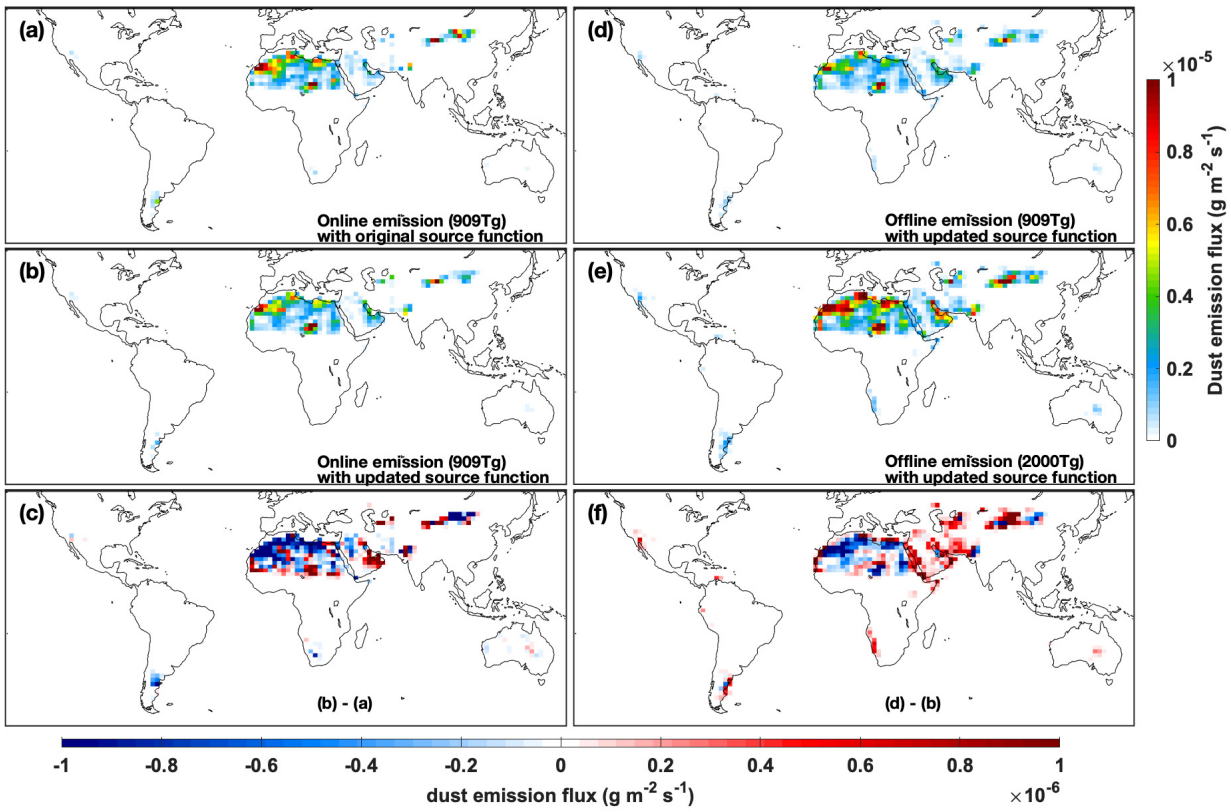

Figure 4-S2. The same as Figure 4-2 but averaged over MAM (March, April and May).

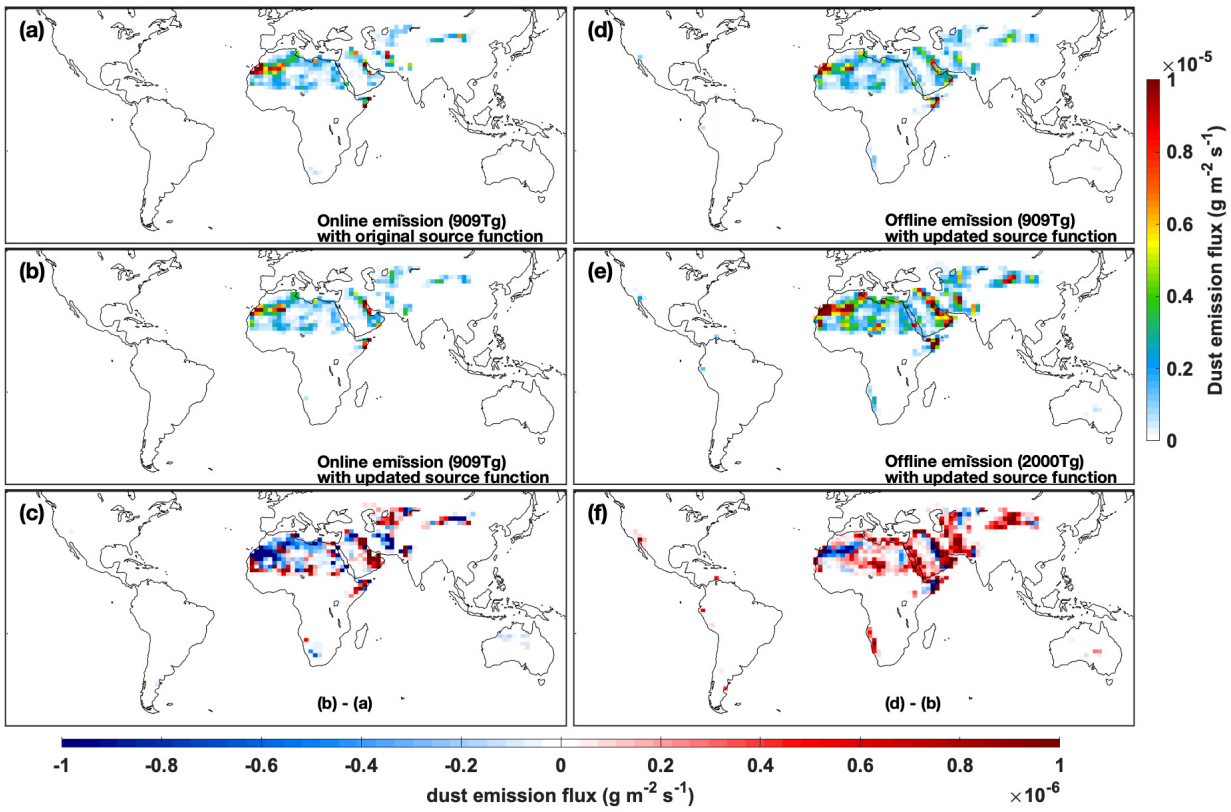

Figure 4-S3. The same as Figure 4-2 but averaged over JJA (June, July and August).

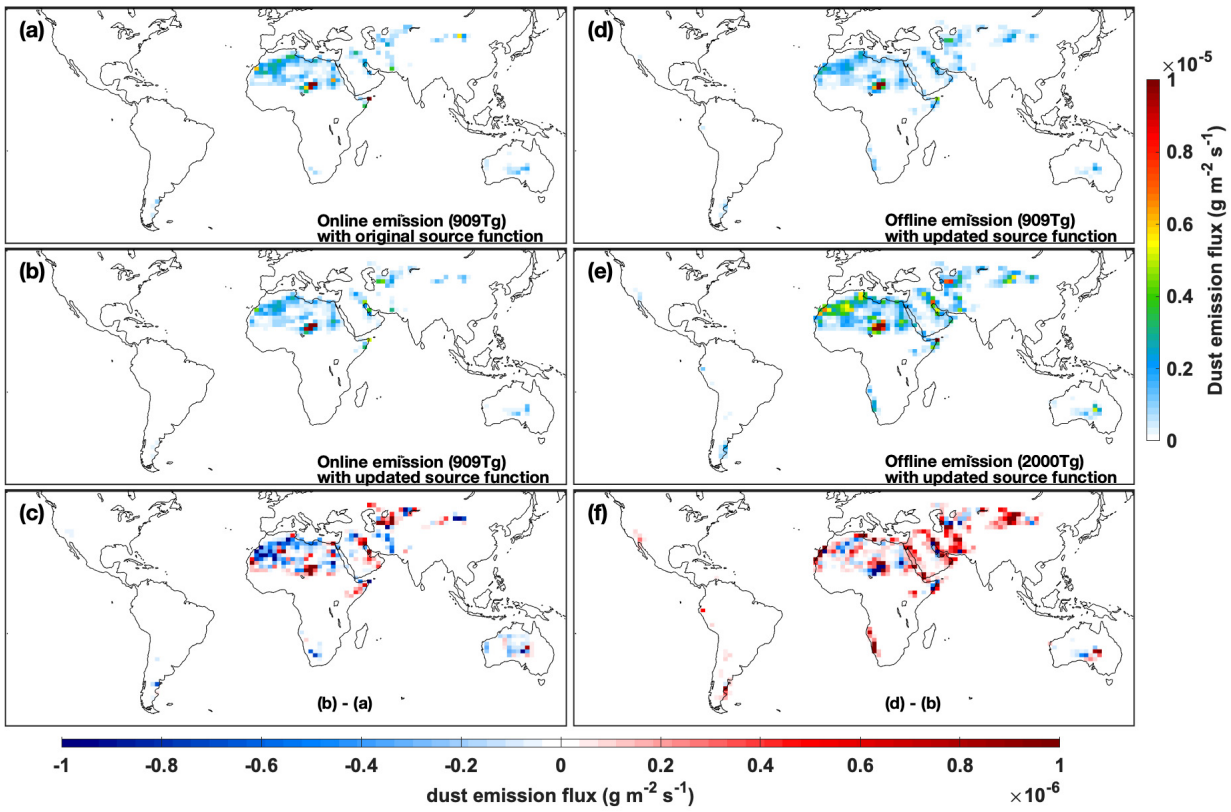

Figure 4-S4. The same as Figure 4-2 but averaged over SON (September, October and November).

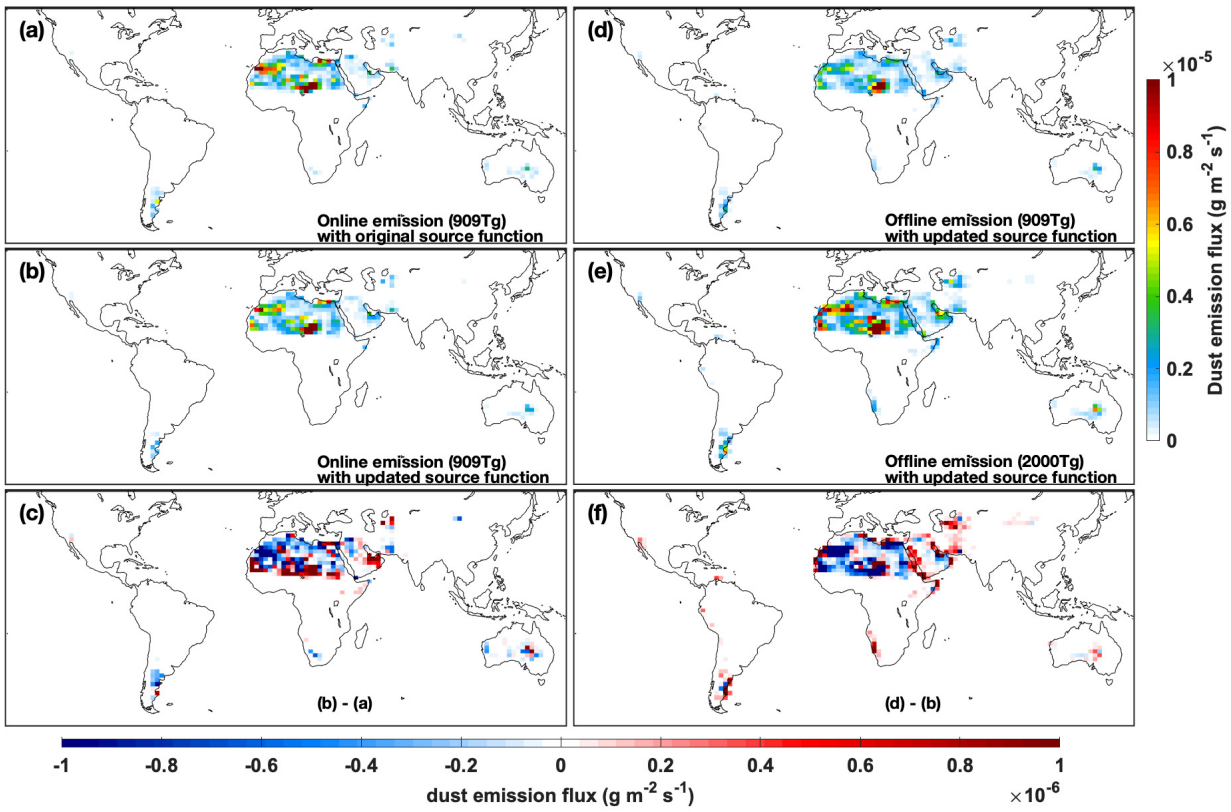

Figure 4-S5. The same as Figure 4-2 but averaged over DJF (December, January and February).

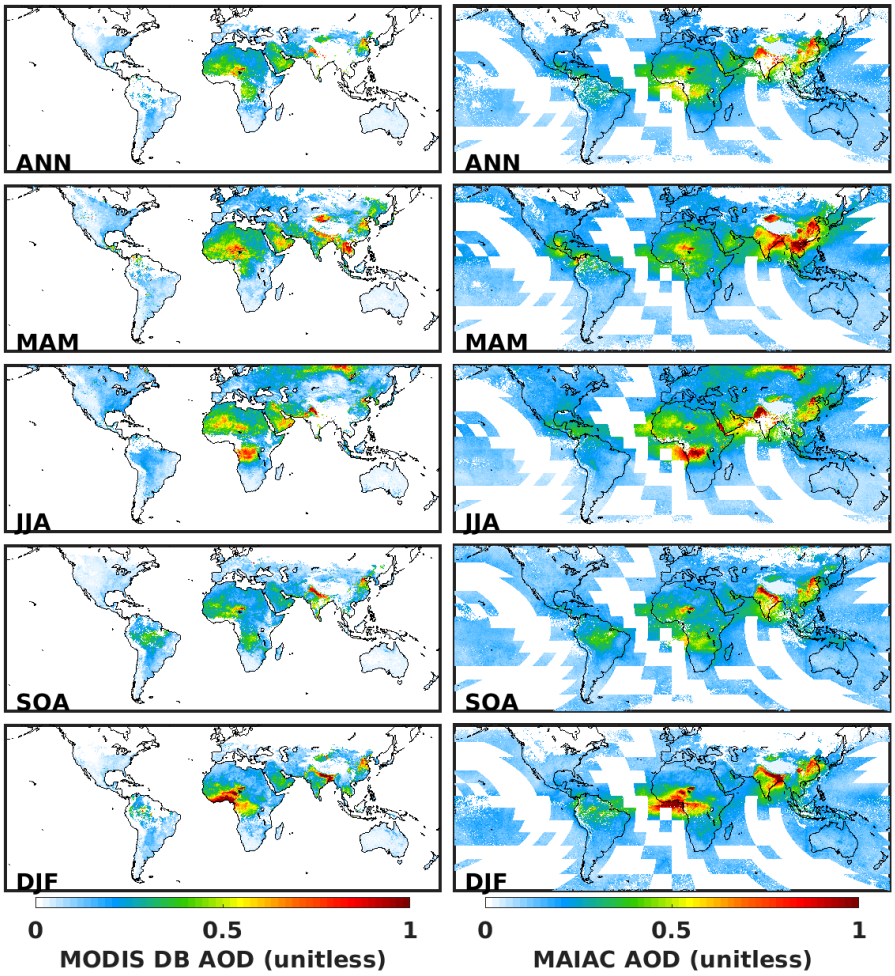

Figure 4-S6. Annual and seasonal satellite AOD from MODIS Deep Blue (DB) and MAIAC algorithms.

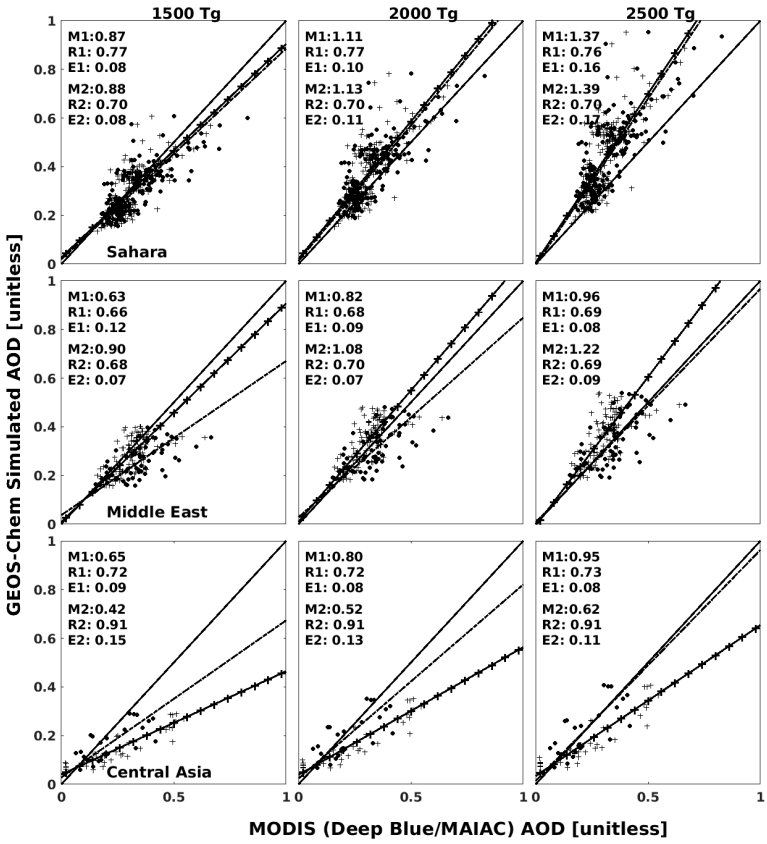

Figure 4-S7. Scatter plots and statistics of comparing GEOS-Chem simulated annual mean AOD with satellite AOD over desert regions. Three columns represent three simulations with total annual dust emissions scaled to the value of 1,500 Tg, 2,000 Tg and 2,500 Tg respectively. The results for the Sahara, Middle East and central Asian deserts are shown in the top, middle and bottom rows respectively. Dots represent the comparison with MODIS DB AOD; the plus signs represent the comparison with MAIAC AOD. Correlation coefficient (R), root mean square error (E), and Slope (M) are reported, in which R1, E1 and M1 show the results of the comparison with MODIS DB AOD; R2, E2 and M2 show the results of the comparison with MAIAC AOD. The best fit lines are lines with corresponding marker signs. The 1:1 line is solid black line.

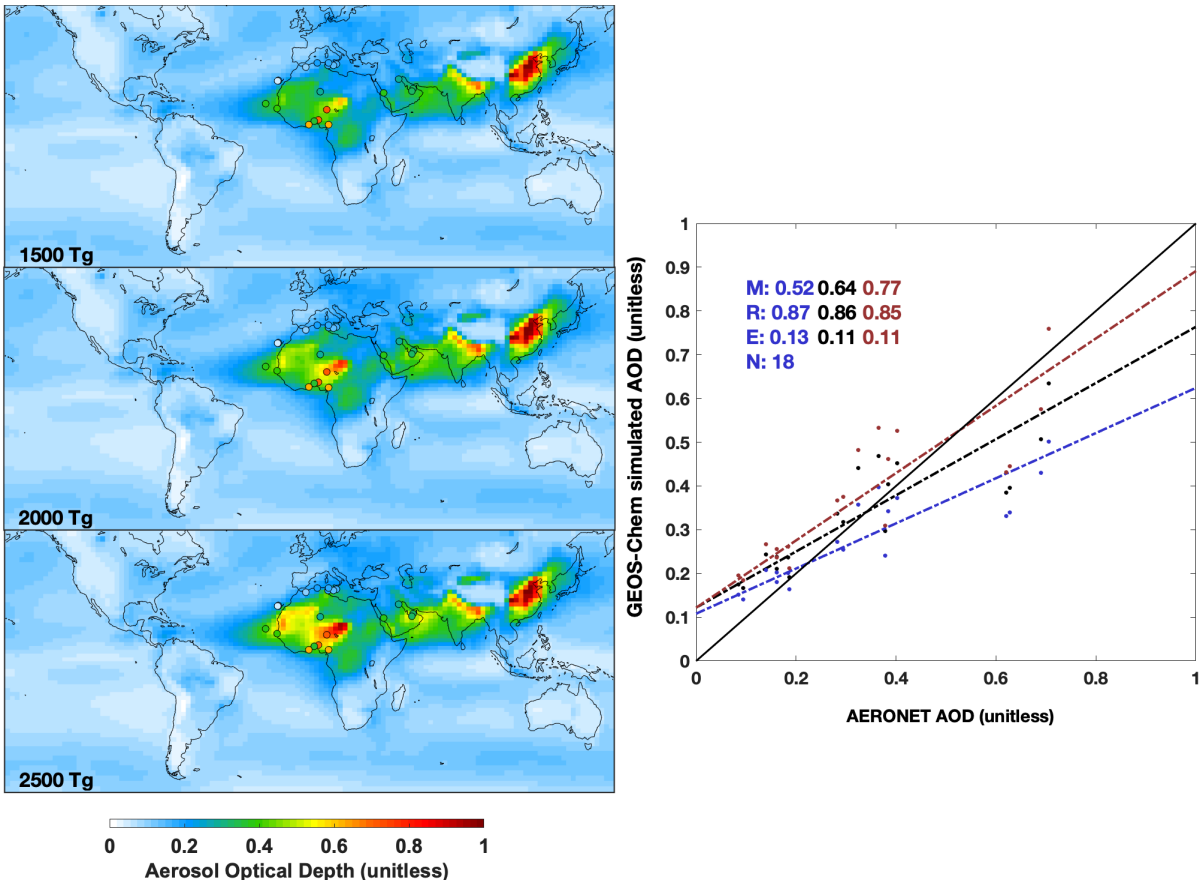

Figure 4-S8. Annual mean simulated AOD from GEOS-Chem simulations for 2016 for simulations with total annual dust emissions of 1,500 Tg, 2,000 Tg and 2,500 Tg, and the comparison against AERONET measured AOD. Sites, shown as filled circles are chosen by where the ratio of simulated DOD and AOD exceeds 0.5. Corresponding statistics, including root mean square error (E), correlation coefficient(R) and slope (M), are inset. Blue, black and red in the scatter plot represent simulations with total annual dust emissions of 1,500 Tg, 2,000 Tg and 2,500 Tg, respectively.

CHAPTER 5 CONCLUSION

5.1 SUMMARY OF THIS PRESENT WORK

$PM_{2.5}$ exposure is a major health concern. Long-term exposure to $PM_{2.5}$ is associated with increased mortality, even at low $PM_{2.5}$ concentrations. Long-term historical $PM_{2.5}$ concentration estimates are needed to investigate concentration-response functions. An enhanced understanding of sectoral contributions to $PM_{2.5}$ is needed to guide future air quality management and inform studies about the health outcomes associated with specific emission sectors. This thesis included three research projects that applied the combination of observations and a chemical transport model to advance understanding of historical $PM_{2.5}$ concentrations and source contributions.

In Chapter 2, we estimated historical $PM_{2.5}$ concentrations over North America from 1981 to 2016 by using the information from different platforms, including chemical transport modeling, satellite remote sensing, and ground-based measurements. We included long-term historical emission inventories in the model simulation. We downscaled the simulation to a resolution of 1km x 1km using a satellite derived $PM_{2.5}$ data set. We constrained the downscaled simulation with ground-based measurements. We evaluated the estimates with direct ground-based $PM_{2.5}$ measurements when available and otherwise with historical estimates of $PM_{2.5}$ inferred from PM_{10} or TSP measurements. The estimated annual mean $PM_{2.5}$ concentrations were generally consistent with direct ground-based $PM_{2.5}$ measurements with R^2 ranging from 0.6 to 0.85 over the comparison period from 1988 onward. The relative RMSD at direct $PM_{2.5}$ sites drops from 30% in the early 1990s to below 20% prior to 1999 when the direct $PM_{2.5}$ measurements became more widespread. The R^2 versus $PM_{2.5}$ data inferred from PM_{10}

measurements increases with the increase of PM_{10} sites for the years 1985-1990 indicating the importance of the historical PM_{10} measurements in the estimates.

The population-weighted annual average $PM_{2.5}$ estimates over North America decreased from 22 ± 6.4 μg m^{-3} in 1981, to 12 ± 3.2 μg m^{-3} in 1998, and to 7.9 ± 2.1 μg m^{-3} in 2016, with an overall trend of -0.33 μg m^{-3} yr^{-1} (95% CI: -0.35 -0.30). The population-weighted trends from our current dataset remain within 0.03 μg m^{-3} yr^{-1} of our prior work (Boys et al., 2014; van Donkelaar et al., 2015), with an advantage that our current study spans a time period (1981-2016) about twice as long by including more trend information from our GEOS-Chem simulation, and includes historical ground-based measurements prior to 1999. The collocated comparison of the trends of population-weighted annual average $PM_{2.5}$ from our estimates and ground-based measurements were highly consistent with RMSD of 0.66 μg m^{-3}.

In Chapter 3, we investigated the sectoral contribution to $PM_{2.5}$ in 2013 for Canada using the GEOS-Chem chemical transport model. We conducted sensitivity simulations by zeroing out each emission sector and downscaled the simulations with satellite-based $PM_{2.5}$ to an exposure-relevant resolution (1 km x 1km). We found that the contributions to $PM_{2.5}$ at the low population-weighted $PM_{2.5}$ concentrations across Canada of 5.5 μg m^{-3} is primarily (81%) from five major anthropogenic sectors and the wildfires sector. The three leading sectoral contributors to population weighted $PM_{2.5}$ over Canada are wildfires with 1.0 μg m^{-3} (17%), transportation with 0.96 μg m^{-3} (16%) and residential combustion with 0.91 μg m^{-3} (15%). The relative contribution to population-weighted $PM_{2.5}$ of different sectors varies regionally with residential combustion as the leading contributor in Central Canada (19%); while wildfires dominate over Northern Canada (59%), Atlantic Canada (34%) and Western Canada (18%). The regionally-varying relative

contribution of different emission sectors across Canada implies that mitigation strategies will benefit from regional policies.

We evaluated the contribution from U.S. sources. We found that over 70% of population-weighted $PM_{2.5}$ originates from Canadian sources followed by 30% from the contiguous United States. The agricultural, transportation and power generation sectors from U.S. sources are the leading contributors. The contribution from U.S. sources is larger over Central Canada (33%) than over Western Canada (17%), Atlantic Canada (17%) and Northern Canada (< 2%). The notable $PM_{2.5}$ contributions from the contiguous United States (~30%) implies benefits from international coordination.

Sectoral contribution analysis for 1990, 2000 and 2010 showed that the contribution from anthropogenic sources to population-weighted $PM_{2.5}$ decreased from 7.1 $\mu g/m^3$ to 3.4 $\mu g/m^3$, which reflects the successful controls on emissions over the last two decades. The contributions of anthropogenic emission sectors decreased with decreasing $PM_{2.5}$ concentrations. This finding could shed light on the investigation of the shape of the concentration-response function for low-level $PM_{2.5}$.

In Chapter 4, we developed a method to calculate and archive offline dust emissions at the native meteorological resolution to promote consistency of dust emissions across different model resolutions, which will benefit the next generation of chemical transport models, such as GCHP, with nimble capability for multiple resolutions. The offline dust emissions based on high resolution meteorological fields can better resolve weak dust source regions, such as southern South America, southern Africa and the southwestern United States. In terms of model development, the offline high resolution dust emissions are expected to ease the evaluation process for global total dust emissions. The native resolution offline dust emissions facilitate

evaluation by scaling according to observations before coupling with the model rather than testing scale factors for different resolutions. We have found that simulation with global total annual dust emission scaled to 2,000 Tg yr^{-1} generally represents observations of AOD from satellite and AERONET.

5.2 Studies Utilizing this Present Work

The estimated historical $PM_{2.5}$ concentration data set in Chapter 2 provides long-term continuous $PM_{2.5}$ information at an exposure-relevant resolution across North America. This data set is being used to study the shape of concentration-response relationship at low $PM_{2.5}$ concentrations. Pappin et al. (2019) linked this dataset with the mobility and mortality data in three Canadian Census Health and Environment Cohorts (CanCHEC) and found that $PM_{2.5}$ was associated with non-accidental mortality at concentrations as low as 5 μg m^{-3}. Similarly, a research report (Brauer et al., 2019) from Health Effects Institute (HEI) provided evidence that the relationship between $PM_{2.5}$ and non-accidental mortality was supralinear without apparent threshold. Crouse et al. (2020) used this data set as one of $PM_{2.5}$ exposures to evaluate the sensitivity of $PM_{2.5}$-mortality associations to the temporal and spatial scale of the $PM_{2.5}$ exposures. The results in this study not only further supported the previous relationship between $PM_{2.5}$ and non-accidental mortality in Pappin et al. (2019) and Brauer et al. (2019), but also highlighted the importance of longer-exposure window and more exposure-relevant spatial resolution of the exposure data in characterizing the relationship. In addition, Muller (2020) applied this dataset in the economy field assessing the long-term air pollution damage in the U.S. economy.

The sectoral contribution analysis for Canada in Chapter 3 provides detailed information about the annual source contributions from each emission sectors in 2013 and selected years in the past three decades (1990, 2000 and 2010). Chen et al. (in prep) are applying the sectoral $PM_{2.5}$ data to a national level epidemiological analysis using the CanCHEC cohort to examine the relationship between sector attributed $PM_{2.5}$ concentrations and cardiovascular disease deaths.

5.3 Outlook

The GEOS-Chem chemical transport model used in this thesis has utility for understanding $PM_{2.5}$ and its chemical compositions. However, model uncertainty remains. Uncertainty could be reduced in the future through development to emission inventories and chemical mechanisms. Contemporary and sophisticated emission inventories will help to identify more reliable and detailed source contribution information. The emission inventories we used in Chapter 3 investigating the sectoral contribution to $PM_{2.5}$ for Canada were updated until 2014. Contemporary emission inventories with detailed subsectors and fuel type information (McDuffie et al., 2020) will benefit future source contribution studies in the global and national level.

Model resolution also plays an important role in reducing uncertainties. As presented in Chapter 2 and Chapter 3 of this thesis, we leveraged the nested grid capability of GEOS-Chem to capture the small-scale variations obtained from fine resolution simulations. However, this feature sacrifices the model resolution elsewhere. The high performance version of GEOS-Chem (GCHP), which enables massive parallelization by using a distributed-memory framework

(Eastham et al., 2018), is expected to overcome this bottleneck with the capability of conducting global simulations with resolutions ranging from C24 (~4°x5°) to C360 (~0.25°).

The offline high resolution grid independent dust emissions developed in Chapter 4 advance the implementation of dust emissions for the next generation of CTMs, such as GCHP, with the capability for multiple resolutions. However, uncertainty remains in the estimated global annual total dust emissions. We have used satellite AOD and AERONET AOD measurements in Chapter 4 to constrain the total dust emissions. Further analyses should be conducted to further narrow the uncertainty gap of the global annual total dust emissions. Additional evaluation with measurements from other platforms, such as vertical profile measurements, should be useful to further constrain the dust emissions at regional scales. Additionally, the parameterization of the dust emission scheme should receive more attention in future development.

Advanced understanding of sectoral contributions to $PM_{2.5}$ and its historical concentrations can be of benefit for the future air quality standards regulation and management. Additionally, it can inform concentration-response relationship and sectoral health outcomes studies. As the Earth system continues to evolve, the impact of climate change on air quality and human health deserves attention. Scientific knowledge in this research field is enhancing the ability of understanding the interrelationships between air quality, human health and climate change.

REFERENCES

Aksoyoglu, S., Ciarelli, G., El-Haddad, I., Baltensperger, U., & Prévôt, A. S. H. (2017). Secondary inorganic aerosols in Europe: sources and the significant influence of biogenic VOC emissions, especially on ammonium nitrate. *Atmospheric Chemistry and Physics*, *17*(12), 7757–7773. https://doi.org/10.5194/acp-17-7757-2017

Amos, H. M., Jacob, D. J., Holmes, C. D., Fisher, J. A., Wang, Q., Yantosca, R. M., et al. (2012). Gas-particle partitioning of atmospheric Hg(II) and its effect on global mercury deposition. *Atmospheric Chemistry and Physics*, *12*(1), 591–603. https://doi.org/10.5194/acp-12-591-2012

Amouroux, D., Roberts, G., Rapsomanikis, S., & Andreae, M. O. (2002). Biogenic Gas (CH4, N2O, DMS) Emission to the Atmosphere from Near-shore and Shelf Waters of the North-western Black Sea. *Estuarine, Coastal and Shelf Science*, *54*(3), 575–587. https://doi.org/10.1006/ecss.2000.0666

Amsalu, E., Wang, T., Li, H., Liu, Y., Wang, A., Liu, X., et al. (2019). Acute effects of fine particulate matter (PM2.5) on hospital admissions for cardiovascular disease in Beijing, China: a time-series study. *Environmental Health*, *18*. https://doi.org/10.1186/s12940-019-0506-2

Baccarelli, A., Wright, R. O., Bollati, V., Tarantini, L., Litonjua, A. A., Suh, H. H., et al. (2009). Rapid DNA methylation changes after exposure to traffic particles. *American Journal of Respiratory and Critical Care Medicine*, *179*(7), 572–578. https://doi.org/10.1164/rccm.200807-1097OC

Barker, H. W. (2012). Isolating the Industrial Contribution of $PM_{2.5}$ in Hamilton and Burlington, Ontario. *Journal of Applied Meteorology and Climatology*, *52*(3), 660–667. https://doi.org/10.1175/JAMC-D-12-0163.1

Beckerman, B. S., Jerrett, M., Serre, M., Martin, R. V., Lee, S.-J., van Donkelaar, A., et al. (2013). A Hybrid Approach to Estimating National Scale Spatiotemporal Variability of $PM_{2.5}$ in the Contiguous United States. *Environmental Science & Technology*, *47*(13), 7233–7241. https://doi.org/10.1021/es400039u

Beelen, R., Hoek, G., van den Brandt, P. A., Goldbohm, R. A., Fischer, P., Schouten, L. J., et al. (2008). Long-Term Effects of Traffic-Related Air Pollution on Mortality in a Dutch Cohort (NLCS-AIR Study). *Environmental Health Perspectives*, *116*(2), 196–202. https://doi.org/10.1289/ehp.10767

Beelen, R., Raaschou-Nielsen, O., Stafoggia, M., Andersen, Z. J., Weinmayr, G., Hoffmann, B., et al. (2014). Effects of long-term exposure to air pollution on natural-cause mortality: an analysis of 22 European cohorts within the multicentre ESCAPE project. *Lancet (London, England)*, *383*(9919), 785–795. https://doi.org/10.1016/S0140-6736(13)62158-3

Behera, S. N., Sharma, M., Aneja, V. P., & Balasubramanian, R. (2013). Ammonia in the atmosphere: a review on emission sources, atmospheric chemistry and deposition on terrestrial bodies. *Environmental Science and Pollution Research International*, *20*(11), 8092–8131. https://doi.org/10.1007/s11356-013-2051-9

Bergin, M. H., Ghoroi, C., Dixit, D., Schauer, J. J., & Shindell, D. T. (2017). Large Reductions in Solar Energy Production Due to Dust and Particulate Air Pollution. *Environmental Science & Technology Letters*, *4*(8), 339–344. https://doi.org/10.1021/acs.estlett.7b00197

Bey, I., Jacob, D. J., Yantosca, R. M., Logan, J. A., Field, B. D., Fiore, A. M., et al. (2001). Global modeling of tropospheric chemistry with assimilated meteorology: Model description and evaluation. *Journal of Geophysical Research: Atmospheres*, *106*(D19), 23073–23095. https://doi.org/10.1029/2001JD000807

Boldo, E., Medina, S., LeTertre, A., Hurley, F., Mücke, H.-G., Ballester, F., et al. (2006). Apheis: Health impact assessment of long-term exposure to $PM_{2.5}$ in 23 European cities. *European Journal of Epidemiology*, *21*(6), 449–458. https://doi.org/10.1007/s10654-006-9014-0

Bond, T. C., Streets, D. G., Yarber, K. F., Nelson, S. M., Woo, J.-H., & Klimont, Z. (2004). A technology-based global inventory of black and organic carbon emissions from combustion. *Journal of Geophysical Research: Atmospheres*, *109*(D14). https://doi.org/10.1029/2003JD003697

Boys, B. L., Martin, R. V., van Donkelaar, A., MacDonell, R. J., Hsu, N. C., Cooper, M. J., et al. (2014). Fifteen-Year Global Time Series of Satellite-Derived Fine Particulate Matter. *Environmental Science & Technology*, *48*(19), 11109–11118. https://doi.org/10.1021/es502113p

Brauer, M., Brook, J. R., Christidis, T., Chu, Y., Crouse, D. L., Erickson, A., et al. (2019). Mortality-Air Pollution Associations in Low-Exposure Environments (MAPLE): Phase 1. *Research Report (Health Effects Institute)*, (203), 1–87.

Breider, T. J., Mickley, L. J., Jacob, D. J., Ge, C., Wang, J., Sulprizio, M. P., et al. (2017). Multidecadal trends in aerosol radiative forcing over the Arctic: Contribution of changes in anthropogenic aerosol to Arctic warming since 1980. *Journal of Geophysical Research: Atmospheres*, *122*(6), 3573–3594. https://doi.org/10.1002/2016JD025321

Briggs, N. L., & Long, C. M. (2016). Critical review of black carbon and elemental carbon source apportionment in Europe and the United States. *Atmospheric Environment*, *144*, 409–427. https://doi.org/10.1016/j.atmosenv.2016.09.002

Bristow, C. S., Hudson-Edwards, K. A., & Chappell, A. (2010). Fertilizing the Amazon and equatorial Atlantic with West African dust. *Geophysical Research Letters*, *37*(14). https://doi.org/10.1029/2010GL043486

Brook, J. R., Lillyman, C. D., Shepherd, M. F., & Mamedov, A. (2002). Regional Transport and Urban Contributions to Fine Particle Concentrations in Southeastern Canada. *Journal of the Air & Waste Management Association*, *52*(7), 855–866. https://doi.org/10.1080/10473289.2002.10470821

Brook, J. R., Poirot, R. L., Dann, T. F., Lee, P. K. H., Lillyman, C. D., & Ip, T. (2007). Assessing Sources of $PM_{2.5}$ in Cities Influenced by Regional Transport. *Journal of Toxicology and Environmental Health, Part A*, *70*(3–4), 191–199. https://doi.org/10.1080/15287390600883000

Brook, J. R., Graham, L., Charland, J. P., Cheng, Y., Fan, X., Lu, G., et al. (2007). Investigation of the motor vehicle exhaust contribution to primary fine particle organic carbon in urban air. *Atmospheric Environment*, *41*(1), 119–135. https://doi.org/10.1016/j.atmosenv.2006.07.050

Brook, R. D., Rajagopalan, S., Pope, C. A., Brook, J. R., Bhatnagar, A., Diez-Roux, A. V., et al. (2010). Particulate matter air pollution and cardiovascular disease: An update to the scientific statement from the American Heart Association. *Circulation*, *121*(21), 2331–2378. https://doi.org/10.1161/CIR.0b013e3181dbece1

Brunsdon, C., Fotheringham, A. S., & Charlton, M. E. (1996). Geographically Weighted Regression: A Method for Exploring Spatial Nonstationarity. *Geographical Analysis*, *28*(4), 281–298. https://doi.org/10.1111/j.1538-4632.1996.tb00936.x

Burnett, R., Chen, H., Szyszkowicz, M., Fann, N., Hubbell, B., Pope, C. A., et al. (2018). Global estimates of mortality associated with long-term exposure to outdoor fine particulate matter. *Proceedings of the National Academy of Sciences of the United States of America*, *115*(38), 9592–9597. https://doi.org/10.1073/pnas.1803222115

Caiazzo, F., Ashok, A., Waitz, I. A., Yim, S. H. L., & Barrett, S. R. H. (2013). Air pollution and early deaths in the United States. Part I: Quantifying the impact of major sectors in 2005. *Atmospheric Environment*, *79*, 198–208. https://doi.org/10.1016/j.atmosenv.2013.05.081

Canadian Council of Ministers of the Environment (CCME). (2011). *Ambient air monitoring protocol for $PM_{2.5}$ and ozone: Canada-wide standards for particulate matter and ozone*. Winnipeg, Man.: Canadian Council of Ministers of the Environment. Retrieved from https://www.ccme.ca/files/Resources/air/pm_ozone/pm_oz_cws_monitoring_protocol_pn1456_e.pdf

Carlton, A. G., Wiedinmyer, C., & Kroll, J. H. (2009). A review of Secondary Organic Aerosol (SOA) formation from isoprene. *Atmospheric Chemistry and Physics*, *9*(14), 4987–5005. https://doi.org/10.5194/acp-9-4987-2009

Carn, S. A., Clarisse, L., & Prata, A. J. (2016). Multi-decadal satellite measurements of global volcanic degassing. *Journal of Volcanology and Geothermal Research*, *311*, 99–134. https://doi.org/10.1016/j.jvolgeores.2016.01.002

Chance, K., & Martin, R. V. (2017). *Spectroscopy and Radiative Transfer of Planetary Atmospheres*. Oxford University Press.

Chen, H., Navea, J. G., Young, M. A., & Grassian, V. H. (2011). Heterogeneous Photochemistry of Trace Atmospheric Gases with Components of Mineral Dust Aerosol. *The Journal of Physical Chemistry A*, *115*(4), 490–499. https://doi.org/10.1021/jp110164j

Cho, S., McEachern, P., Morris, R., Shah, T., Johnson, J., & Nopmongcol, U. (2012). Emission sources sensitivity study for ground-level ozone and $PM_{2.5}$ due to oil sands development using air quality modeling system: Part I- model evaluation for current year base case simulation. *Atmospheric Environment*, *55*, 533–541. https://doi.org/10.1016/j.atmosenv.2012.02.026

Claiborn, C. S., Finn, D., Larson, T. V., & Koenig, J. Q. (2000). Windblown dust contributes to high PM2.5 concentrations. *Journal of the Air & Waste Management Association (1995)*, *50*(8), 1440–1445. https://doi.org/10.1080/10473289.2000.10464179

Cohen, A. J., Brauer, M., Burnett, R., Anderson, H. R., Frostad, J., Estep, K., et al. (2017). Estimates and 25-year trends of the global burden of disease attributable to ambient air pollution: an analysis of data from the Global Burden of Diseases Study 2015. *The Lancet*, *389*(10082), 1907–1918. https://doi.org/10.1016/S0140-6736(17)30505-6

Crouse, D. L., Peters, P. A., van Donkelaar, A., Goldberg, M. S., Villeneuve, P. J., Brion, O., et al. (2012). Risk of nonaccidental and cardiovascular mortality in relation to long-term exposure to low concentrations of fine particulate matter: a Canadian national-level cohort study. *Environmental Health Perspectives*, *120*(5), 708–714. https://doi.org/10.1289/ehp.1104049

Crouse, D. L., Erickson, A. C., Christidis, T., Pinault, L., van Donkelaar, A., Li, C., et al. (2020). Evaluating the Sensitivity of PM2.5-Mortality Associations to the Spatial and Temporal Scale of Exposure Assessment. *Epidemiology (Cambridge, Mass.)*, *31*(2), 168–176. https://doi.org/10.1097/EDE.0000000000001136

Dabek-Zlotorzynska, E., Dann, T. F., Kalyani Martinelango, P., Celo, V., Brook, J. R., Mathieu, D., et al. (2011). Canadian National Air Pollution Surveillance (NAPS) $PM_{2.5}$ speciation program: Methodology and $PM_{2.5}$ chemical composition for the years 2003–2008. *Atmospheric Environment*, *45*(3), 673–686. https://doi.org/10.1016/j.atmosenv.2010.10.024

De Longueville, F., Hountondji, Y.-C., Henry, S., & Ozer, P. (2010). What do we know about effects of desert dust on air quality and human health in West Africa compared to other regions? *The Science of the Total Environment*, *409*(1), 1–8. https://doi.org/10.1016/j.scitotenv.2010.09.025

van Donkelaar, A., Martin, R. V., Brauer, M., Kahn, R., Levy, R., Verduzco, C., & Villeneuve, P. J. (2010). Global Estimates of Ambient Fine Particulate Matter Concentrations from Satellite-Based Aerosol Optical Depth: Development and Application. *Environmental Health Perspectives*, *118*(6), 847–855. https://doi.org/10.1289/ehp.0901623

van Donkelaar, A., Martin, R. V., Spurr, R. J. D., & Burnett, R. T. (2015). High-Resolution Satellite-Derived $PM_{2.5}$ from Optimal Estimation and Geographically Weighted Regression over North America. *Environmental Science & Technology*, *49*(17), 10482–10491. https://doi.org/10.1021/acs.est.5b02076

van Donkelaar, A., Martin, R. V., Li, C., & Burnett, R. T. (2019). Regional Estimates of Chemical Composition of Fine Particulate Matter Using a Combined Geoscience-Statistical Method with Information from Satellites, Models, and Monitors. *Environmental Science & Technology*, *53*(5), 2595–2611. https://doi.org/10.1021/acs.est.8b06392

Drury, E., Jacob, D. J., Spurr, R. J. D., Wang, J., Shinozuka, Y., Anderson, B. E., et al. (2010). Synthesis of satellite (MODIS), aircraft (ICARTT), and surface (IMPROVE, EPA-AQS, AERONET) aerosol observations over eastern North America to improve MODIS aerosol retrievals and constrain surface aerosol concentrations and sources. *Journal of Geophysical Research: Atmospheres*, *115*(D14). https://doi.org/10.1029/2009JD012629

Du, Y., Xu, X., Chu, M., Guo, Y., & Wang, J. (2016). Air particulate matter and cardiovascular disease: the epidemiological, biomedical and clinical evidence. *Journal of Thoracic Disease*, *8*(1), E8–E19. https://doi.org/10.3978/j.issn.2072-1439.2015.11.37

Eastham, S. D., Long, M. S., Keller, C. A., Lundgren, E., Yantosca, R. M., Zhuang, J., et al. (2018). GEOS-Chem High Performance (GCHP v11-02c): a next-generation implementation of the GEOS-Chem chemical transport model for massively parallel applications. *Geoscientific Model Development*, *11*(7), 2941–2953. https://doi.org/10.5194/gmd-11-2941-2018

Eeftens, M., Beelen, R., de Hoogh, K., Bellander, T., Cesaroni, G., Cirach, M., et al. (2012). Development of Land Use Regression models for $PM_{2.5}$, $PM_{2.5}$ absorbance, PM_{10} and PM_{coarse} in 20 European study areas; results of the ESCAPE project. *Environmental Science & Technology*, *46*(20), 11195–11205. https://doi.org/10.1021/es301948k

Eney, A. B., & Petzold, D. E. (1987). The problem of acid rain: An overview. *Environmentalist*, *7*(2), 95–103. https://doi.org/10.1007/BF02240291

Environment and Climate Change Canada. (2015, January 26). Air Pollutant Emissions Inventory: overview. [program descriptions;navigation page]. Retrieved September 15, 2018, from https://www.canada.ca/en/environment-climate-change/services/pollutants/air-emissions-inventory-overview.html

Environment and Climate Change Canada. (2018). Canadian environmental sustainability indicators: Air pollutant emissions. Retrieved September 15, 2018, from https://www.canada.ca/en/environment-climate-change/services/environmental-indicators/air-pollutant-emissions.html

Evans, M. J., & Jacob, D. J. (2005). Impact of new laboratory studies of N_2O_5 hydrolysis on global model budgets of tropospheric nitrogen oxides, ozone, and OH. *Geophysical Research Letters*, *32*(9). https://doi.org/10.1029/2005GL022469

Fairlie, T. D., Jacob, D. J., & Park, R. J. (2007). The impact of transpacific transport of mineral dust in the United States. *Atmospheric Environment*, *41*(6), 1251–1266. https://doi.org/10.1016/j.atmosenv.2006.09.048

Fisher, J. A., Jacob, D. J., Wang, Q., Bahreini, R., Carouge, C. C., Cubison, M. J., et al. (2011). Sources, distribution, and acidity of sulfate–ammonium aerosol in the Arctic in winter–spring. *Atmospheric Environment*, *45*(39), 7301–7318. https://doi.org/10.1016/j.atmosenv.2011.08.030

Fountoukis, C., & Nenes, A. (2007). ISORROPIA II: A computationally efficient thermodynamic equilibrium model for K^+-Ca^{2+}-Mg^{2+}-NH_4^+-Na^+-SO_4^{2-}-NO_3^--Cl^--H_2O aerosols. *Atmospheric Chemistry and Physics*, *7*(17), 4639–4659. https://doi.org/10.5194/acp-7-4639-2007

Friedl, M. A., Sulla-Menashe, D., Tan, B., Schneider, A., Ramankutty, N., Sibley, A., & Huang, X. (2010). MODIS Collection 5 global land cover: Algorithm refinements and characterization of new datasets. *Remote Sensing of Environment*, *114*(1), 168–182. https://doi.org/10.1016/j.rse.2009.08.016

Fu, P., Guo, X., Cheung, F. M. H., & Yung, K. K. L. (2019). The association between PM2.5 exposure and neurological disorders: A systematic review and meta-analysis. *Science of The Total Environment*, *655*, 1240–1248. https://doi.org/10.1016/j.scitotenv.2018.11.218

Gakidou, E., Afshin, A., Abajobir, A. A., Abate, K. H., Abbafati, C., Abbas, K. M., et al. (2017). Global, regional, and national comparative risk assessment of 84 behavioural, environmental and occupational, and metabolic risks or clusters of risks, 1990–2016: a systematic analysis for the Global Burden of Disease Study 2016. *The Lancet*, *390*(10100), 1345–1422. https://doi.org/10.1016/S0140-6736(17)32366-8

Giglio, L., Randerson, J. T., & Werf, G. R. van der. (2013). Analysis of daily, monthly, and annual burned area using the fourth-generation global fire emissions database (GFED4). *Journal of Geophysical Research: Biogeosciences*, *118*(1), 317–328. https://doi.org/10.1002/jgrg.20042

Giles, D. M., Sinyuk, A., Sorokin, M. G., Schafer, J. S., Smirnov, A., Slutsker, I., et al. (2019). Advancements in the Aerosol Robotic Network (AERONET) Version 3 database – automated near-real-time quality control algorithm with improved cloud screening for Sun photometer aerosol optical depth (AOD) measurements. *Atmospheric Measurement Techniques*, *12*(1), 169–209. https://doi.org/10.5194/amt-12-169-2019

Gillette, D. A. (1999). A qualitative geophysical explanation for hot spot dust emitting source regions. *A Qualitative Geophysical Explanation for Hot Spot Dust Emitting Source Regions*, *72*(1), 67–77.

Gillette, D. A., & Passi, R. (1988). Modeling dust emission caused by wind erosion. *Journal of Geophysical Research: Atmospheres*, *93*(D11), 14233–14242. https://doi.org/10.1029/JD093iD11p14233

Ginoux, P., Chin, M., Tegen, I., Prospero, J. M., Holben, B., Dubovik, O., & Lin, S.-J. (2001). Sources and distributions of dust aerosols simulated with the GOCART model. *Journal of Geophysical Research: Atmospheres*, *106*(D17), 20255–20273. https://doi.org/10.1029/2000JD000053

Ginoux, P., Prospero, J. M., Gill, T. E., Hsu, N. C., & Zhao, M. (2012). Global-scale attribution of anthropogenic and natural dust sources and their emission rates based on MODIS Deep Blue aerosol products: ANTHROPOGENIC AND NATURAL DUST SOURCES. *Reviews of Geophysics*, *50*(3). https://doi.org/10.1029/2012RG000388

Glass, N. R., Glass, G. E., & Rennie, P. J. (1980). Effects of acid precipitation in North America. *Environment International*, *4*(5), 443–452. https://doi.org/10.1016/0160-4120(80)90025-2

Global Population Count Grid Time Series Estimates, v1: Population Dynamics | SEDAC. (n.d.). Retrieved August 8, 2018, from http://sedac.ciesin.columbia.edu/data/set/popdynamics-global-pop-count-time-series-estimates

Goldberg, D. L., Lamsal, L. N., Loughner, C. P., Swartz, W. H., Lu, Z., & Streets, D. G. (2017). A high-resolution and observationally constrained OMI NO_2 satellite retrieval. *Atmospheric Chemistry and Physics*, *17*(18), 11403–11421. https://doi.org/10.5194/acp-17-11403-2017

Goodarzi, F. (2006). The rates of emissions of fine particles from some Canadian coal-fired power plants. *Fuel*, *85*(4), 425–433. https://doi.org/10.1016/j.fuel.2005.07.008

Gridded Population of the World (GPW), v4, SEDAC. (2018). Retrieved August 8, 2018, from http://sedac.ciesin.columbia.edu/data/collection/gpw-v4

Grythe, H., Ström, J., Krejci, R., Quinn, P., & Stohl, A. (2014). A review of sea-spray aerosol source functions using a large global set of sea salt aerosol concentration measurements. *Atmospheric Chemistry and Physics*, *14*(3), 1277–1297. https://doi.org/10.5194/acp-14-1277-2014

Guenther, A. B., Jiang, X., Heald, C. L., Sakulyanontvittaya, T., Duhl, T., Emmons, L. K., & Wang, X. (2012). The Model of Emissions of Gases and Aerosols from Nature version 2.1 (MEGAN2.1): an extended and updated framework for modeling biogenic emissions. *Geosci. Model Dev.*, *5*(6), 1471–1492. https://doi.org/10.5194/gmd-5-1471-2012

Hales, S., Blakely, T., & Woodward, A. (2012). Air pollution and mortality in New Zealand: cohort study. *Journal of Epidemiology and Community Health*, *66*(5), 468–473. https://doi.org/10.1136/jech.2010.112490

Hammer, M. S., Martin, R. V., van Donkelaar, A., Buchard, V., Torres, O., Ridley, D. A., & Spurr, R. J. D. (2016). Interpreting the ultraviolet aerosol index observed with the OMI satellite instrument to understand absorption by organic aerosols: implications for atmospheric oxidation and direct radiative effects. *Atmospheric Chemistry and Physics*, *16*(4), 2507–2523. https://doi.org/10.5194/acp-16-2507-2016

Hamra, G. B., Guha, N., Cohen, A., Laden, F., Raaschou-Nielsen, O., Samet, J. M., et al. (2014). Outdoor particulate matter exposure and lung cancer: a systematic review and meta-analysis. *Environmental Health Perspectives*, *122*(9), 906–911. https://doi.org/10.1289/ehp/1408092

Hand, J. L., Schichtel, B. A., Pitchford, M., Malm, W. C., & Frank, N. H. (2012). Seasonal composition of remote and urban fine particulate matter in the United States. *Journal of Geophysical Research: Atmospheres*, *117*(D5). https://doi.org/10.1029/2011JD017122

Heald, C. L., Jr, C., L, J., Lee, T., Benedict, K. B., Schwandner, F. M., et al. (2012). Atmospheric ammonia and particulate inorganic nitrogen over the United States. *Atmospheric Chemistry and Physics*, *12*(21), 10295–10312. https://doi.org/10.5194/acp-12-10295-2012

Hinton, D., Sune, J., Suggs, J., & Barnard, W. F. (2002). *Inhalable Particulate Network Report: Operation and Data Summary (mass concentrations only). Vol. 1. April 1979-December 1982*. U.S. Environmental Protection Agency, Washington, D.C., EPA/600/4-84/088A (NTIS PB85148682). Retrieved from https://cfpub.epa.gov/si/si_public_record_report.cfm?Lab=NERL&dirEntryId=42103

Hoesly, R. M., Smith, S. J., Feng, L., Klimont, Z., Janssens-Maenhout, G., Pitkanen, T., et al. (2018). Historical (1750–2014) anthropogenic emissions of reactive gases and aerosols from the Community Emissions Data System (CEDS). *Geoscientific Model Development*, *11*(1), 369–408. https://doi.org/10.5194/gmd-11-369-2018

Holben, B. N., Eck, T. F., Slutsker, I., Tanré, D., Buis, J. P., Setzer, A., et al. (1998). AERONET—A Federated Instrument Network and Data Archive for Aerosol Characterization. *Remote Sensing of Environment*, *66*(1), 1–16. https://doi.org/10.1016/S0034-4257(98)00031-5

Holt, J., Selin, N. E., & Solomon, S. (2015). Changes in Inorganic Fine Particulate Matter Sensitivities to Precursors Due to Large-Scale US Emissions Reductions. *Environmental Science & Technology*, *49*(8), 4834–4841. https://doi.org/10.1021/acs.est.5b00008

Hong, K. Y., King, G. H., Saraswat, A., & Henderson, S. B. (2017). Seasonal ambient particulate matter and population health outcomes among communities impacted by road dust in British Columbia, Canada. *Journal of the Air & Waste Management Association (1995)*, *67*(9), 986–999. https://doi.org/10.1080/10962247.2017.1315348

Hsu, N. C., Jeong, M.-J., Bettenhausen, C., Sayer, A. M., Hansell, R., Seftor, C. S., et al. (2013). Enhanced Deep Blue aerosol retrieval algorithm: The second generation. *Journal of Geophysical Research: Atmospheres*, *118*(16), 9296–9315. https://doi.org/10.1002/jgrd.50712

Huang, R.-J., Zhang, Y., Bozzetti, C., Ho, K.-F., Cao, J.-J., Han, Y., et al. (2014). High secondary aerosol contribution to particulate pollution during haze events in China. *Nature*, *514*(7521), 218–222. https://doi.org/10.1038/nature13774

Huang, Y., Shen, H., Chen, Y., Zhong, Q., Chen, H., Wang, R., et al. (2015). Global organic carbon emissions from primary sources from 1960 to 2009. *Atmospheric Environment*, *122*, 505–512. https://doi.org/10.1016/j.atmosenv.2015.10.017

Hudman, R. C., Moore, N. E., Martin, R. V., Russell, A. R., Valin, L. C., & Cohen, R. C. (2012). A mechanistic model of global soil nitric oxide emissions : implementation and space based-constraints - Semantic Scholar. Retrieved August 1, 2018, from /paper/A-mechanistic-model-of-global-soil-nitric-oxide-%3A-Hudman-Moore/cce0d0ce67a101f264b70bf43e10288f67307468

Hudman, R. C., Jacob, D. J., Turquety, S., Leibensperger, E. M., Murray, L. T., Wu, S., et al. (2018). Surface and lightning sources of nitrogen oxides over the United States: Magnitudes, chemical evolution, and outflow. *Journal of Geophysical Research: Atmospheres*. https://doi.org/10.1029/2006JD007912@10.1002/(ISSN)2169-8996.INTEX1

Huneeus, N., Schulz, M., Balkanski, Y., Griesfeller, J., Prospero, J., Kinne, S., et al. (2011). Global dust model intercomparison in AeroCom phase I. *Atmospheric Chemistry and Physics*, *11*(15), 7781–7816. https://doi.org/10.5194/acp-11-7781-2011

Hurteau, M. D., Westerling, A. L., Wiedinmyer, C., & Bryant, B. P. (2014). Projected Effects of Climate and Development on California Wildfire Emissions through 2100. *Environmental Science & Technology*, *48*(4), 2298–2304. https://doi.org/10.1021/es4050133

Information (NCEI), N. C. for E. (n.d.). ETOPO1 1 Arc-Minute Global Relief Model. Retrieved November 9, 2018, from https://data.nodc.noaa.gov/cgi-bin/iso?id=gov.noaa.ngdc.mgg.dem:316

IPCC. (2013). *Climate Change 2013: The Physical Science Basis. Contribution of Working Group I to the Fifth Assessment Report of the Intergovernmental Panel on Climate Change [Stocker, T.F., D. Qin, G.-K. Plattner, M. Tignor, S.K. Allen, J. Boschung, A. Nauels, Y. Xia, V. Bex and P.M. Midgley (eds.)]. Cambridge University Press, Cambridge, United Kingdom and New York, NY, USA, 1535 pp.*

Jacob, D. J. (2000). Heterogeneous chemistry and tropospheric ozone. *Atmospheric Environment*, *34*(12), 2131–2159. https://doi.org/10.1016/S1352-2310(99)00462-8

Jacobson, M. C., Hansson, H.-C., Noone, K. J., & Charlson, R. J. (2000). Organic atmospheric aerosols: Review and state of the science. *Reviews of Geophysics*, *38*(2), 267–294. https://doi.org/10.1029/1998RG000045

Jaeglé, L., Quinn, P. K., Bates, T. S., Alexander, B., & Lin, J.-T. (2011). Global distribution of sea salt aerosols: new constraints from in situ and remote sensing observations. *Atmospheric Chemistry and Physics*, *11*(7), 3137–3157. https://doi.org/10.5194/acp-11-3137-2011

Jeong, C.-H., Evans, G. J., Dann, T., Graham, M., Herod, D., Dabek-Zlotorzynska, E., et al. (2008). Influence of biomass burning on wintertime fine particulate matter: Source contribution at a valley site in rural British Columbia. *Atmospheric Environment*, *42*(16), 3684–3699. https://doi.org/10.1016/j.atmosenv.2008.01.006

Keller, C. A., Long, M. S., Yantosca, R. M., Da Silva, A. M., Pawson, S., & Jacob, D. J. (2014). HEMCO v1.0: a versatile, ESMF-compliant component for calculating emissions in atmospheric models. *Geoscientific Model Development*, *7*(4), 1409–1417. https://doi.org/10.5194/gmd-7-1409-2014

Kim, P. S., Jacob, D. J., Fisher, J. A., Travis, K., Yu, K., Zhu, L., et al. (2015). Sources, seasonality, and trends of southeast US aerosol: an integrated analysis of surface, aircraft, and satellite observations with the GEOS-Chem chemical transport model. *Atmospheric Chemistry and Physics*, *15*(18), 10411–10433. https://doi.org/10.5194/acp-15-10411-2015

Kim, S.-Y., Olives, C., Sheppard, L., Sampson, P. D., Larson, T. V., Keller, J. P., & Kaufman, J. D. (2017). Historical Prediction Modeling Approach for Estimating Long-Term Concentrations of $PM_{2.5}$ in Cohort Studies before the 1999 Implementation of Widespread Monitoring. *Environmental Health Perspectives*, *125*(1), 38–46. https://doi.org/10.1289/EHP131

Kosmopoulos, P. G., Kazadzis, S., Taylor, M., Athanasopoulou, E., Speyer, O., Raptis, P. I., et al. (2017). Dust impact on surface solar irradiance assessed with model simulations, satellite observations and ground-based measurements. *Atmospheric Measurement Techniques*, *10*(7), 2435–2453. https://doi.org/10.5194/amt-10-2435-2017

Krewski, D., Jerrett, M., Burnett, R. T., Ma, R., Hughes, E., Shi, Y., et al. (2009). Extended follow-up and spatial analysis of the American Cancer Society study linking particulate air pollution and mortality. *Research Report (Health Effects Institute)*, (140), 5–114; discussion 115-136.

Kroll, J. H., & Seinfeld, J. H. (2008). Chemistry of secondary organic aerosol: Formation and evolution of low-volatility organics in the atmosphere. *Atmospheric Environment*, *42*(16), 3593–3624. https://doi.org/10.1016/j.atmosenv.2008.01.003

Kuhns, H., Knipping, E. M., & Vukovich, J. M. (2005). Development of a United States-Mexico Emissions Inventory for the Big Bend Regional Aerosol and Visibility Observational (BRAVO) Study. *Journal of the Air & Waste Management Association (1995)*, *55*(5), 677–692.

Lall, R., Kendall, M., Ito, K., & Thurston, G. D. (2004). Estimation of historical annual $PM_{2.5}$ exposures for health effects assessment. *Atmospheric Environment*, *38*(31), 5217–5226. https://doi.org/10.1016/j.atmosenv.2004.01.053

Landis, M. S., Edgerton, E. S., White, E. M., Wentworth, G. R., Sullivan, A. P., & Dillner, A. M. (2018). The impact of the 2016 Fort McMurray Horse River Wildfire on ambient air pollution levels in the Athabasca Oil Sands Region, Alberta, Canada. *The Science of the Total Environment*, *618*, 1665–1676. https://doi.org/10.1016/j.scitotenv.2017.10.008

Latimer, R. N. C., & Martin, R. V. (2019). Interpretation of measured aerosol mass scattering efficiency over North America using a chemical transport model. *Atmospheric Chemistry and Physics*, *19*(4), 2635–2653. https://doi.org/10.5194/acp-19-2635-2019

Lee, C., Martin, R. V., van Donkelaar, A., Lee, H., Dickerson, R. R., Hains, J. C., et al. (2011). SO_2 emissions and lifetimes: Estimates from inverse modeling using in situ and global, space-based (SCIAMACHY and OMI) observations. *Journal of Geophysical Research: Atmospheres*, *116*(D6). https://doi.org/10.1029/2010JD014758

Lelieveld, J., Evans, J. S., Fnais, M., Giannadaki, D., & Pozzer, A. (2015). The contribution of outdoor air pollution sources to premature mortality on a global scale. *Nature*, *525*(7569), 367–371. https://doi.org/10.1038/nature15371

Lepeule, J., Laden, F., Dockery, D., & Schwartz, J. (2012). Chronic exposure to fine particles and mortality: an extended follow-up of the Harvard Six Cities study from 1974 to 2009. *Environmental Health Perspectives*, *120*(7), 965–970. https://doi.org/10.1289/ehp.1104660

Li, C., Martin, R. V., van Donkelaar, A., Boys, B. L., Hammer, M. S., Xu, J.-W., et al. (2017). Trends in Chemical Composition of Global and Regional Population-Weighted Fine Particulate Matter Estimated for 25 Years. *Environmental Science & Technology*, *51*(19), 11185–11195. https://doi.org/10.1021/acs.est.7b02530

Li, L., Wu, A. H., Cheng, I., Chen, J.-C., & Wu, J. (2017). Spatiotemporal estimation of historical $PM_{2.5}$ concentrations using PM_{10}, meteorological variables, and spatial effect. *Atmospheric Environment*, *166*, 182–191. https://doi.org/10.1016/j.atmosenv.2017.07.023

Li, Y., Henze, D. K., Jack, D., & Kinney, P. L. (2016). The influence of air quality model resolution on health impact assessment for fine particulate matter and its components. *Air Quality, Atmosphere & Health*, *9*(1), 51–68. https://doi.org/10.1007/s11869-015-0321-z

Liu, H., J. Jacob, D., Bey, I., & Yantosca, R. (2001). Constraints from 210Pb and 7Be on wet deposition and transport in a global three-dimensional chemical tracer model driven by assimilated meteorological fields. *Journal of Geophysical Research: Atmospheres*, *106*. https://doi.org/10.1029/2000JD900839

Lohmann, U., & Feichter, J. (2005). Global indirect aerosol effects: a review. *Atmospheric Chemistry and Physics*, *5*(3), 715–737. https://doi.org/10.5194/acp-5-715-2005

Lyapustin, A., Martonchik, J., Wang, Y., Laszlo, I., & Korkin, S. (2011). Multiangle implementation of atmospheric correction (MAIAC): 1. Radiative transfer basis and look-up tables. *Journal of Geophysical Research*, *116*(D3). https://doi.org/10.1029/2010JD014985

Lyapustin, A., Wang, Y., Laszlo, I., Kahn, R., Korkin, S., Remer, L., et al. (2011). Multiangle implementation of atmospheric correction (MAIAC): 2. Aerosol algorithm. *Journal of Geophysical Research*, *116*(D3). https://doi.org/10.1029/2010JD014986

Lyapustin, A., Wang, Y., Korkin, S., & Huang, D. (2018). MODIS Collection 6 MAIAC algorithm. *Atmospheric Measurement Techniques*, *11*(10), 5741–5765. https://doi.org/10.5194/amt-11-5741-2018

Ma, Q., Cai, S., Wang, S., Zhao, B., Martin, R. V., Brauer, M., et al. (2017). Impacts of coal burning on ambient $PM_{2.5}$ pollution in China. *Atmospheric Chemistry and Physics*, *17*(7), 4477–4491. https://doi.org/10.5194/acp-17-4477-2017

Ma, Z., Hu, X., Sayer, A. M., Levy, R., Zhang, Q., Xue, Y., et al. (2016). Satellite-Based Spatiotemporal Trends in $PM_{2.5}$ Concentrations: China, 2004-2013. *Environmental Health Perspectives*, *124*(2), 184–192. https://doi.org/10.1289/ehp.1409481

Mao, J., Fan, S., Jacob, D. J., & Travis, K. R. (2013). Radical loss in the atmosphere from Cu-Fe redox coupling in aerosols. *Atmospheric Chemistry and Physics*, *13*(2), 509–519. https://doi.org/10.5194/acp-13-509-2013

Marais, E. A., Jacob, D. J., Jimenez, J. L., Campuzano-Jost, P., Day, D. A., Hu, W., et al. (2016). Aqueous-phase mechanism for secondary organic aerosol formation from isoprene: Application to the southeast United States and co-benefit of SO_2 emission controls. *Atmospheric Chemistry and Physics*, *16*(3), 1603–1618. https://doi.org/10.5194/acp-16-1603-2016

Martin, R. V., Jacob, D. J., Yantosca, R. M., Chin, M., & Ginoux, P. (2003). Global and regional decreases in tropospheric oxidants from photochemical effects of aerosols. *Journal of Geophysical Research: Atmospheres*, *108*(D3). https://doi.org/10.1029/2002JD002622

McDuffie, E. E., Smith, S. J., O'Rourke, P., Tibrewal, K., Venkataraman, C., Marais, E. A., et al. (2020). A global anthropogenic emission inventory of atmospheric pollutants from sector- and fuel-specific sources (1970–2017): An application of the Community Emissions Data System (CEDS). *Earth System Science Data Discussions*, 1–49. https://doi.org/10.5194/essd-2020-103

Meng, J., Li, C., Martin, R. V., van Donkelaar, A., Hystad, P., & Brauer, M. (2019a). Estimated Long-term (1981-2016) Concentrations of Ambient Fine Particulate Matter across North America from Chemical Transport Modeling, Satellite Remote Sensing and Ground-based Measurements. *Environmental Science & Technology*. https://doi.org/10.1021/acs.est.8b06875

Meng, J., Li, C., Martin, R. V., van Donkelaar, A., Hystad, P., & Brauer, M. (2019b). Historical PM2.5 dataset across North America. https://doi.org/10.5281/zenodo.2616769

Molod, A., Takacs, L., Suarez, M., & Bacmeister, J. (2015). Development of the GEOS-5 atmospheric general circulation model: evolution from MERRA to MERRA2. *Geoscientific Model Development*, *8*(5), 1339–1356. https://doi.org/10.5194/gmd-8-1339-2015

Muller, N. Z. (2020). Long-Run Environmental Accounting in the US Economy. *Environmental and Energy Policy and the Economy*, *1*, 158–191. https://doi.org/10.1086/706798

Murray, L. T., Jacob, D. J., Logan, J. A., Hudman, R. C., & Koshak, W. J. (2012). Optimized regional and interannual variability of lightning in a global chemical transport model constrained by LIS/OTD satellite data. *Journal of Geophysical Research: Atmospheres*, *117*(D20). https://doi.org/10.1029/2012JD017934

Pappin, A. J., & Hakami, A. (2013). Source Attribution of Health Benefits from Air Pollution Abatement in Canada and the United States: An Adjoint Sensitivity Analysis. *Environmental Health Perspectives*, *121*(5), 572–579. https://doi.org/10.1289/ehp.1205561

Pappin, A. J., Christidis, T., Pinault, L. L., Crouse, D. L., Brook, J. R., Erickson, A., et al. (2019). Examining the Shape of the Association between Low Levels of Fine Particulate Matter and Mortality across Three Cycles of the Canadian Census Health and Environment Cohort. *Environmental Health Perspectives*, *127*(10), 107008. https://doi.org/10.1289/EHP5204

Park, R. J., Jacob, D. J., Chin, M., & Martin, R. V. (2003). Sources of carbonaceous aerosols over the United States and implications for natural visibility. *Journal of Geophysical Research: Atmospheres*, *108*(D12), 4355. https://doi.org/10.1029/2002JD003190

Park, R. J., Jacob, D. J., Field, B. D., Yantosca, R. M., & Chin, M. (2004). Natural and transboundary pollution influences on sulfate-nitrate-ammonium aerosols in the United States: Implications for policy. *Journal of Geophysical Research: Atmospheres*, *109*(D15). https://doi.org/10.1029/2003JD004473

Parkhurst, W. J., Tanner, R. L., Weatherford, F. P., Valente, R. J., & Meagher, J. F. (1999). Historic $PM_{2.5}/PM_{10}$ concentrations in the southeastern United States - Potential implications of the revised particulate matter standard. *Journal of the Air & Waste Management Association*, *49*(9), 1060–1067. https://doi.org/10.1080/10473289.1999.10463894

Parrella, J. P., Jacob, D. J., Liang, Q., Zhang, Y., Mickley, L. J., Miller, B., et al. (2012). Tropospheric bromine chemistry: implications for present and pre-industrial ozone and mercury. *Atmospheric Chemistry and Physics*, *12*(15), 6723–6740. https://doi.org/10.5194/acp-12-6723-2012

Philip, S., Martin, R. V., Pierce, J. R., Jimenez, J. L., Zhang, Q., Canagaratna, M. R., et al. (2014). Spatially and seasonally resolved estimate of the ratio of organic mass to organic carbon. *Atmospheric Environment*, *87*, 34–40. https://doi.org/10.1016/j.atmosenv.2013.11.065

Philip, S., Martin, R. V., & Keller, C. A. (2016). Sensitivity of chemistry-transport model simulations to the duration of chemical and transport operators: a case study with GEOS-Chem v10-01. *Geosci. Model Dev.*, *9*(5), 1683–1695. https://doi.org/10.5194/gmd-9-1683-2016

Philip, S, Martin, R. V., Snider, G., Weagle, C. L., Donkelaar, A. van, Brauer, M., et al. (2017). Anthropogenic fugitive, combustion and industrial dust is a significant, underrepresented fine particulate matter source in global atmospheric models. *Environmental Research Letters*, *12*(4), 044018. https://doi.org/10.1088/1748-9326/aa65a4

Pinault, L., Tjepkema, M., Crouse, D. L., Weichenthal, S., van Donkelaar, A., Martin, R. V., et al. (2016). Risk estimates of mortality attributed to low concentrations of ambient fine particulate matter in the Canadian community health survey cohort. *Environmental Health: A Global Access Science Source*, *15*, 18. https://doi.org/10.1186/s12940-016-0111-6

Pinault, L., van Donkelaar, A., & Martin, R. V. (2017). Exposure to fine particulate matter air pollution in Canada. *Health Reports*, *28*(3), 9–16.

Pope, C. A., Ezzati, M., & Dockery, D. W. (2009). Fine-Particulate Air Pollution and Life Expectancy in the United States. *New England Journal of Medicine*, *360*(4), 376–386. https://doi.org/10.1056/NEJMsa0805646

Pye, H. O. T., Liao, H., Wu, S., Mickley, L. J., Jacob, D. J., Henze, D. K., & Seinfeld, J. H. (2009). Effect of changes in climate and emissions on future sulfate-nitrate-ammonium aerosol levels in the United States. *Journal of Geophysical Research: Atmospheres*, *114*(D1). https://doi.org/10.1029/2008JD010701

Pye, H. O. T., Chan, A. W. H., Barkley, M. P., & Seinfeld, J. H. (2010). Global modeling of organic aerosol: The importance of reactive nitrogen (NOx and NO_3). *Atmospheric Chemistry and Physics*, *10*(22), 11261–11276. https://doi.org/10.5194/acp-10-11261-2010

Qu, Y., An, J., He, Y., & Zheng, J. (2016). An overview of emissions of SO2 and NOx and the long-range transport of oxidized sulfur and nitrogen pollutants in East Asia. *Journal of Environmental Sciences (China)*, *44*, 13–25. https://doi.org/10.1016/j.jes.2015.08.028

Querol, X., Tobías, A., Pérez, N., Karanasiou, A., Amato, F., Stafoggia, M., et al. (2019). Monitoring the impact of desert dust outbreaks for air quality for health studies. *Environment International*, *130*, 104867. https://doi.org/10.1016/j.envint.2019.05.061

Ramanathan, V., Crutzen, P. J., Kiehl, J. T., & Rosenfeld, D. (2001). Aerosols, climate, and the hydrological cycle. *Science (New York, N.Y.)*, *294*(5549), 2119–2124. https://doi.org/10.1126/science.1064034

Randerson, J. T., Chen, Y., Werf, G. R. van der, Rogers, B. M., & Morton, D. C. (2012). Global burned area and biomass burning emissions from small fires. *Journal of Geophysical Research: Biogeosciences*, *117*(G4). https://doi.org/10.1029/2012JG002128

Reff, A., Bhave, P. V., Simon, H., Pace, T. G., Pouliot, G. A., Mobley, J. D., & Houyoux, M. (2009). Emissions Inventory of $PM_{2.5}$ Trace Elements across the United States. *Environmental Science & Technology*, *43*(15), 5790–5796. https://doi.org/10.1021/es802930x

Ridley, D. A., Heald, C. L., & Ford, B. (2012). North African dust export and deposition: A satellite and model perspective. *Journal of Geophysical Research: Atmospheres*, *117*(D2). https://doi.org/10.1029/2011JD016794

Ridley, D. A., Heald, C. L., Pierce, J. R., & Evans, M. J. (2013). Toward resolution-independent dust emissions in global models: Impacts on the seasonal and spatial distribution of dust. *Geophysical Research Letters*, *40*(11), 2873–2877. https://doi.org/10.1002/grl.50409

Ridley, D. A., Heald, C. L., Kok, J. F., & Zhao, C. (2016). An observationally constrained estimate of global dust aerosol optical depth, *16*(23), 15097–15117. https://doi.org/10.5194/acp-16-15097-2016

Ridley, D. A., Heald, C. L., Ridley, K. J., & Kroll, J. H. (2018). Causes and consequences of decreasing atmospheric organic aerosol in the United States. *Proceedings of the National Academy of Sciences*, *115*(2), 290–295. https://doi.org/10.1073/pnas.1700387115

Sayer, A. M., Munchak, L. A., Hsu, N. C., Levy, R. C., Bettenhausen, C., & Jeong, M.-J. (2014). MODIS Collection 6 aerosol products: Comparison between Aqua's e-Deep Blue, Dark Target, and "merged" data sets, and usage recommendations. *Journal of Geophysical Research: Atmospheres*, *119*(24), 13,965-13,989. https://doi.org/10.1002/2014JD022453

Schepanski, K., Tegen, I., & Macke, A. (2012). Comparison of satellite based observations of Saharan dust source areas. *Remote Sensing of Environment*, *123*, 90–97. https://doi.org/10.1016/j.rse.2012.03.019

Schepanski, Kerstin. (2018). Transport of Mineral Dust and Its Impact on Climate. *Geosciences*, *8*(5), 151. https://doi.org/10.3390/geosciences8050151

Schultz, M. G., Heil, A., Hoelzemann, J. J., Spessa, A., Thonicke, K., Goldammer, J. G., et al. (2008). Global wildland fire emissions from 1960 to 2000. *Global Biogeochemical Cycles*, *22*(2), GB2002. https://doi.org/10.1029/2007GB003031

Schwartz, J. (2000). Harvesting and Long Term Exposure Effects in the Relation between Air Pollution and Mortality. *American Journal of Epidemiology*, *151*(5), 440–448. https://doi.org/10.1093/oxfordjournals.aje.a010228

Schwartz, J., Bind, M.-A., & Koutrakis, P. (2017). Estimating Causal Effects of Local Air Pollution on Daily Deaths: Effect of Low Levels. *Environmental Health Perspectives*, *125*(1), 23–29. https://doi.org/10.1289/EHP232

Seinfeld, J. H., & Pandis, S. N. (2016). *Atmospheric chemistry and physics: from air pollution to climate change* (Third Edition).

Shah, V., Jaeglé, L., Thornton, J. A., Lopez-Hilfiker, F. D., Lee, B. H., Schroder, J. C., et al. (2018). Chemical feedbacks weaken the wintertime response of particulate sulfate and nitrate to emissions reductions over the eastern United States. *Proceedings of the National Academy of Sciences*, *115*(32), 8110–8115. https://doi.org/10.1073/pnas.1803295115

Shao, Y., Raupach, M. R., & Findlater, P. A. (1993). Effect of saltation bombardment on the entrainment of dust by wind. *Journal of Geophysical Research: Atmospheres*, *98*(D7), 12719–12726. https://doi.org/10.1029/93JD00396

Shi, L., Zanobetti, A., Kloog, I., Coull, B. A., Koutrakis, P., Melly, S. J., & Schwartz, J. D. (2016). Low-Concentration $PM_{2.5}$ and Mortality: Estimating Acute and Chronic Effects in a Population-Based Study. *Environmental Health Perspectives*, *124*(1), 46–52. https://doi.org/10.1289/ehp.1409111

Silva, R. A., Adelman, Z., Fry, M. M., & West, J. J. (2016). The Impact of Individual Anthropogenic Emissions Sectors on the Global Burden of Human Mortality due to Ambient Air Pollution. *Environmental Health Perspectives*, *124*(11), 1776–1784. https://doi.org/10.1289/EHP177

Sofowote, U., & Dempsey, F. (2015). Impacts of forest fires on ambient near–real–time $PM_{2.5}$ in Ontario, Canada: Meteorological analyses and source apportionment of the July 2011–2013 episodes. *Atmospheric Pollution Research*, *6*(1), 1–10. https://doi.org/10.5094/APR.2015.001

Solomon, P. A., Crumpler, D., Flanagan, J. B., Jayanty, R. K. M., Rickman, E. E., & McDade, C. E. (2014). U.S. national PM2.5 Chemical Speciation Monitoring Networks-CSN and IMPROVE: description of networks. *Journal of the Air & Waste Management Association (1995)*, *64*(12), 1410–1438. https://doi.org/10.1080/10962247.2014.956904

Squizzato, S., Masiol, M., Brunelli, A., Pistollato, S., Tarabotti, E., Rampazzo, G., & Pavoni, B. (2013). Factors determining the formation of secondary inorganic aerosol: a case study in the Po Valley (Italy). *Atmospheric Chemistry and Physics*, *13*(4), 1927–1939. https://doi.org/10.5194/acp-13-1927-2013

Stettler, M. E. J., Eastham, S., & Barrett, S. R. H. (2011). Air quality and public health impacts of UK airports. Part I: Emissions. *Atmospheric Environment*, *45*(31), 5415–5424. https://doi.org/10.1016/j.atmosenv.2011.07.012

Tai, A. P. K., Mickley, L. J., Heald, C. L., & Wu, S. (2013). Effect of CO_2 inhibition on biogenic isoprene emission: Implications for air quality under 2000 to 2050 changes in climate, vegetation, and land use. *Geophysical Research Letters*, *40*(13), 3479–3483. https://doi.org/10.1002/grl.50650

Tang, M., Huang, X., Lu, K., Ge, M., Li, Y., Cheng, P., et al. (2017). Heterogeneous reactions of mineral dust aerosol: implications for tropospheric oxidation capacity. *Atmospheric Chemistry and Physics*, *17*(19), 11727–11777. https://doi.org/10.5194/acp-17-11727-2017

The International GEOS-Chem User Community. (2019). *geoschem/geos-chem: GEOS-Chem 12.5.0 (Version 12.5.0)*. Zenodo. https://doi.org/10.5281/zenodo.3403111

Tomczak, A., Miller, A. B., Weichenthal, S. A., To, T., Wall, C., van Donkelaar, A., et al. (2016). Long-term exposure to fine particulate matter air pollution and the risk of lung cancer among participants of the Canadian National Breast Screening Study. *International Journal of Cancer*, *139*(9), 1958–1966. https://doi.org/10.1002/ijc.30255

Tzompa-Sosa, Z. A., Henderson, B. H., Keller, C. A., Travis, K., Mahieu, E., Franco, B., et al. (2019). Atmospheric Implications of Large C2-C5 Alkane Emissions From the U.S. Oil and Gas Industry. *Journal of Geophysical Research: Atmospheres*, *124*(2), 1148–1169. https://doi.org/10.1029/2018JD028955

U.S. EPA. (2018). Air Quality Improves as America Grows. Retrieved November 11, 2018, from https://gispub.epa.gov/air/trendsreport/2017/

Venkataraman, C., Brauer, M., Tibrewal, K., Sadavarte, P., Ma, Q., Cohen, A., et al. (2018). Source influence on emission pathways and ambient $PM_{2.5}$ pollution over India (2015–2050). *Atmospheric Chemistry and Physics*, *18*(11), 8017–8039. https://doi.org/10.5194/acp-18-8017-2018

Wallace, P. J. (2001). Volcanic SO2 emissions and the abundance and distribution of exsolved gas in magma bodies. *Journal of Volcanology and Geothermal Research*, *108*(1), 85–106. https://doi.org/10.1016/S0377-0273(00)00279-1

Wang, D., Hu, J., Xu, Y., Lv, D., Xie, X., Kleeman, M., et al. (2014). Source contributions to primary and secondary inorganic particulate matter during a severe wintertime PM2.5 pollution episode in Xi'an, China. *Atmospheric Environment*, *97*, 182–194. https://doi.org/10.1016/j.atmosenv.2014.08.020

Wang, Q., Jacob, D. J., Fisher, J. A., Mao, J., Leibensperger, E. M., Carouge, C. C., et al. (2011). Sources of carbonaceous aerosols and deposited black carbon in the Arctic in winter-spring: implications for radiative forcing. *Atmospheric Chemistry and Physics*, *11*(23), 12453–12473. https://doi.org/10.5194/acp-11-12453-2011

Wang, Q., Jacob, D. J., Spackman, J. R., Perring, A. E., Schwarz, J. P., Moteki, N., et al. (2014). Global budget and radiative forcing of black carbon aerosol: Constraints from pole-to-

pole (HIPPO) observations across the Pacific. *Journal of Geophysical Research: Atmospheres*, *119*, 195–206. https://doi.org/10.1002/2013JD020824

Wang, Y. X., McElroy, M. B., Jacob, D. J., & Yantosca, R. M. (2004). A nested grid formulation for chemical transport over Asia: Applications to CO. *Journal of Geophysical Research: Atmospheres*, *109*(D22). https://doi.org/10.1029/2004JD005237

Weagle, C. L., Snider, G., Li, C., van Donkelaar, A., Philip, S., Bissonnette, P., et al. (2018). Global Sources of Fine Particulate Matter: Interpretation of PM2.5 Chemical Composition Observed by SPARTAN using a Global Chemical Transport Model. *Environmental Science & Technology*, *52*(20), 11670–11681. https://doi.org/10.1021/acs.est.8b01658

Weichenthal, S., Villeneuve, P. J., Burnett, R. T., van Donkelaar, A., Martin, R. V., Jones, R. R., et al. (2014). Long-term exposure to fine particulate matter: association with nonaccidental and cardiovascular mortality in the agricultural health study cohort. *Environmental Health Perspectives*, *122*(6), 609–615. https://doi.org/10.1289/ehp.1307277

Weichenthal, S., Kulka, R., Lavigne, E., van Rijswijk, D., Brauer, M., Villeneuve, P. J., et al. (2017). Biomass Burning as a Source of Ambient Fine Particulate Air Pollution and Acute Myocardial Infarction. *Epidemiology (Cambridge, Mass.)*, *28*(3), 329–337. https://doi.org/10.1097/EDE.0000000000000636

Yu, H., Chin, M., Yuan, T., Bian, H., Remer, L. A., Prospero, J. M., et al. (2015). The fertilizing role of African dust in the Amazon rainforest: A first multiyear assessment based on data from Cloud-Aerosol Lidar and Infrared Pathfinder Satellite Observations. *Geophysical Research Letters*, *42*(6), 1984–1991. https://doi.org/10.1002/2015GL063040

Yu, Y., Kalashnikova, O. V., Garay, M. J., Lee, H., & Notaro, M. (2018). Identification and Characterization of Dust Source Regions Across North Africa and the Middle East Using MISR Satellite Observations. *Geophysical Research Letters*, *45*(13), 6690–6701. https://doi.org/10.1029/2018GL078324

Yue, X., Mickley, L. J., Logan, J. A., & Kaplan, J. O. (2013). Ensemble projections of wildfire activity and carbonaceous aerosol concentrations over the western United States in the mid-21st century. *Atmospheric Environment (Oxford, England: 1994)*, *77*, 767–780. https://doi.org/10.1016/j.atmosenv.2013.06.003

Zender, Charles S., Bian, H., & Newman, D. (2003). Mineral Dust Entrainment and Deposition (DEAD) model: Description and 1990s dust climatology. *Journal of Geophysical Research: Atmospheres*, *108*(D14). https://doi.org/10.1029/2002JD002775

Zender, Charles S., Miller, R. L. R. L., & Tegen, I. (2004). Quantifying mineral dust mass budgets:Terminology, constraints, and current estimates. *Eos, Transactions American Geophysical Union*, *85*(48), 509–512. https://doi.org/10.1029/2004EO480002

Zhang, L., Kok, J. F., Henze, D. K., Li, Q., & Zhao, C. (2013). Improving simulations of fine dust surface concentrations over the western United States by optimizing the particle size distribution. *Geophysical Research Letters*, *40*(12), 3270–3275. https://doi.org/10.1002/grl.50591

Zhang, Y., West, J. J., Mathur, R., Xing, J., Hogrefe, C., Roselle, S. J., et al. (2018). Long-term trends in the ambient $PM_{2.5}$- and O_3-related mortality burdens in the United States under emission reductions from 1990 to 2010. *Atmospheric Chemistry and Physics*, *18*(20), 15003–15016. https://doi.org/10.5194/acp-18-15003-2018